

MIT OpenCourseWare
<http://ocw.mit.edu>

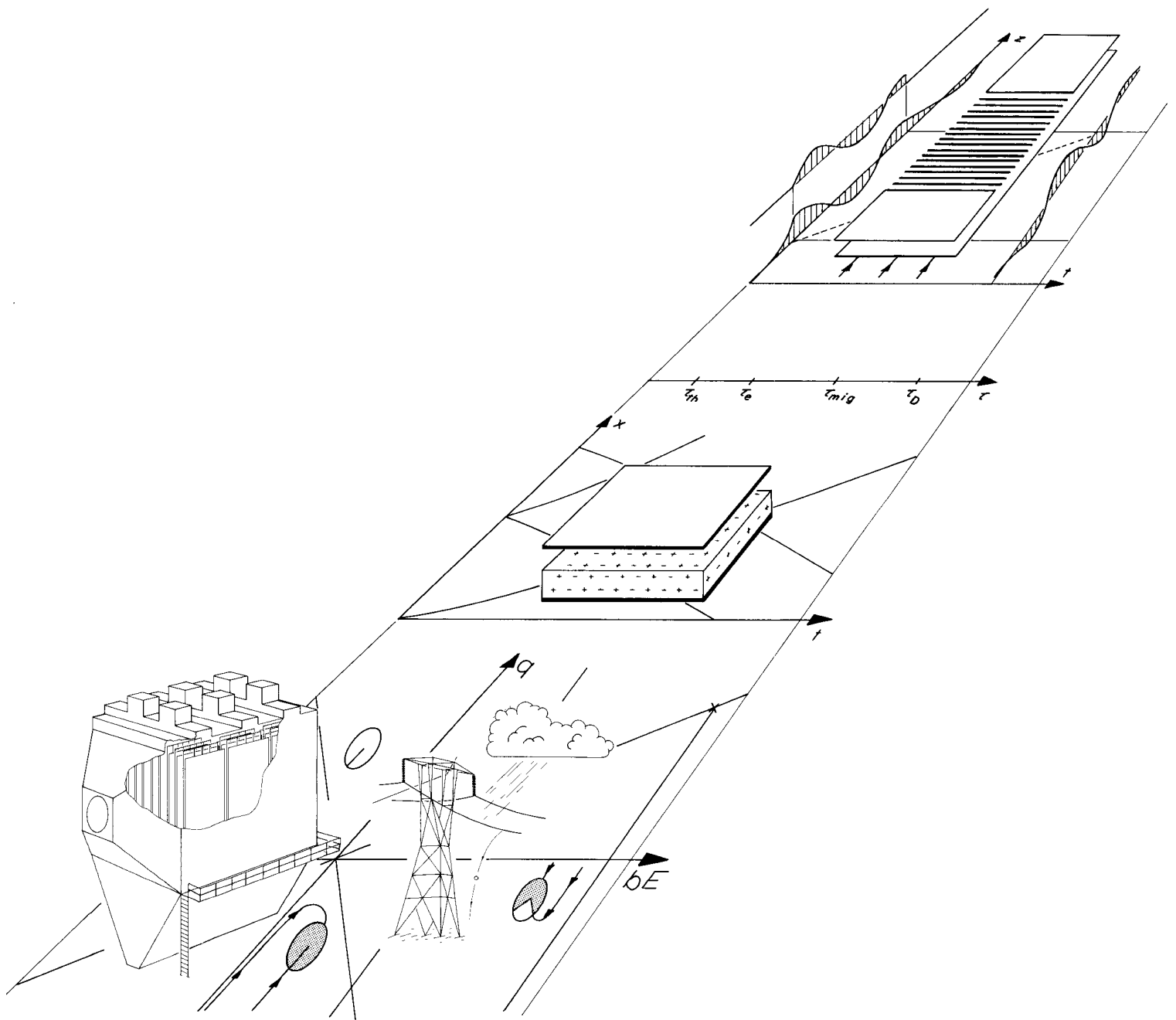
Continuum Electromechanics

For any use or distribution of this textbook, please cite as follows:

Melcher, James R. *Continuum Electromechanics*. Cambridge, MA: MIT Press, 1981. Copyright Massachusetts Institute of Technology. ISBN: 9780262131650. Also available online from MIT OpenCourseWare at <http://ocw.mit.edu> (accessed MM DD, YYYY) under Creative Commons license Attribution-NonCommercial-Share Alike.

For more information about citing these materials or our Terms of Use, visit:
<http://ocw.mit.edu/terms>.

Charge Migration, Convection and Relaxation



5.1 Introduction

In Chap. 4, the subject is electromechanical kinematics. Field sources are physically constrained to have predetermined spatial distributions and the relative motion is prescribed. As a result, in a typical example, the electromechanical dynamics can be incapsulated in a lumped-parameter model. In this and the next chapter, the mechanics remain kinematic, in that the material deformations are again prescribed. However, now material may be suffering relative deformations, represented by a given velocity field $\vec{v}(\vec{r}, t)$. More important, in this and the next chapter, electrodes and wires are no longer used to constrain the "free" field sources. Rather, the distribution of free charge and current is now determined by the field laws themselves, augmented by conservation laws and constitutive relations.

The physical situations now considered are electroquasistatic and the sources are therefore charge densities. In Chap. 6, magnetoquasistatic systems are of interest, the relevant sources are the free current density and magnetization density, and the subject is magnetic diffusion in the face of material convection.

In the next section, equations are deduced that represent the fate of each species of charge. Throughout this chapter, the charge carriers are dominated in their motions by collisions with neutral particles and with each other. On the average, collisions are so frequent that the inertia of each carrier can be ignored. Such collision-dominated carrier motions are introduced in Secs. 3.2 and 3.3, where the observation is made that it is only if the particle inertia is ignorable that the electrical force on the carrier can be taken as instantaneously transmitted to the media through which it moves. If the carrier inertia is important, the carrier densities constitute mechanical continua in their own right. Such examples are the electron beam in vacuum and the ions and electrons that constitute a "cold" plasma. These models are therefore appropriately included in Chaps. 7 and 8, where fluids and fluid-like continua are studied.

The conservation of charge equations, together with the electroquasistatic field laws and the specified material deformation, constitute a description of the way in which the fields and their sources self-consistently evolve. Whether to gain insights concerning the implications of these equations, or to solve these equations in a specific situation, characteristic coordinates are valuable. Thus, the characteristic approach to partial differential equations is introduced in the context of charge-carrier migration, relaxation and convection. The method of characteristics will be used extensively to describe other phenomena involving propagation in later sections and chapters.

Examples treated in Secs. 5.4 and 5.5, which illustrate "imposed field and flow" dynamics of systems of carriers, involve a space charge due to the charge carriers that is ignorable in its contribution to the field. The impact charging of macroscopic particles treated in Sec. 5.5 results in a model widely used in atmospheric sciences, macroscopic particle physics and air-pollution control.

When space-charge effects are significant, it is necessary to be more specialized in the treatment. In Sec. 5.6 only one species of charge carrier is presumed to be significant. The unipolar carriers might be ions injected by a corona discharge into a neutral gas or into a highly insulating liquid. They might also be charged macroscopic particles carrying a constant charge per particle and migrating through a gas or liquid. Section 5.7 considers steady-flow one-dimensional unipolar conduction and its relation to the d-c family of energy converters.

Bipolar conduction, discussed in Secs. 5.8 and 5.9, has as a limiting model ohmic conduction. These sections have two major objectives, to illustrate charge migration and convection phenomena with more than one species of carrier, and to put the ohmic conduction model in perspective. In Sec. 5.10, charge relaxation is described in general terms by again resorting to the method of characteristics. The remaining sections are based on the ohmic conduction model.

The transfer relations for regions of uniform conductivity are discussed in Sec. 5.12 and applied to important illustrative physical situations in Secs. 5.13 and 5.14. These case studies are profitably contrasted with their magnetic counterparts developed in Secs. 6.4 and 6.5.

Temporal transients, initiated from spatially periodic initial conditions, are considered in Sec. 5.15. Just as the natural modes are closely related to the driven response of lumped-parameter linear systems, the natural modes of the continuum systems discussed in terms of their responses to spatially periodic drives in Secs. 5.13 and 5.14 are found to be closely related to the natural modes for distributed systems. This section, which is the first to illustrate the third category of response for linear systems that are uniform in at least one direction, as presaged in Sec. 1.2, also illustrates how heterogeneous systems of uniform ohmic conductors (which support a charge relaxation process in each bulk region) can display charge diffusion in the system taken as a whole. This type of diffusion should be discriminated from diffusion at the carrier (microscopic) level. Diffusion in the latter sense is included in Sec. 5.2 so that the domain of validity of migration and convection proc-

esses in which diffusion is neglected can be appreciated. Molecular diffusion and its effect on charge evolution, introduced in Sec. 5.2, is largely delayed until Chap. 10.

Finally, in Sec. 5.16, the response of an Ohmic moving sheet is used to introduce the fourth type of continuum linear response eluded to in Sec. 1.2, a spatially transient response to a drive that is temporarily in the sinusoidal steady state.

5.2 Charge Conservation with Material Convection

With the objective of deriving a law obeyed by each species of charge carrier in its self-consistent evolution, consider a volume V of the deforming material having a fixed identity. That is, in a macroscopic sense, the surface S enclosing this volume is always composed of the same material particles: $S = S(t)$. The i th species of charge carrier is defined as having a number density n_i (particles per unit volume), charge magnitude q_i (per particle) and hence a magnitude of charge density $\rho_i = n_i q_i$. Positive and negative charge or charge density will be denoted explicitly by upper and lower signs respectively.

A statement that the total charge of the i th species is lost from V at a rate determined by the net outward current flux and accrued at a rate determined by the net effect of volumetric processes is

$$\frac{d}{dt} \int_V \pm \rho_i dV = - \oint_S \vec{J}_i' \cdot \vec{n} da \pm \int_V (G - R) dV \quad (1)$$

Generation and recombination of the carriers within the volume are represented by G and R , respectively, which have the units of charge/unit volume/sec. Because S is fixed relative to the media, \vec{J}_i' is defined as the i th species current density measured in the materials frame of reference.

The generalized Leibnitz rule for differentiation of an integral over a time-varying volume, Eq. 2.6.5, makes it possible to take the time derivative inside the integral on the left in Eq. 1. In using Eq. 2.6.5 for this purpose, note that the velocity of the surface S is the material velocity \vec{v} . Thus Eq. 1 is converted to

$$\int_V \frac{\partial \pm \rho_i}{\partial t} dV + \oint_S \pm \rho_i \vec{v} \cdot \vec{n} da = - \oint_S \vec{J}_i' \cdot \vec{n} da \pm \int_V (G - R) dV \quad (2)$$

By Gauss' theorem, Eq. 2.6.2, the surface integrations are converted to volume integrations. Because the volume V is arbitrary, it follows that

$$\frac{\partial \rho_i}{\partial t} + \nabla \cdot [\rho_i \vec{v} \pm \vec{J}_i'] = G - R \quad (3)$$

To make use of this differential law, the current density must be related to the charge density, and the rates of generation and recombination must be specified.

Carriers, dominated by collisions in their motion through a neutral medium, are usually described by the current density

$$\vec{J}_i' = n_i b_i q_i \vec{E} \mp K_{Di} \nabla (q_i n_i) \equiv b_i \rho_i \vec{E} \mp K_{Di} \nabla \rho_i \quad (4)$$

The term proportional to $q_i \vec{E}$ represents migration and is familiar from Sec. 3.2. Because of the electric field, a charged particle sustains a net migration as it undergoes frequent thermally induced collisions with neutral particles. These collisions are so frequent that on the time scale of interest there is an instantaneous equilibrium between the electrical force and an effective drag force. In terms of a friction coefficient ($m_i \nu_i$), this force equilibrium is expressed by

$$\pm q_i \vec{E} = (m_i \nu_i) \vec{v}_i \quad (5)$$

The particle velocity \vec{v}_i relative to the neutral medium is expressed in terms of the mobility b_i as

$$\vec{v}_i = \pm b_i \vec{E} \quad (6)$$

where $b_i \equiv q_i / m_i \nu_i$. Thus, the first term in Eq. 4 is the product of the charge density $\pm \rho_i$ and the

particle velocity \vec{v}_i . Large molecules and macroscopic particles in gases¹ and liquids² are often modeled as being spherical and obeying Stokes's law (Sec. 7.21), in which case the friction factor is $m_i v_i = 6\pi\eta a$, where η and a are the fluid viscosity and particle radius respectively. For such particles, the mobility is

$$b_i = \frac{q_i}{6\pi\eta a} \quad (7)$$

The second term in Eq. 4 recognizes that because of the thermally induced motions of the particles, on the average there will be a particle flux away from regions of high concentration. This flux is proportional to the spatial rate of change of concentration.

As might be expected from their common origins in the thermal particle motions, the diffusion coefficient K_{Di} and the mobility are related properties of the medium through which given particles migrate and diffuse. For ideal gases and liquids, K_{Di} and b_i are linked by the Einstein relation

$$K_{Di} = \left(\frac{kT}{q_i}\right)b_i; \quad \frac{kT}{e} = 26.6 \times 10^{-3} \text{ volts at } T = 20^\circ\text{C} \quad (8)$$

where k is the Boltzmann constant, T is the absolute temperature in degrees Kelvin and q_i is the particle charge. The quantity kT/q is measured in volts and at room temperature for q equal to the electron charge, e , has the value given with Eq. 8.

Physical examples to which Eq. 4 applies are given in Table 5.2.1, together with typical values for the mobility and diffusion coefficient.

In inserting Eq. 4 into the charge conservation equation, Eq. 3, it is now assumed that the material deformations of interest are incompressible in the sense that $\nabla \cdot \vec{v} = 0$, so that

$$\frac{\partial \rho_i}{\partial t} + (\vec{v} \pm b_i \vec{E}) \cdot \nabla \rho_i = \nabla \cdot (K_{Di} \nabla \rho_i) \mp \rho_i \nabla \cdot b_i \vec{E} + G - R \quad (9)$$

Each of n species contributing to the transfer of charge is described by an expression of the form of Eq. 9. The evolution of one species is linked to the others through Gauss' law, which recognizes that the net charge from all of the species is the source for the electric field:

$$\nabla \cdot \epsilon \vec{E} = \sum_{i=1}^n \pm \rho_i \quad (10)$$

Of course, in the electroquasistatic approximation \vec{E} is irrotational, a condition that is automatically met by requiring that

$$\vec{E} = -\nabla \phi \quad (11)$$

Given appropriate source and recombination functions G and R , and the material velocity distribution $\vec{v}(r,t)$, Eqs. 9-11 constitute $n+1$ scalar expressions and one vector equation describing n charge densities, ϕ and the vector \vec{E} .

In the remainder of this chapter, certain of the physical implications of these relations are explored, with emphasis on the interplay of the material convection and the charge transport processes. Approximations are necessary if practical use is to be made of these relations. In this regard, the relative importance of the migration and diffusion contributions to the current density, Eq. 4, is important. To approximate the ratio of diffusion and migration terms for a given species, the charge density gradient is characterized by ρ_i/ℓ , where ℓ is a typical length. For media described by the Einstein relation, Eq. 8,

$$\frac{\text{diffusion current density}}{\text{migration current density}} = \frac{kT/q_i}{\ell |\vec{E}|} \quad (12)$$

Suppose that each carrier supports one electronic charge. Then if $|\vec{E}| = 1$ V/m, the influence of diffusion equals or exceeds that of migration for length scales shorter than about 2.5 cm. But, for

1. C. Orr, Jr., Particle Technology, Macmillan Company, New York, 1966, p. 296.

2. F. Daniels and R. A. Alberty, Physical Chemistry, 3rd ed., John Wiley & Sons, New York, 1967, pp. 405-406.

Table 5.2.1. Typical mobilities of various charged particles.

Macroscopic Particles in Fluids										
<p>Charged to saturation by ion impact, the particle charge is given by Eq. 5.5.1. Introduced into Eq. 7, this charge implies the mobility</p> $b = \frac{2\epsilon_0 aE}{\eta} \tag{a}$ <p>where a is the particle radius, E is the electric field in which the charging occurs, and η is the viscosity of the gas or liquid. In air under standard conditions this expression is valid for radii down to about $0.5 \mu\text{m}$, below which the finite mean free path of air molecules and diffusional charging become important.³ For air, this expression becomes $8.8 \times 10^{-7} aE$, so that for $a = 1 \mu\text{m}$ and $E = 10^6 \text{ V/m}$ the mobility is $10^{-7} \text{ (m/sec)/(V/m)}$.</p>										
Ions in Gases										
<p>At atmospheric pressure, ions are typically generated by a corona discharge. Ions drawn from the discharge by an electric field are usually not distinguished. Reported ion mobilities distinguish among various gases, but do not specify the type of ion. Some published values, unless otherwise indicated for atmospheric pressure and 20°C, are:</p>										
Gas	Air (dry)	CCl_4	CO_2	H_2	H_2O (100°C)	H_2S	N_2	N_2 Very pure	O_2	SO_2
b_+ (units of $10^{-4} \text{ m}^2/\text{V sec}$)	1.36	0.30	0.84	5.9	1.1	0.62	1.27	1.28	1.31	0.41
b_- (units of $10^{-4} \text{ m}^2/\text{V sec}$)	2.1	0.31	0.98	8.15	0.95	0.56	1.84	145	1.8	0.41
<p>Low mobilities in impure gases are thought to result from formation of "clusters," while extremely high negative mobilities are attributed to an "ion" spending part of its time as a free electron.⁴</p>										
Ions in Highly Insulating Liquids										
<p>Approximate formulas relate mobility to the viscosity,</p> $b_+ \approx 1.5 \times 10^{-11}/\eta; \quad b_- \approx 3 \times 10^{-11}/\eta \tag{b}$ <p>Thus, for a liquid having the viscosity of water, $\eta \approx 10^{-3}$, mobilities are 1.5×10^{-8} and 3×10^{-8} respectively. For a careful evaluation with liquid and type of ion specified see Adamczewski.⁵</p>										
Ions in Water at 25°C Forming an Electrolyte at Infinite Dilution ⁶										
Ion	Na^+	K^+	H^+	Cl^-	I^-	OH^-	Ca^{2+}	SO_4^{2-}	NO_3^-	
b_{\pm} (units of $10^{-8} \text{ m}^2/\text{V sec}$)	5.20	7.62	36.3	7.90	7.96	20.5	6.16	8.27	7.40	

3. H. J. White, Industrial Electrostatic Precipitation, Addison-Wesley Publishing Company, Reading, Mass., 1963, p. 137.
4. Handbook of Physics, E. U. Condon and H. Odishaw, Eds., McGraw-Hill Book Company, New York, 1958, pp. 4-161.
5. I. Adamczewski, Ionization, Conductivity and Breakdown in Dielectric Liquids, Taylor & Francis, London, 1969, pp. 224-225.
6. Ref. 2, p. 395.

fields of the order of 10^4 V/m, the length scale must be shorter than $2.5 \mu\text{m}$ for this to be true. In relatively conducting materials, such as electrolytes, fields of interest might be no more than 1 V/m. But, motions of ions in insulating liquids and gases, with fields typically exceeding 10^4 V/m, are not influenced by diffusion except in accounting for certain processes in the immediate vicinity of boundaries.

5.3 Migration in Imposed Fields and Flows

In this section, the spatial scale of interest is such that the diffusion current can be considered negligible compared to the migration current. In addition, the medium is one in which generation and recombination of the charged species is negligible. Hence, the first and last two terms in Eq. 5.2.9 can be dropped. For carriers having a constant mobility, what remains on the right in Eq. 5.2.9 is proportional to the divergence of the electric field. By Gauss' law, this term is therefore proportional to the net space charge. If the density of carriers is small, Gauss' law, Eq. 5.2.4, requires that \vec{E} be solenoidal:

$$\nabla \cdot \vec{E} = 0 \quad (1)$$

and Eq. 5.2.9 therefore reduces to

$$\frac{\partial \rho_1}{\partial t} + (\vec{v} \pm b_1 \vec{E}) \cdot \nabla \rho_1 = 0 \quad (2)$$

In this "imposed field" approximation, the electric field is essentially determined by charges outside of the region of interest. Typically, these charges reside on boundaries and, in terms of the potential, \vec{E} is governed by Laplace's equation. Thus, as an example, if the potentials of all boundaries were constrained, \vec{E} would be determined by solving Laplace's equation subject to these boundary conditions, and that value of \vec{E} "imposed" in Eq. 2. For such a physical situation, each species migrates independently of the others, as is evident from the fact that the coupling between species afforded by Gauss' law is now absent.

The assumption that the electric field distribution is not appreciably affected by the migrating species says that the net charge density is small but not necessarily zero. In general there is an electrical force density acting throughout the moving medium. As in all of this chapter, it is assumed that the effect of this force density on the relative velocity distribution $v(r,t)$ is negligible. In this sense, the flow is also "imposed."

The imposed field and flow approximation gives the opportunity to study the effect of convection on the migration of charged particles. As can be seen from Table 5.2.1, ions moving in a field of 10^5 V/m through air have a migration velocity $b_1 \vec{E}$ on the order of 20 m/sec. Thus, an air velocity on this order could have a large influence on an ion trajectory. Macroscopic charged particles, such as dust in an electrostatic precipitator, typically have a considerably lesser mobility, and are therefore strongly influenced by modest motions of the gas. Although typical velocities of a liquid are likely to be less than for a gas, because of the relatively lower mobilities of ions and macroscopic particles in highly insulating liquids, the effects of convection can again be appreciable.

With the replacement of the velocity by the ion velocity $\vec{v} \pm b_1 \vec{E}$, Eq. 2 takes the form of a convective derivative. It states that the time rate of change of the species charge density as viewed by a charged particle of fixed identity is zero (see Sec. 2.4 for a discussion of the physical significance of the convective derivative):

$$\frac{d\rho_1}{dt} = 0 \quad (3)$$

on

$$\frac{d\vec{r}}{dt} = \vec{v} \pm b_1 \vec{E} \quad (4)$$

In what amounts to a rederivation of the convective derivative, consider the transition from Eq. 2 to the representation of Eqs. 3 and 4 in a somewhat more formal way. The three spatial coordinates and time constitute a four-dimensional space. Each set of coordinates (\vec{r}, t) in this space has an associated solution $\rho_1(\vec{r}, t)$. An incremental change in the coordinates therefore leads to a change in ρ_1 given by

$$d\rho_1 = dt \frac{\partial \rho_1}{\partial t} + dx \frac{\partial \rho_1}{\partial x} + dy \frac{\partial \rho_1}{\partial y} + dz \frac{\partial \rho_1}{\partial z} \quad (5)$$

As it stands, this expression is nothing more than a prescription for computing $d\rho_1$ for a given change

$(d\vec{r}, dt)$ in the coordinates of the (\vec{r}, t) space. But, can these incremental changes be specified so that Eq. 2 reduces to an ordinary differential equation? Division of Eq. 5 by dt and comparison to Eq. 2 shows that the desired specification is Eq. 4. Along a given characteristic line, represented by Eq. 4, Eq. 2 becomes Eq. 3. These lines have the physical significance of being the trajectories of the carriers.

If the evolution of the charge species is to be determined within a given volume V , then the charge density of each species must be specified where the associated characteristic line "enters" the volume of interest. The "direction" of a characteristic line is one of increasing time. Formally, with n taken as positive if directed outward from the volume of interest, the boundary condition is imposed on the i th species wherever

$$\vec{n} \cdot (\vec{v} \pm b_i \vec{E}) < 0 \quad (6)$$

Boundary conditions consistent with causality seem obvious in the transient case, but Eqs. 4 and 5 pertain also to steady flows in which rates of change with respect to time for an observer at a fixed location are zero.

Steady Migration with Convection: In the laboratory frame of reference, \vec{v}, \vec{E} and the boundary conditions represented by Eq. 6 are all invariant. Even so, the time rate of change for the particle, as expressed by Eq. 4, is finite. Explicit expressions for the particle trajectories can be found in a wide class of physically interesting situations, following the approach now illustrated.

Both \vec{v} and \vec{E} are solenoidal, and hence can be represented in terms of vector potentials. The discussion of Sec. 2.18 centers around four common configurations in which only a single component of these vector potentials is required to describe the vector functions. By way of illustration, the polar and axisymmetric spherical configurations are now considered, with the results applied to specific problems in the next two sections.

In polar coordinates, define vector potentials such that

$$\begin{bmatrix} \vec{E} \\ \vec{v} \end{bmatrix} = \begin{bmatrix} \hat{i}_r \frac{1}{r} \frac{\partial}{\partial \theta} - \hat{i}_\theta \frac{\partial}{\partial r} \end{bmatrix} \begin{bmatrix} A_E \\ A_V \end{bmatrix} \quad (7)$$

as suggested by Table 2.18,1. Similarly, in spherical coordinates

$$\begin{bmatrix} \vec{E} \\ \vec{v} \end{bmatrix} = \frac{1}{r \sin \theta} \begin{bmatrix} \hat{i}_r \frac{1}{r} \frac{\partial}{\partial \theta} - \hat{i}_\theta \frac{\partial}{\partial r} \end{bmatrix} \begin{bmatrix} \Lambda_E \\ \Lambda_V \end{bmatrix} \quad (8)$$

In terms of these functions, in the respective configurations, Eq. 4 becomes

Polar		Axisymmetric spherical	
$\frac{dr}{dt} = \frac{1}{r} \frac{\partial}{\partial \theta} (A_V \pm b_i A_E)$		$\frac{dr}{dt} = \frac{1}{r \sin \theta} \left[\frac{1}{r} \frac{\partial}{\partial \theta} \right] (\Lambda_V \pm b_i \Lambda_E)$	(9)

	$r \frac{d\theta}{dt} = - \frac{\partial}{\partial r} (A_V \pm b_i A_E)$		$r \frac{d\theta}{dt} = - \frac{1}{r \sin \theta} \frac{\partial}{\partial r} (\Lambda_V \pm b_i \Lambda_E)$	(10)
--	--	--	--	------

Remember that steady-state conditions prevail, so that the quantities on the right are independent of time. Time is therefore eliminated as a parameter by solving each of these expressions for dt and setting the respective equations equal to each other

$$\frac{\partial}{\partial r} (A_V \pm b_i A_E) dr + \frac{\partial}{\partial \theta} (A_V \pm b_i A_E) d\theta = 0 \quad \left| \quad \frac{\partial}{\partial r} (\Lambda_V \pm b_i \Lambda_E) dr + \frac{\partial}{\partial \theta} (\Lambda_V \pm b_i \Lambda_E) d\theta = 0 \quad (11)$$

Because there is no time dependence to the potential functions, these expressions constitute total derivatives, and can be just as well written as

$$d(A_V \pm b_i A_E) = 0 \quad \left| \quad d(\Lambda_V \pm b_i \Lambda_E) = 0 \quad (12)$$

The lines along which a species charge density is constant are implicitly given by

$$A_V \pm b_i A_E = \text{constant} \quad \left| \quad \Lambda_V \pm b_i \Lambda_E = \text{constant} \quad (13)$$

Quasistationary Migration with Convection: To integrate the particle equations of motion, and thus arrive at Eqs. 13, it is necessary to require that the particles be in essentially the same field and flow distribution throughout their motions through the volume of interest. In that sense, the motions are steady. But the particle transit times may be brief compared to a dynamical time of interest, perhaps that required for a surface upon which the particles impinge to charge, and hence change the electric field intensity. Thus, over a longer time scale, the flow and field distribution, hence the functions (A_E, A_V) and (λ_E, λ_V) , may be functions of time. This is often the situation during impact charging of macroscopic particles, discussed in Sec. 5.5.

For unipolar migration, the assumption that the electric field is solenoidal (that space charge has a negligible effect on the electric field distribution) is equivalent to the postulate of quasistationary migration (that the transit time for a particle through the volume of interest is short compared to the time required to charge a boundary). This point is best made in Sec. 5.6 after a quasistationary process is considered in Sec. 5.5.

5.4 Ion Drag Anemometer

The example of this section is intended to illustrate how charged particle trajectories can be computed using the approximations introduced in Sec. 5.3. A pair of electrodes is embedded in the wall bounding a fluid moving uniformly to the right, as shown in Fig. 5.4.1. A potential, V , applied to the right electrode gives an electric field intensity which terminates on the left electrode. In the neighborhood of the coordinate origin this field can be approximated as azimuthal. Thus, the imposed velocity and electric field intensity distributions are

$$\vec{v} = U[\sin \theta \vec{i}_r + \cos \theta \vec{i}_\theta] \quad (1)$$

$$\vec{E} = -\frac{V}{\pi r} \vec{i}_\theta \quad (2)$$

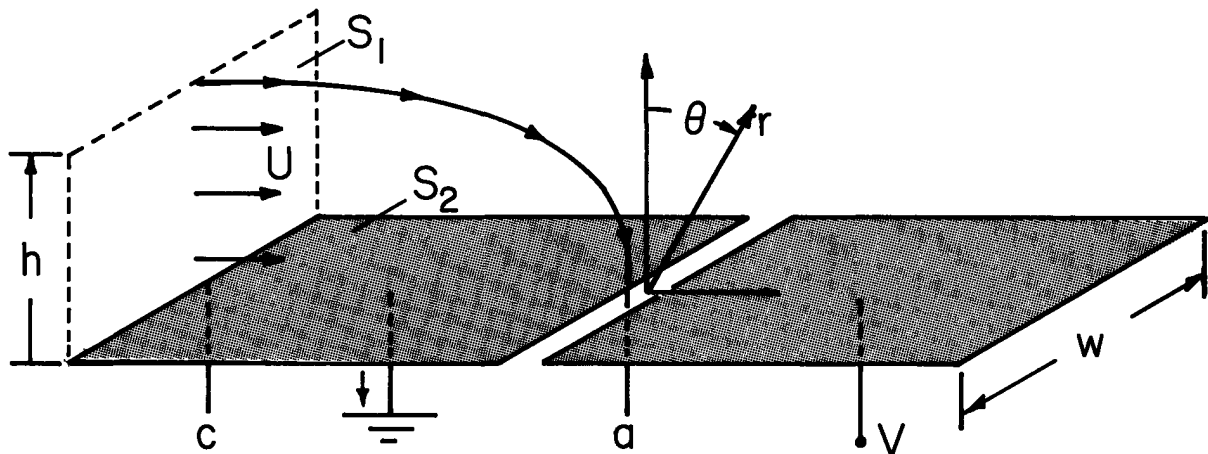


Fig. 5.4.1. Electrodes embedded in a smooth wall have the potential difference V . Ions enter from the left, entrained in the uniform velocity U . With a positive V , the left electrode intercepts some of the ions from the flow.

Fluid flow is represented as inviscid, and hence uniform right up to the electrode surfaces. Positive ions, present in the stream entering from the left, are sampled by the electrodes. The flux of ions to the left electrode caused by applying a positive voltage V to the right electrode is to be computed with a view toward obtaining the associated current i as a way of measuring the gas velocity.¹

It follows from Eqs. 5.3.3 that

$$A_E = \frac{V}{\pi} \ln \left(\frac{r}{a} \right) \quad (3)$$

$$A_V = -Ur \cos \theta \quad (4)$$

The characteristic lines, along which the charge density is constant, are given by Eq. 5.3.13, which in view of Eqs. 3 and 4 becomes

$$-Ur \cos \theta + \frac{bV}{\pi} \ln \left(\frac{r}{a} \right) = \text{constant} \quad (5)$$

1. K. J. Nygaard, "Anemometric Characteristics of a Wire-to-Plane Electrical Discharge," Rev. Sci. Instr. 36, 1771 (1965).

The constant is evaluated by fixing attention on the characteristic line entering at an altitude h over the left edge of the left electrode. Thus, at $r \sin \theta = -c$, $r \cos \theta = h$ and $r = \sqrt{h^2 + c^2}$. Then, Eq. 5 becomes

$$V \ln \left[\frac{\sqrt{h^2 + c^2}}{r} \right] = h - r \cos \theta \quad (6)$$

where normalization of (V, h, r) is introduced:

$$\underline{v} = \frac{bV}{\pi U c}, \quad \underline{h} = \frac{h}{c}, \quad \underline{r} = \frac{r}{c}$$

The quantity on the right is the distance downward (toward the electrode) measured from the initial altitude, \underline{h} , of a particle. Hence, the particle trajectories can be simply plotted by specifying the normalized voltage \underline{v} and \underline{h} for the trajectory of interest. With compass in hand, a graphical construction of a trajectory is obtained by picking a normalized radial coordinate \underline{r} , computing the left-hand side of Eq. 6, and finding the azimuthal angle θ at which the distance downward from the initial height \underline{h} , is as computed.

Typical plots are shown in Fig. 5.4.2. Concern is with positive ions only so that characteristic lines emanating from the wall to the right of the origin enter the volume of interest where there is no source of charge. Hence, the constant charge density to be associated with those lines is zero. On lines entering from the left, the charge density is a constant determined by conditions to the left.

The point $(r, \theta) = (0.5, 0)$ shown in Fig. 5.4.2 is one of zero force. Setting the r and θ components of $v + bE$ to zero shows that this critical point is at $\underline{r} = \underline{v}$ and $\theta = 0$. At this point, characteristic lines entering from the left split into those that remain in the stream and those that reach the plane $\theta = -\pi/2$.

The characteristic line passing through the critical point is found by evaluating Eq. 5 at $\underline{r} = \underline{v}, \theta = 0$:

$$-r \cos \theta + V \ln \left(r \frac{c}{a} \right) = -V + V \ln \left(V \frac{c}{a} \right) \quad (7)$$

The position $\underline{r} = \underline{r}^*$ on the surface $\theta = -\pi/2$ where this critical characteristic line impinges then follows by evaluating Eq. 7 with $\theta = -\pi/2$:

$$\underline{r}^* = \frac{V}{e} \quad (8)$$

Thus, the critical characteristic line impinges on the electrode if $\underline{r}^* > (a/c)$, i.e., if

$$\underline{v} > \left(\frac{a}{c} \right) e \quad (9)$$

For lesser values of \underline{v} , all of the electrode surface collects particles entering from the left, and the total current i is the integral of $-\rho b E_\theta$ over the entire electrode surface:

$$i = w \int_a^c \frac{\rho b V}{\pi} \frac{dr}{r} = (\rho U c w) \underline{v} \ln \left(\frac{c}{a} \right) \quad (10)$$

This dependence of i on V is presented graphically in Fig. 5.4.3, valid so long as $\underline{v} < \frac{a}{c} e$.

If V is increased beyond this value, only that portion of the electrode to the left of $\underline{r} = \underline{r}^*$ collects particles. The rest intercepts characteristic lines carrying no charge because they originate on the boundary $\theta = \pi/2$ to the right. Thus, the current is

$$i = w \int_{\underline{r}^*}^c \frac{\rho b V}{\pi} \frac{dr}{r} = \rho U c w \underline{v} (1 - \ln \underline{v}) \quad (11)$$

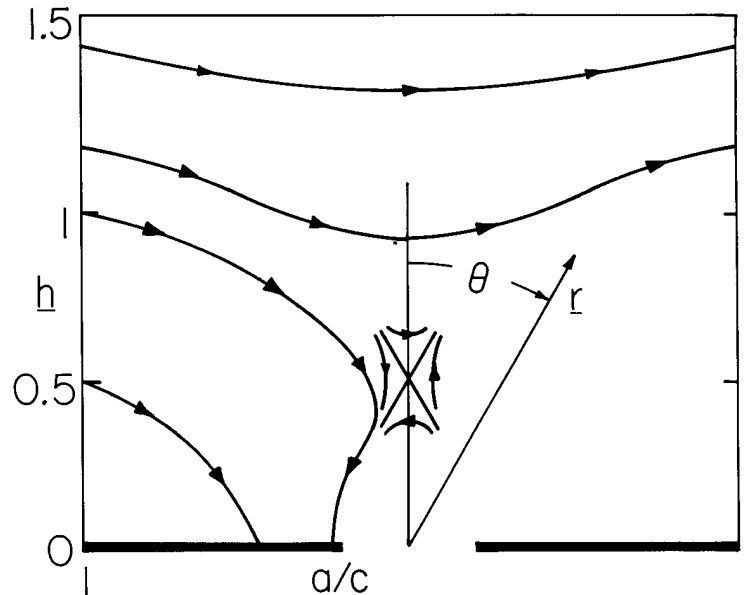


Fig. 5.4.2. Characteristic (force) lines for the physical configuration of Fig. 5.4.1. Vertical and horizontal distances have been normalized to c , with the left electrode then extending from $1 \rightarrow a/c$. In this sketch, $\underline{v} = 0.5$.

X

X
4/20/96

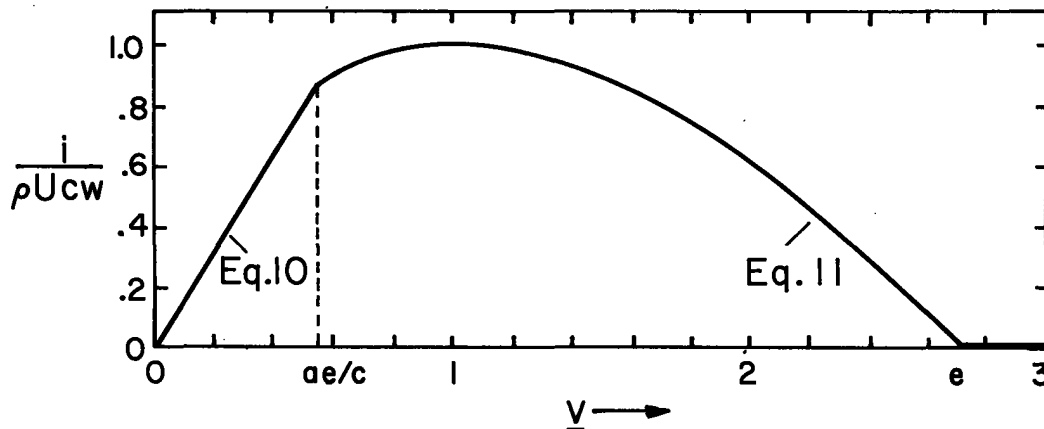


Fig. 5.4.3. Normalized current to electrode in Fig. 5.4.1 as function of normalized voltage $V = bV/\pi U c$.

With V beyond the value e , all of the characteristic lines reaching the electrode surface originate to the right where there is no source of particles. For voltages greater than this, the electric field diverts the particles completely before they can reach the electrode, and $i = 0$. The current dependence given by Eq. 11 is also summarized in Fig. 5.4.3.

It should be clear from the i - V characteristic summarized by Fig. 5.4.3 that there are many ways in which practical use could be made of the charged particle collection process. The peak current is a measure of U , while the voltage at which the curve peaks, or cuts off, gives a measure of either the velocity or the mobility.

5.5 Impact Charging of Macroscopic Particles: The Whipple and Chalmers Model

Electrostatic precipitators, used for the collection of particulate from gases in air-pollution control systems, make use of ion impact charging. A typical configuration is shown in Fig. 5.5.1. Dust laden gas enters the metallic tube from the bottom, and the object is to separate the dust from the gas before the latter leaves at the top. The high-voltage wire supported at the center of the tube sustains a corona discharge, a type of electrical breakdown that remains localized around the wire. Within this corona discharge, both positive and negative ions are created. Positive ions are drawn outside the immediate vicinity of the corona where they migrate along the lines of force toward the grounded coaxial electrode.

A particle of dust that interrupts the electric field also interrupts the ion migration. As a result the particle becomes charged.

Once charged, it too is subject to an electrical force and hence also tends to migrate to the cylindrical wall. The final stage of particle collection consists in rapping the electrode so that compacted dust falls from the walls into a hopper below.¹

Provided that the contribution of the migrating ions to the electric field in the immediate vicinity of the particle is negligible, the model developed in this section describes the charging process. As the particle acquires charge, its own contribution to the field is altered, so this example gives the opportunity to exemplify the quasistationary migration presaged in Sec. 5.3.

Typical electric fields in an electrostatic precipitator are 5×10^5 V/m. Thus, ions having a mobility of about 2×10^{-4} (m/sec)/(V/m) have velocities $bE \approx 100$ m/sec. Typical gas velocities are only 1-2 m/sec, so the effects of convection on the charging process are usually not significant.

But convection is an important factor in other situations to which the impact charging model pertains. It is well known that as drops of water fall through the atmosphere, they become charged because of interactions with ions. In a thunderstorm, a system of ions and drops can be subject to a significant electric field.

The particle shown in Fig. 5.5.2 is taken as spherical with an "imposed" electric field E that is locally uniform and if positive directed as shown. As envisioned by meteorologists, the particle is a

1. H. J. White, Industrial Electrostatic Precipitation, Addison-Wesley Publishing Company, Reading, Mass., 1963, pp. 33-48.

water drop falling through the atmosphere, so from the frame of reference of the particle, there is an ambient gas velocity U directed upward in the $-z$ direction. For the meteorologist the question is, given ions of a certain density carried by the combined field and flow, what is the charging law for the particle? How fast does it become charged and to what final value? Whipple and Chalmers² were interested in a quantitative model of Wilson's theory of thunderstorm electrification, which centered around how a particle could acquire charge while falling through essentially equal densities of positive and negative ions.²

In the following discussion, the particle being charged will be called the "drop," while the impacting particles will be termed ions. In fact, the "ions" might be fine macroscopic particulate being collected (scrubbed) by charged drops.³

At the outset, two useful parameters are identified. Regimes of charging are demarked by the critical charge

$$q_c \equiv 12\pi\epsilon_0 R^2 E \quad (1)$$

which can be positive or negative, depending on the sign of E . Rates of charging will be characterized by the currents

$$I_{\pm} = \pi R^2 b_{\pm} \rho_{\pm} E = q_c \frac{b_{\pm} \rho_{\pm}}{\epsilon_0 12} \quad (2)$$

which are also determined in sign by E . The magnitudes of the positive and negative ion charge densities are ρ_{\pm} respectively, uniformly distributed at "infinity," where the ions enter the volume neighboring the drops.

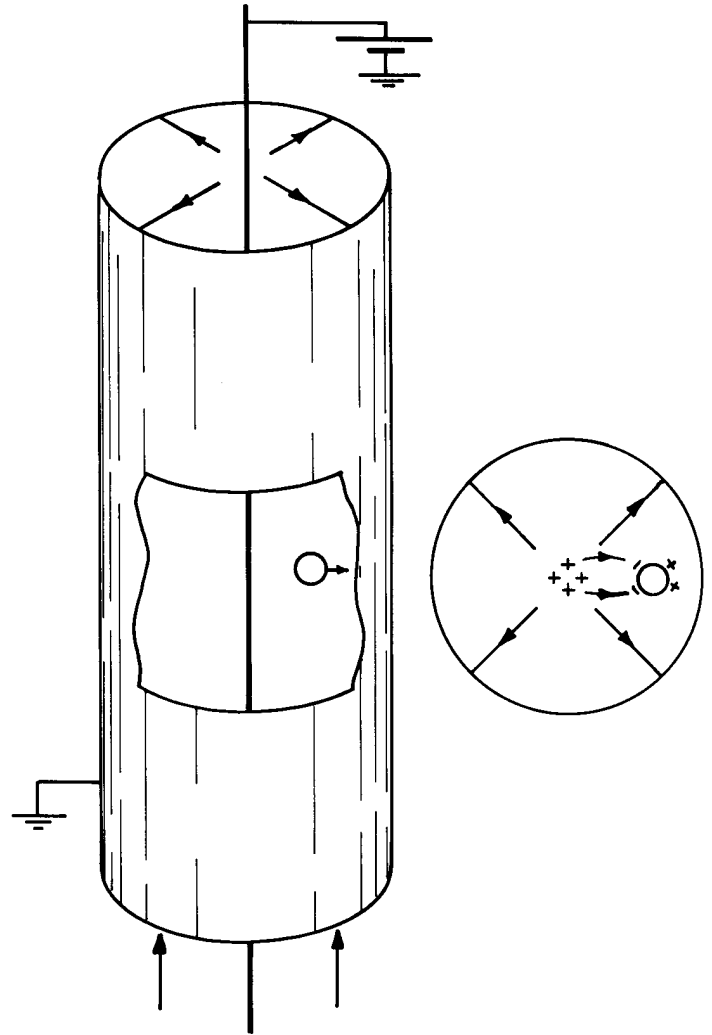
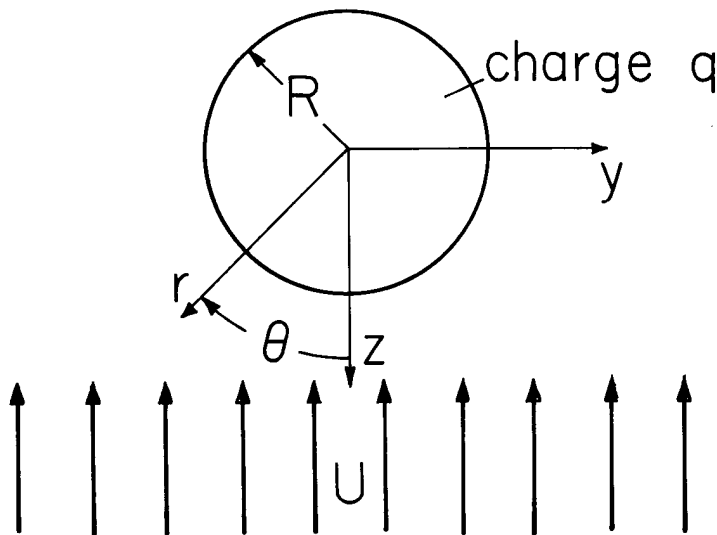
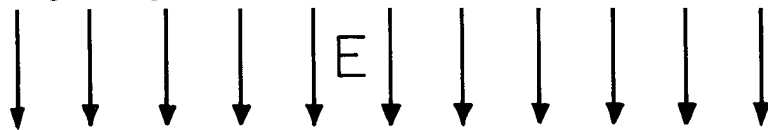


Fig. 5.5.1. Single-stage tube-type electrostatic precipitator.

Fig. 5.5.2.

Spherical conducting drop in imposed electric field E and relative flow U that are uniform at infinity. In general, the electric field intensity E can be either positive or negative with E and U positive if directed as shown.

2. F. J. W. Whipple and J. A. Chalmers, "On Wilson's Theory of the Collection of Charge by Falling Drops," *Quart. J. Roy. Meteorol. Soc.* 70, 103 (1944).
3. J. R. Melcher, K. S. Sachar and E. P. Warren, "Overview of Electrostatic Devices for Control of Submicrometer Particles," *Proc. IEEE* 65, 1659 (1977).

That the charging rate is to be calculated implies that the electric field and hence the ion motions are not in the steady state. However, as discussed in Sec. 5.3, it is assumed that ion transit times through several particle radii R are short compared to charging times of interest. Hence, at any instant the particle charge is taken as a known constant, which then makes a contribution to the instantaneous electric field intensity.

The particle is taken as perfectly conducting. The electric potential is therefore constant at $r = R$, becomes $-E_0 r \cos \theta$ far from the particle and is consistent with there being a net charge q on the particle. The appropriate combination of the potentials (satisfying Laplace's equation, as discussed in Sec. 2.16) $r \cos \theta$, $\cos \theta/r^2$ and $q/4\pi\epsilon_0 r$ therefore is the "imposed" field:

$$\vec{E} = -\nabla\phi = \left\{ E \left(\frac{2R^3}{3} + 1 \right) \cos \theta + \frac{q}{4\pi\epsilon_0 r^2} \right\} \vec{i}_r + \left\{ E \left(\frac{R^3}{3} - 1 \right) \sin \theta \right\} \vec{i}_\theta \quad (3)$$

It follows from this result and Eq. 5.3.8a that the "stream" function for the electric field intensity is

$$\Lambda_E = ER^2 \left[\frac{R}{r} + \frac{1}{2} \left(\frac{r}{R} \right)^2 \right] \sin^2 \theta - \frac{q \cos \theta}{4\pi\epsilon_0} \quad (4)$$

The velocity distribution in the neighborhood of the particle must have both tangential and normal components that vanish on the particle surface, and must approach the uniform flow at infinity. Written in terms of a stream function, in accordance with Eq. 5.3.8b, the velocity distribution automatically is solenoidal (the flow is incompressible). Conservation of momentum supplies the additional law to determine the velocity distribution, but there is no exact analytical solution valid for all velocities. As is shown in Sec. 7.20, if forces due to viscosity dominate those due to inertia, Stokes's flow around a sphere applies, and the associated stream function is (from Eqs. 7.20.13 and 7.20.17)

$$\Lambda_v = \frac{-UR^2}{2} \left[\left(\frac{r}{R} \right)^2 - \frac{3}{2} \left(\frac{r}{R} \right) + \frac{1}{2} \frac{R}{r} \right] \sin^2 \theta \quad (5)$$

The flow field found by using Eq. 5.3.8b is valid, provided the Reynolds number (Sec. 7.20) $R_v = \rho RU/\eta < 1$, where η is the fluid viscosity. A fifty micron radius water droplet in free fall through air has $R_v \approx 0.7$.

Given Eqs. 4 and 5, the characteristic lines are determined by substituting into Eq. 5.3.13b to obtain

$$\frac{1}{2} \frac{U}{b_{\pm} E} \left[\left(\frac{r}{R} \right)^2 + \frac{1}{2} \left(\frac{R}{r} \right) - \frac{3}{2} \left(\frac{r}{R} \right) \right] \sin^2 \theta \mp \left[\frac{R}{r} + \frac{1}{2} \left(\frac{r}{R} \right)^2 \right] \sin^2 \theta \pm \frac{3q}{q_c} \cos \theta = C \quad (6)$$

The upper and lower signs, respectively, refer to positive and negative migrating particles and C is a constant which identifies the particular characteristic line.

Just what constant charge density should be associated with each of these lines is determined by a single boundary condition imposed wherever the line "enters" the volume of interest.

In terms of parameters now introduced, the object is to obtain the net instantaneous electrical current to the particle, $i_{\pm}(q, E, U, \rho_{\pm})$. With the imposed field, velocity and charge densities held fixed, this expression then serves to evaluate the drop rate of charging

$$\frac{dq}{dt} = i_{\pm}(q) \quad (7)$$

Permutations and combinations of flow velocity, imposed field, instantaneous drop charge, and sign of the incident particles are large, so an orderly approach is required to sort out the possible collection regimes. These are conveniently pictured in the (q, bE) plane: for positive particles Fig. 5.5.3, for negative ones Fig. 5.5.4.

First, recognize the surfaces which satisfy the condition of Eq. 5.3.6, and hence at which boundary conditions on the charge density are imposed. For positive particles (upper sign) and $b_{+}E > U$ the distribution of particle densities for particles entering at $z \rightarrow -\infty$ is required. Otherwise, the charge density is imposed as $z \rightarrow +\infty$ because the positive particles enter from below. These conditions therefore respectively apply to the left and right of the line $b_{+}E = U$ in Fig. 5.5.3. Characteristic lines originating on the particle surface carry zero charge density. Also, at the particle surface the normal fluid velocity is zero; hence the characteristic lines degenerate to $\pm b_{\pm} \vec{E}$. This greatly simplifies the charging process, because the electric field intensity given by Eq. 3 can be used to decide whether or not a given point on the particle surface can accept charge. Evaluation shows that

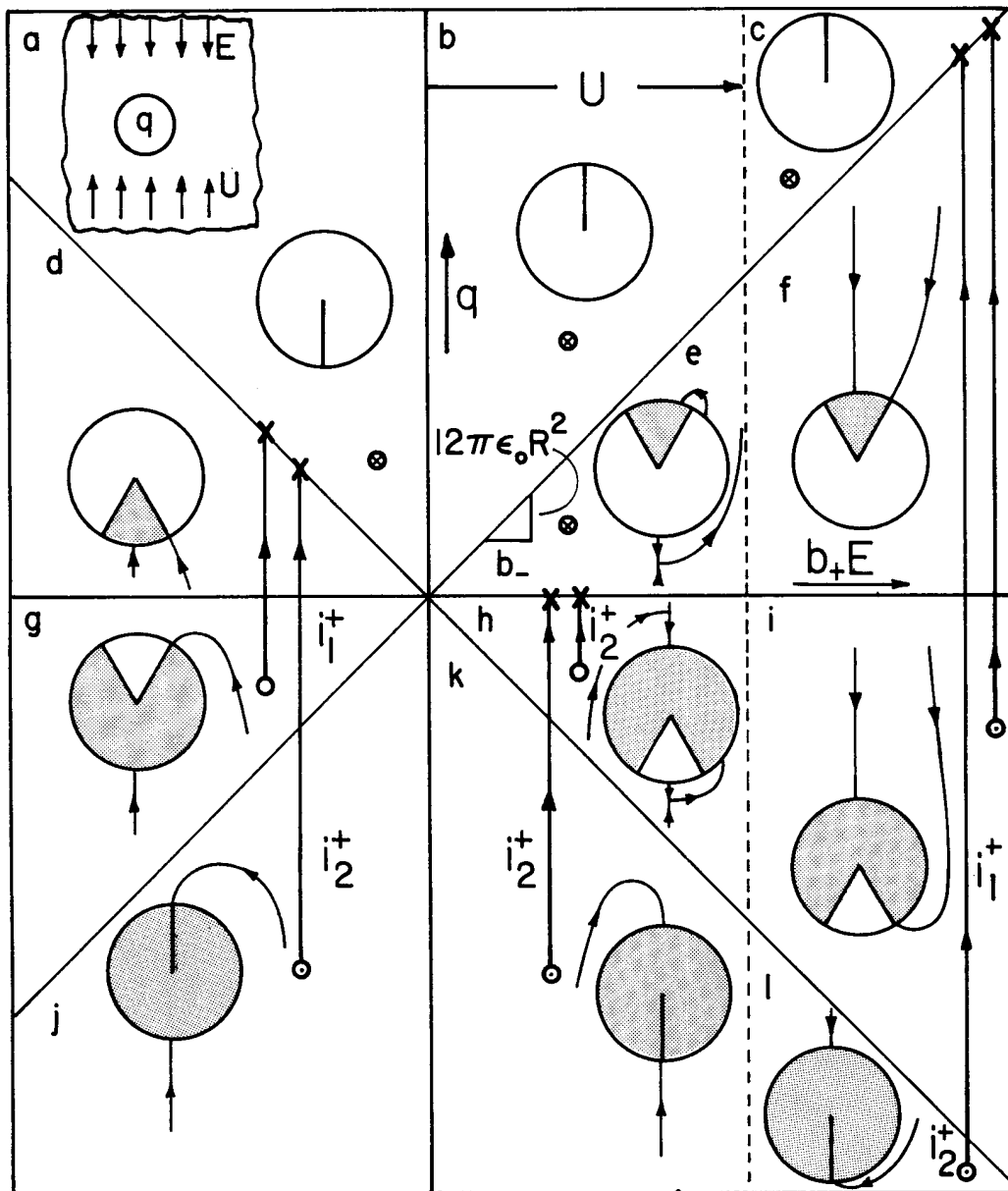


Fig. 5.5.3. Positive ion charging diagram. Charging regimes depicted in the plane of drop charge q and mobility-field product b_+E . With increasing fluid velocity, the vertical line of demarcation indicated by U moves to the right. Initial charges, indicated by \odot , follow the trajectories shown until they reach a final value given by \otimes . If there is no charging, the final and initial charges are identical, and indicated by \otimes . The inserted diagrams show the force lines $\vec{v} \pm b_{\pm} \vec{E}$.

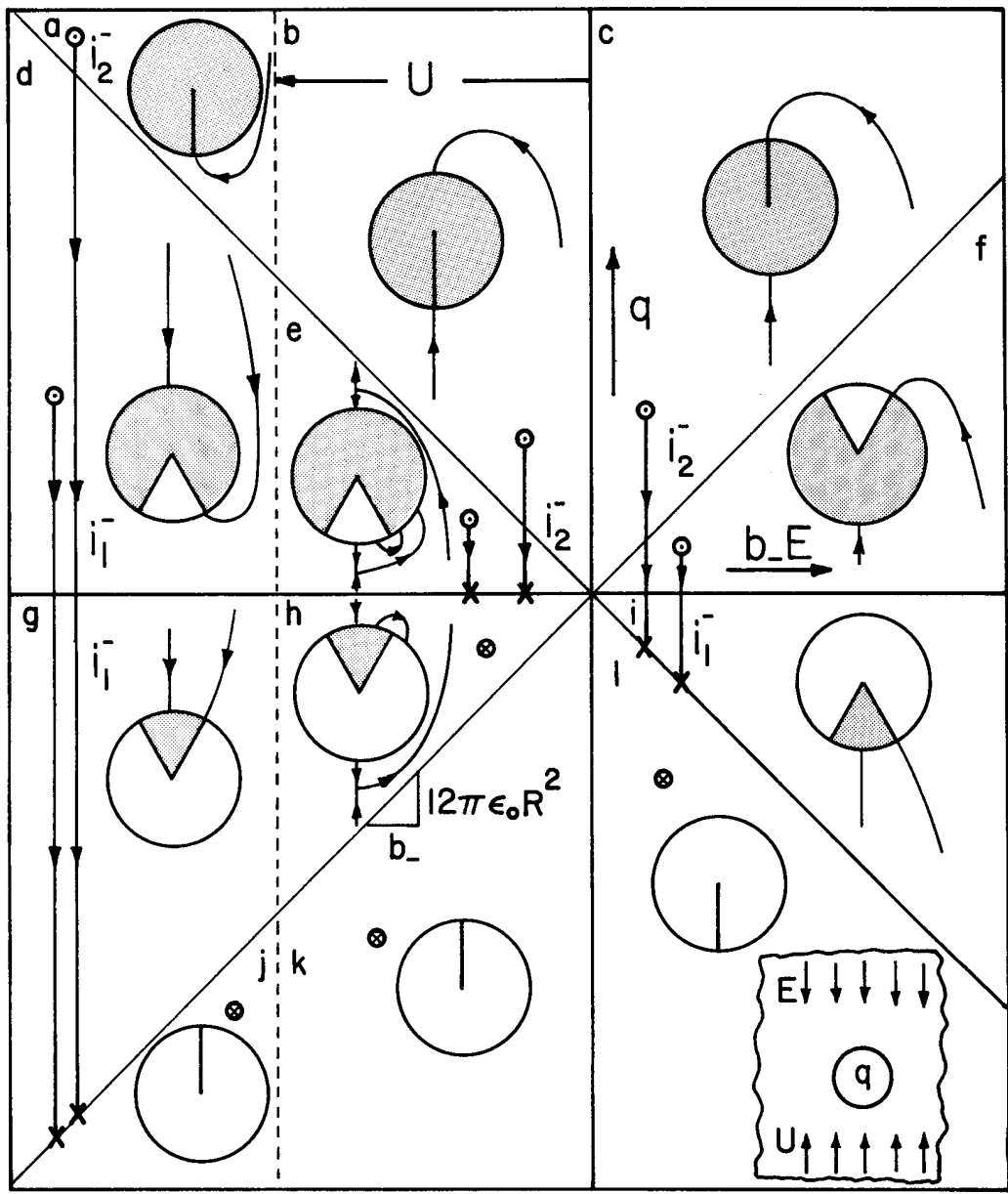


Fig. 5.5.4. Negative particle charging diagram. Conventions are as in Fig. 5.5.3. With increasing fluid velocity, the line of demarcation indicated by U moves to the left.

characteristic lines are directed into the particle surface wherever

$$\theta_c < \theta < \pi \quad \begin{cases} \text{positive ions, } E > 0 \\ \text{negative ions, } E < 0 \end{cases} \quad (8)$$

$$0 < \theta < \theta_c; \quad \begin{cases} \text{positive ions, } E < 0 \\ \text{negative ions, } E > 0 \end{cases} \quad (9)$$

where the critical angle, θ_c , demarking regions of inward and outward force lines, follows from the radial component of Eq. 3 evaluated at $r = R$:

$$\cos \theta_c = - \frac{q}{q_c} \quad (10)$$

A graphical representation of what has been determined is given by the direction of incident force lines on the particle surfaces sketched in Figs. 5.5.3 and 5.5.4. Where directed inward, these force lines indicate a possible electric current density. Whether or not the current is finite depends on whether the given characteristic line originates elsewhere on the drop boundary or at infinity.

In any case, if a characteristic line is directed outward, there is no charging current density to the particle, and so without further derivations, regimes (a), (b) and (c) for the positive particles (Fig. 5.5.3) and (j), (k) and (l) for the negative particles (Fig. 5.5.4) give no charging current. From Eq. 7, within these regimes the drop charge remains at its initial value.

Regimes (f) and (i) for Positive Ions; (d) and (g) for Negative Ions: To continue the characterization of each regime shown in Figs. 5.5.3 and 5.5.4, upper and lower signs respectively will be used to refer to the positive and negative ion cases.

The characteristic line terminating at the critical angle on the drop surface reaches the $z \rightarrow -\infty$ surface at the radius y^* shown in the respective regimes in the Fig. 5.5.3. Particles entering within that radius strike the surface of the drop within the range of angles wherein the drop can accept ions. Hence, to compute the instantaneous drop charging current, simply find this radius y^* and compute the total current passing within that radius at $z \rightarrow -\infty$. The particular line is defined by Eq. 6 evaluated at the critical angle, and on the particle surface: $\theta = \theta_c$, $r = R$. Thus, the constant is evaluated as

$$C = \mp \frac{3}{2} \left[1 + \left(\frac{q}{q_c} \right)^2 \right] \quad (11)$$

To find y^* , take the limit of Eq. 6 ($r \rightarrow \infty$, $y^* = (r \sin \theta)$ and $\cos \theta \rightarrow -1$) using the constant of Eq. 11 to determine that

$$(y^*)^2 \left(1 \mp \frac{U}{b_{\pm} E} \right) = 3R^2 \left[1 - \frac{q}{q_c} \right]^2 \quad (12)$$

The current passing through the surface with radius y^* is simply the product of the current density and the circumscribed area:

$$i_{\pm}^{\pm} = \pm n_{\pm} q_{\pm} (\pm b_{\pm} E - U) \pi (y^*)^2 \quad (13)$$

The combination of Eqs. 12 and 13 is

$$i_{\pm}^{\pm} = 3I_{\pm} \left(1 - \frac{q}{q_c} \right)^2 = \pm 3 |I_{\pm}| \left(1 \mp \frac{q}{q_c} \right)^2 \quad (14)$$

The second equality is written by recognizing the sign of E in the respective regimes.

In the positive ion regimes (f) and (i), the charging current is positive, tending to increase the drop charge until it reaches the limiting value $q = |q_c|$. Charging trajectories are shown in the figures, with i_1 the rate of charging, whether the initial drop charge is within the respective regimes or the charge passes from another regime into one of these regimes, and then passes on to its final value, $|q_c|$. For example, in the case of the positive ion charging, it will be shown that a drop charges at one rate in regime (l) and then, on reaching regime (i), assumes the charging rate given by Eq. 14, which it obeys until the charge reaches a final value on the boundary between regimes (f) and (c).

Also sketched in Figs. 5.5.3 and 5.5.4 are the characteristic lines, and the critical angles defining those portions of the drop over which conduction can occur. As a drop charges and then passes from regime (i) to (f), and finally to the boundary between regimes (f) and (c) in the positive particle case, the angle over which the drop can accept particles decreases from a maximum of 2π to π at $q = 0$, and finally to zero when $q = |q_c|$. It is the closing of this "window" through which charge can be accepted to the particle surface which limits the drop charge to the critical or "saturation" value q_c .

Regimes (d) and (g) for Positive Ions; (f) and (i) for Negative Ions: These regimes are analogous to the four just discussed except that the particles enter at $z \rightarrow \infty$, rather than at $z \rightarrow -\infty$. The derivation is therefore as just described except that the limiting form of Eq. 6 is taken as $\theta \rightarrow 0$, with C again given by Eq. 11 to obtain

$$(y^*)^2 \left(1 \mp \frac{U}{b_{\pm} E} \right) = 3R^2 \left(1 + \frac{q}{q_c} \right)^2 \quad (15)$$

Then, the particle currents can be evaluated as

$$i_1^+ = -3I_{\pm}(1 + \frac{q}{q_c})^2 = \pm 3|I_{\pm}|(1 \mp \frac{q}{|q_c|})^2 \quad (16)$$

As would be expected on physical grounds, the positive ion case gives charging currents and final drop charges in regimes (d) and (g) which are the same as those in (f) and (i).

Regimes (j) and (k) for Positive Ions; (b) and (c) for Negative Ions: For these regimes, the total surface of the drop can accept particles. The radius for the circular cross section of ions reaching the surface of the drop from $z \rightarrow \infty$ is determined by the line intersecting the drop surface at $\theta = \pi$. This line is defined by evaluating Eq. 6 at $r = R$, $\theta = \pi$ to obtain

$$C = \mp \frac{3q}{q_c} \quad (17)$$

Then, if the limit is taken $r \rightarrow \infty$, $\theta \rightarrow 0$ of Eq. 6, y^* is obtained and the current can be evaluated as

$$i_2^+ = \frac{\pm n_{\pm} q_{\pm} (\pm b_{\pm} E + U) \pi (y^*)^2}{|q_c|} = \frac{12|I_{\pm}|}{|q_c|} q \quad (18)$$

Note that in the positive ion regimes, q is negative, so the result indicates that the particle charges at this rate until it leaves the respective regimes when the charge $q = -|q_c|$.

Regime (l) for Positive Ions; (a) for Negative Ions: The situation here is similar to that for the previous cases, except that ions enter at $z \rightarrow -\infty$, so the appropriate constant for the critical characteristic lines given by Eq. 6 evaluated at $r = R$, $\theta = 0$, is the negative of Eq. 17. The limit of that equation given as $r \rightarrow \infty$, $\theta \rightarrow \pi$ gives y^* and evaluation of the current gives a value identical to that found with Eq. 18. In regime (l), for positive particles, where the initial charge is negative, the charging current is positive, and tends to reduce the magnitude of the drop charge until it enters regime (i), where its rate of charging shifts to i_1 and it continues to acquire positive charge until it reaches the final value $|q_c|$ indicated on the diagram.

Regime (e), Positive Ions; Regime (h), Negative Ions: In regimes (e) and (h) for either sign of particles, the window through which the drop can accept a particle flux is on the opposite side from the incident particles. Typical force lines are drawn in Fig. 5.5.5. Force lines terminating within the window through which the drop can accept ions originate on the particle; hence, there is no charging. In that case, the charge density on the characteristic line is zero, since the drop surface is incapable of providing particles.

To determine the particle charge that just prevents force lines originating at $z \rightarrow \infty$ from terminating on the particle surface, follow a line from the z axis where the drops enter at infinity back to the drop surface. That line has a constant determined by evaluating Eq. 6 with $\theta = 0$

$$C = \mp \frac{3q}{q_c} \quad (19)$$

Now, if Eq. 6 is evaluated using this constant, and $r = R$, an expression is found for the angular position at which that characteristic line meets the drop surface

$$\frac{3}{2} \sin \theta = \frac{3q}{q_c} (\cos \theta - 1) \quad (20)$$

Note that the quantity on the right is always negative if q/q_c is positive, as it is in regimes (e) for the positive particles and (h) for the negative. Thus, in regime (e) for the positive particles and (h) for the negative, the rate of charging vanishes and the drop remains at its initial charge.

Regime (h) for Positive Ions; (e) for Negative Ions: In these regimes, q/q_c is negative and Eq. 20 gives an angle at which the characteristic line along the z axis meets the drop surface. Typical force lines are shown in Fig. 5.5.6. To compute the rate of charging, the solution to this equation is

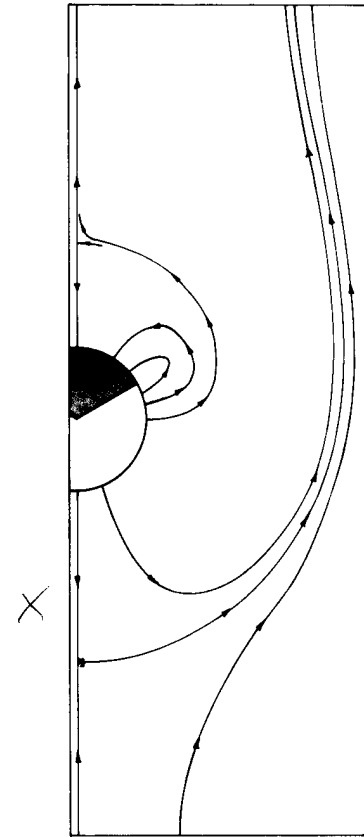


Fig. 5.5.5. Force lines in detail for regimes (e) for positive ions and (h) for negative ions. Here, all of the characteristic lines terminating on the particle also originate on the particle; hence, there is no charging. For the case shown, $U = \pm 2bE$, $q = \pm q_c/2$.

not required because a circular area of incidence for ions at $z \rightarrow \infty$ is then determined by the characteristic line reaching the drop at $\theta = \pi$. Actually, no new calculation is necessary because that radius is the same as that found for regime (k) for the positive ions and (b) for the negative. The charging current is i_2^\pm , as given by Eq. 18. Drops in these regimes discharge until they reach zero charge. Moreover, if the initial drop charges place the drop in regimes (k) for the positive ions or (b) for the negative ions, the rate of discharge follows the same law through regimes (h) for the positive ions and (e) for the negative until the drop reaches zero charge.

As a matter of interest, in regimes (e) and (h) for both positive and negative ions a doughnut-shaped island of closed force lines is attached to the critical line if $0.5 < |bE|/U < 1$. An illustration is Fig. 5.5.7.

Positive and Negative Particles Simultaneously: If both positive and negative particles are present simultaneously, the drop charging is characterized by simply superimposing the results summarized with Figs. 5.5.3 and 5.5.4. (The independence of species migration is discussed in Sec. 5.3.) The diagrams are superimposed with their origins (marked 0) coincident. A given point in either plane then specifies the drop charge and associated field experienced by both families of charges. This justifies superimposing the respective currents at the given point to find the total charging current:

$$\frac{dq}{dt} = i_+(q) + i_-(q) \quad (21)$$

Here, i_+ is i_1^+ , i_2^+ or 0, in accordance with the charging regime and similarly, i_- is the appropriate current due to negative ions.

Drop Charging Transient: The quasistationary charging process is illustrated specifically by considering the fate of a drop starting out in regime (l) of Fig. 5.5.3, in a field $b_+E > U$ and with a charge $q < -|q_c|$. Then, Eq. 7 with i_2^+ given by Eq. 18, becomes

$$\int_{q_0}^q \frac{dq}{q} = - \int_0^t \frac{12|I_+|}{|q_c|} dt = - \int_0^t \frac{\rho_+ b_+}{\epsilon_0} dt \quad (22)$$

where q_0 is the drop charge when $t = 0$. Thus, so long as the charge remains in regime (l), the charging transient is

$$q = q_0 e^{-t/\tau} \quad ; \quad \tau \equiv \epsilon_0 / \rho_+ b_+ \quad (23)$$

When the drop has been discharged to $q = -|q_c|$, the rate of discharge switches to i_1^+ , given by Eq. 16. Thus, the charging equation is

$$\int_{-q_c}^q \frac{dq}{(1 + \frac{q}{|q_c|})^2} = +3|I_+| \int_0^{t'} dt' \quad (24)$$

where t' is the time measured relative to when the drop switches into regime (i). Integration gives a charging transient

$$q = |q_c| \left(\frac{t'/4\tau - \frac{1}{2}}{t'/4\tau + \frac{1}{2}} \right) \quad (25)$$

which completes the discharging of the drop and goes on in regime (f) to charge the drop positively until it approaches the saturation charge q_0 .

Note that although the detailed temporal dependence of Eqs. 23 and 25 is quite different, the same charge relaxation time $\epsilon_0 / \rho_+ b_+$ characterizes the charging dynamics. It is this time that must be long compared to the particle transient time to justify the quasistationary model. The same time constant has a second complementary significance, brought out in the next section. There, it is possible to appreciate the relation of space-charge effects to the quasistationary model used in this section.

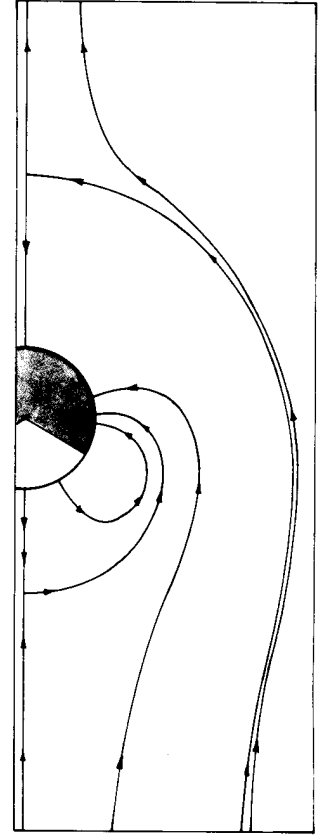


Fig. 5.5.6. Regimes (h) for positive ions and (e) for negative ions. Some of the characteristic lines extend to where the charge enters. $U = +2b_+E$, $q = +q_c/2$.

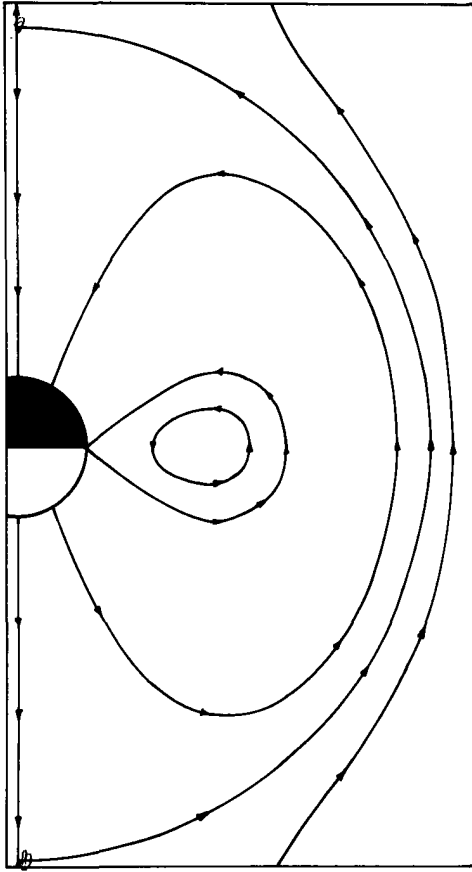


Fig. 5.5.7

In regimes (e) and (h) with $0.5 < |bE|/|U|$, a "doughnut" of closed force lines is attached to critical line around drop. Positive particles are illustrated with $q = 0$ and $b_+E/U = 0.75$.

5.6 Unipolar Space Charge Dynamics: Self-Precipitation

Complementary assumptions in Secs. 5.3 - 5.5 are that the effect of the electric field on the flow can be ignored, and that the volume space charge density makes a negligible contribution to the imposed field. Although often good approximations in predicting the trajectories of dilute ions and charged macroscopic particles in moving gases and liquids, these are usually not good assumptions if there is to be an appreciable coupling between the electric field and the neutral fluid through which the charged particles migrate.

What are the effects of "self-fields" (space-charge contributions) left out in the imposed field approximation used in Secs 5.3 - 5.5? In this and the next section, this question is addressed while again considering a single species of either positively or negatively charged particles.

The pertinent laws are Eqs. 5.2.9 - 5.2.11 without source or recombination contributions ($G=R=0$) and with lengths of interest large enough to justify ignoring diffusion. In writing Eq. 5.2.9, the creation of a field divergence by the space charge is recognized by substituting on the right with Gauss' law, Eq. 5.2.10:

$$\frac{\partial \rho_{\pm}}{\partial t} + (\vec{v}_{\pm} + b_{\pm} \vec{E}) \cdot \nabla \rho_{\pm} = - \frac{\rho_{\pm}^2 b_{\pm}}{\epsilon} \quad (1)$$

This expression is converted to one describing how the charge density changes with time for an observer moving along a characteristic (or force) line by following the procedure developed in Sec. 5.3.2. Instead of Eq. 5.3.3, Eq. 1 becomes

$$\frac{d\rho_{\pm}}{dt} = - \frac{\rho_{\pm}^2 b_{\pm}}{\epsilon} \quad (2)$$

along the characteristic lines

$$\frac{d\vec{r}}{dt} = \vec{v}_{\pm} + b_{\pm} \vec{E} \quad (3)$$

Although the velocity \vec{v} is still considered to be imposed, \vec{E} in Eq. 3 has contributions from not only charges on the boundaries, but from those within the volume of interest as well. So it is that the time dependence of the charge density can be determined from an integration of Eq. 2. For a characteristic line originating when $t = 0$ where $\rho_{\pm} = \rho_0$

$$\int_{\rho_0}^{\rho_{\pm}} \frac{d\rho_{\pm}}{\rho_{\pm}^2} = -\frac{b_{\pm}}{\epsilon} \int_0^t dt \quad (4)$$

Thus,

$$\frac{\rho_{\pm}}{\rho_0} = \frac{1}{1 + t/\tau_e}; \quad \tau_e = \frac{\epsilon}{\rho_0 b_{\pm}} \quad (5)$$

This result is both remarkably general and somewhat deceiving. Without apparent regard for the particulars of a physical situation, for the boundary conditions and hence for any imposed component of the field and for the locations of charges that image those evolving in the volume, the decay law of Eq. 5 is deduced. But, the law applies for an observer measuring time as he follows a given particle along a characteristic line, defined by Eq. 3, originating when $t = 0$ where $\rho_{\pm} = \rho_0$. At each step in the evolution, all of the charge (in the volume and on the boundaries) instantaneously contributes to \vec{E} . This contribution is embodied in Gauss' law. The characteristic viewpoint is now used to make some general deductions, and then by way of illustration, to make specific predictions.

General Properties: Suppose that when $t = 0$ the charged particles are uniformly distributed over some confined region V within the total volume, as suggested by Fig. 5.6.1. When $t = 0$, the volume of interest consists of regions either occupied by no charge density or by the uniform density ρ_u . At a later time, the cloud of charged particles has changed its shape and general location. Particles initially at the locations A , B and C are respectively found at A' , B' and C' . At a point like A' , with a characteristic line originating within the initial cloud of particles, the charge density is given by Eq. 5 as

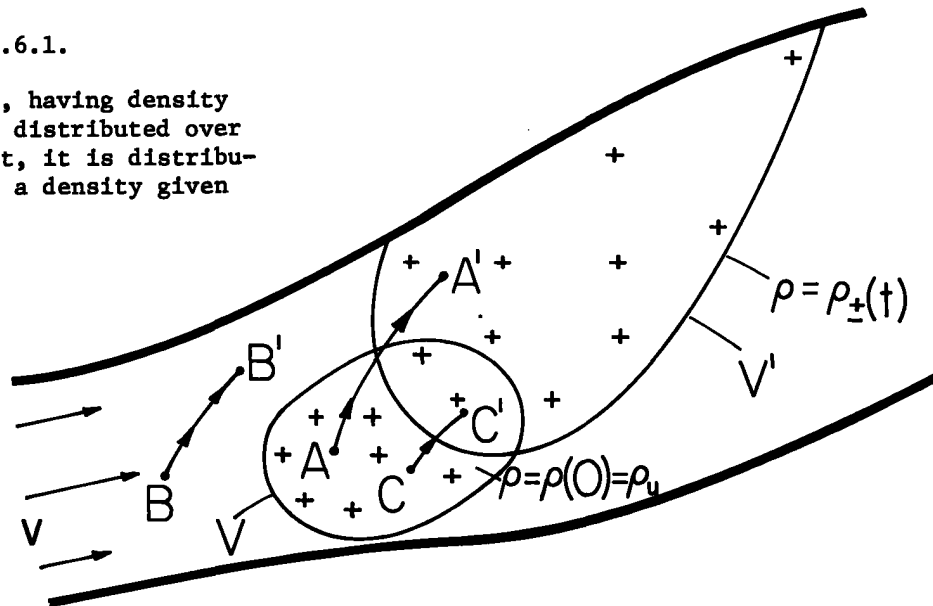
$$\rho_{\pm} = \frac{\rho_u}{1 + t/\tau_e}; \quad \tau_e \equiv \frac{\epsilon}{\rho_u b_{\pm}} \quad (6)$$

Note that τ_e is itself dependent on the initial charge density.

Now, consider the time dependence of ρ_{\pm} at a fixed location A' . So long as A' is within the region occupied by the charge cloud, this time dependence is also given by Eq. 6. At each instant, the point in question can be traced backward in time to a location in the cloud when $t = 0$ where the charge density is the same number, ρ_u . As time progresses, different locations originate the characteristic A' , but because ρ_u is the same throughout the initial cloud, each of these has the same charge density ρ_u or no charge density at all. That is, at a position like B' , the characteristic originates on no charge density, and there is no charge density at the instant in question.

Fig. 5.6.1.

When $t=0$, charge, having density ρ_u , is uniformly distributed over V . By the time t , it is distributed over V' with a density given by Eq. 6.



So it is that the charge transient at any fixed location consists of either a charge density decaying according to Eq. 6 or no charge density at all. Generally, at a position like A', the charge density is zero until the "front" arrives. Then, the position A' is enveloped by the particle cloud which is expanding under its self-field so that the density decays in accordance with Eq. 6. At a position like C', there is no delay in the arrival of this front so that the decay is given by Eq. 6 from time $t = 0$. But, the time may come when the cloud passes beyond the point in question and the decay in charge density is then abruptly terminated by the density going to zero. When the front arrives and when the cloud has passed by is a matter that must be resolved by integrating to find the characteristic lines.

The tendency of the cloud to expand or self-precipitate, as the cloud as a whole is carried by the deforming medium and the total field, is described by a decay that is relatively slow. Figure 5.6.2 emphasizes this point by comparing Eq. 7 to an exponential decay.

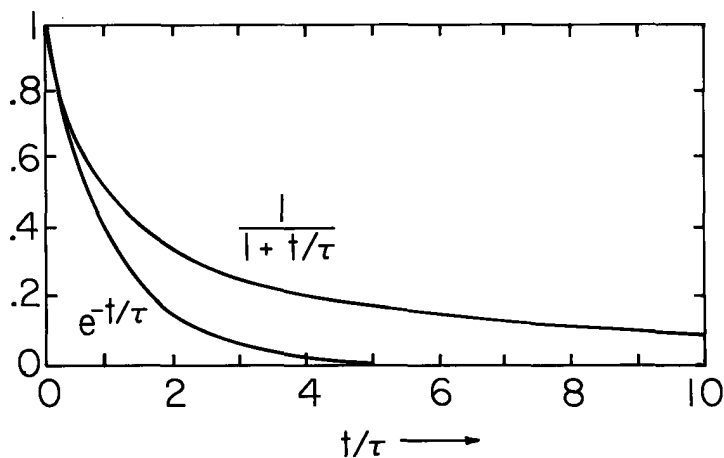


Fig. 5.6.2. Comparison of self-precipitation transient to exponential decay.

The rate of decay along a characteristic line represented by τ_e is the same as the charging time constant for the "drop" in Sec. 5.5. An important observation can now be made relevant to taking into account space-charge effects on the collection of charged particles by isolated drops. If space-charge effects are really important, then processes of interest must occur on the time scale of τ_e . This implies that the drop described in Sec. 5.5 must change its charge in a time on this same scale. But, the drop charge contributes to the electric field, and in the analysis of Sec. 5.5 the electric field is assumed to be constant during the time that a particle migrates several drop radii. Thus it is apparent that if space-charge contributions to the field are to be taken into account, the quasi-steady approximation is not valid.

A Space-Charge Transient: As a simple illustration of the fate of a cloud of charged particles that is initially of uniform charge density, consider the radially symmetric configuration of Fig. 5.6.3. When $t=0$, the particles occupy the annular region $R_1 < r < R_0$. Image charges are presumed sufficiently remote that the field can be regarded as radially symmetric. There is a source of fluid inside the region $r < R_1$ giving rise to a volume rate of flow Φ_v (m^3/sec). Because the flow is incompressible, the resulting velocity distribution is determined by the requirement that the material flux at any radius r be the same: $4\pi r^2 v_r = \Phi_v$. The characteristic lines are then found from the one nontrivial component of Eq. 3:

$$\frac{dr}{dt} = \frac{\Phi_v}{4\pi r^2} \pm b \pm E_r \quad (7)$$

Because the initial charge distribution is uniform, any region within the cloud is known to have a density that decays according to Eq. 6. In this simple example it is easy to find the position of the outward propagating front, and hence locate the region where this decay applies. By the integral form of Gauss' law, Eq. 2.7.1a, the electric field at r , the leading edge of the cloud, is

$$E_r = \pm \frac{1}{3} \frac{(R_0^3 - R_1^3) \rho_u}{\epsilon_0 r^2} \quad (8)$$

Substitution of this expression into Eq. 7 and integration gives

$$\frac{r}{R_0} = \left\{ 1 + \left[\frac{3\Phi_v \tau_e}{4\pi R_0^3} + 1 - \left(\frac{R_1}{R_0} \right)^3 \right] \frac{t}{\tau_e} \right\}^{1/3} \quad (9)$$

Similar arguments apply to the trailing edge, where $E_r = 0$ and hence

$$\frac{r}{R_0} = \left[\left(\frac{R_1}{R_0} \right)^3 + \left(\frac{3\Phi_v \tau_e}{4\pi R_0^3} \right) \frac{t}{\tau_e} \right]^{1/3} \quad (10)$$

These last two expressions define the region occupied by the charged particles. During the time that

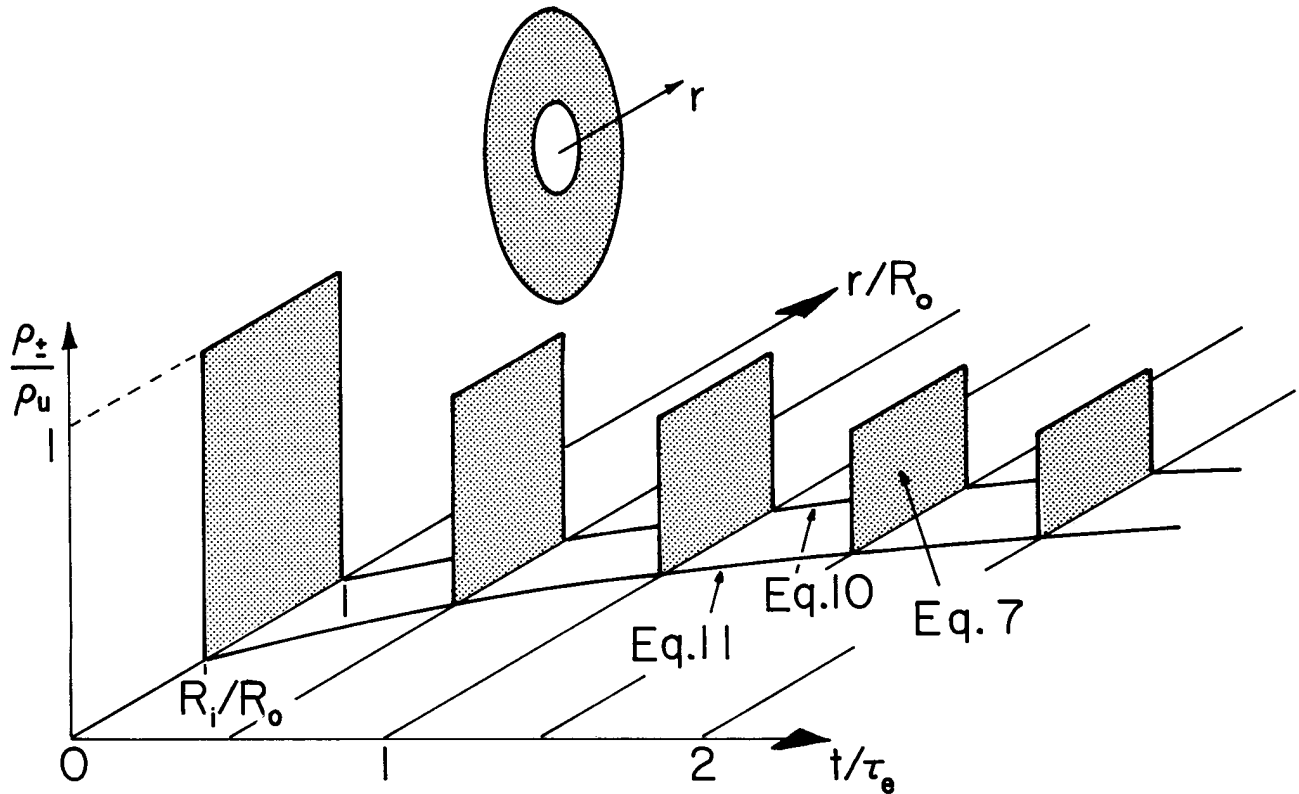


Fig. 5.6.3. When $t = 0$, a uniform density ρ_u of charged particles fills the spherical shell $R_1 < r < R_0$. A source of gas at the origin imparts a radial velocity. For this plot, $R_0/R_1 = 0.5$, $3\Phi_v\tau_e/4\pi R_0^3 = 1$. Remember that the charge is self-precipitating in three dimensions. At any time, the product of the charge density and the volume of the region filled by the charge is constant.

the particles surround a given fixed radial location, the temporal decay at that radius is given by Eq. 6. The evolution of the cloud is illustrated in Fig. 5.6.3. Fig,

Steady-State Space-Charge Precipitator: What from the laboratory frame of reference appears to be steady or stationary phenomenon is from the particle frame of reference still a transient. The characteristic time is typically a transport time ℓ/U , and the ratio

$$R_e = \frac{\tau_e}{\ell/U} = \frac{U\epsilon_0}{\lambda\rho_0 b_{\pm}} \quad (11)$$

represents the degree to which convection competes with self-field migration in determining the distribution of the charged particles. R_e is defined as the electric Reynolds number.

As a specific illustration, consider the circular cylindrical duct shown in Fig. 5.6.4. Gas enters at the left with a uniform velocity profile carrying a uniform distribution of charged particles. The channel wall is at zero potential, and hence only the self-fields contribute to the migration. With the assumption that variations in the z direction of the particle density occur relatively slowly goes the quasi-one-dimensional model of an electric field that is dominantly in the radial direction. Hence, the characteristic lines are determined from Eq. 3 approximated as

$$\frac{d\vec{r}}{dt} = U\vec{i}_z \pm b_{\pm} E_r(r)\vec{i}_r \quad (12)$$

The z component of this expression can be integrated to describe the characteristic line associated with the solution given by Eq. 6, i.e., for the particles entering at $z = 0$, where $\rho_+ = \rho_0 = \rho_u$ when $t = 0$:

$$z = Ut \quad (13)$$

Hence, the distribution of charge density with z is obtained directly by substituting Eq. 13 into Eq. 6.

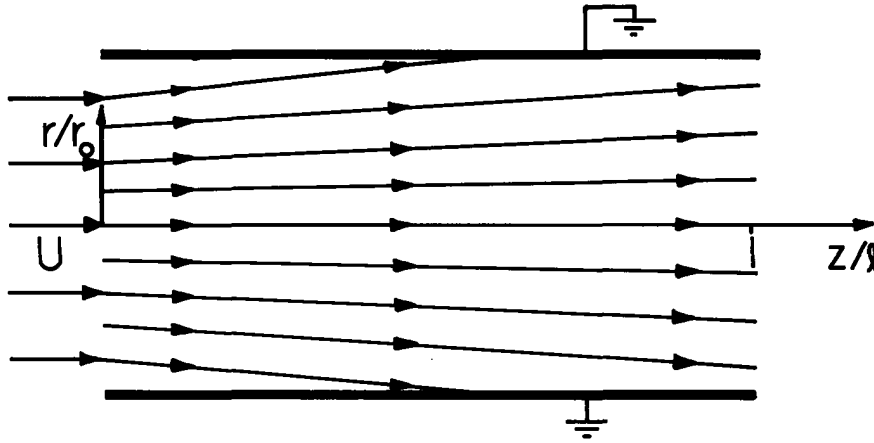


Fig. 5.6.4

Space-charge precipitator having circular cylindrical cross section and $Re = 1$ showing characteristic lines.

$$\rho_{\pm} = \frac{\rho_u}{1 + \frac{z}{l} \left(\frac{l}{U\tau_e} \right)} \quad (14)$$

The fact that the axial component of \vec{E} is neglected has made it possible to find the spatial distribution of ρ_{\pm} without solving the self-consistent characteristic equations.

A length l of the channel might be used as a precipitator, for the removal of pollutant particles which are charged upstream. The cleaning efficiency of such a device follows from Eq. 14 integrated over the channel cross section A at $z = l$ and $z = 0$,

$$\eta \equiv \frac{\int_A \rho_u da - \int_A \rho_{\pm}(l) da}{\int_A \rho_u da} = \frac{R_e^{-1}}{1 + R_e^{-1}} \quad (15)$$

and is determined by the ratio of transport time to τ_e . The dependence of η on R_e^{-1} is shown in Fig. 5.6.5. The relatively poor efficiency even with a residence time several times τ_e has its origins in the relatively slow decay depicted by Fig. 5.6.2.

The trajectories of the particles are determined from both the radial and axial components of Eq. 12. Gauss' law relates the charge density at a given cross section along the z axis to E_r :

$$\frac{1}{r} \frac{\partial}{\partial r} (rE_r) = \pm \frac{\rho_{\pm}}{\epsilon_0} \quad (16)$$

This expression can be integrated in the radial direction to give

$$E_r = \pm \frac{1}{r} \int_0^r \frac{r}{\epsilon_0} \frac{\rho_u dr}{\left(1 + \frac{z}{l} R_e^{-1}\right)} = \pm \frac{1}{2} \frac{r}{\epsilon_0} \frac{\rho_u}{\left(1 + \frac{z}{l} R_e^{-1}\right)} \quad (17)$$

Thus, the radial component of Eq. 12 becomes

$$\frac{dr}{dt} = \frac{1}{2} b_{\pm} \frac{r}{\epsilon_0} \frac{\rho_u}{1 + \frac{z}{l} R_e^{-1}} \quad (18)$$

But, in view of the axial component of this same equation,

$$\frac{dr}{dt} = \frac{dr}{dz} \frac{dz}{dt} = U \frac{dr}{dz} \quad (19)$$

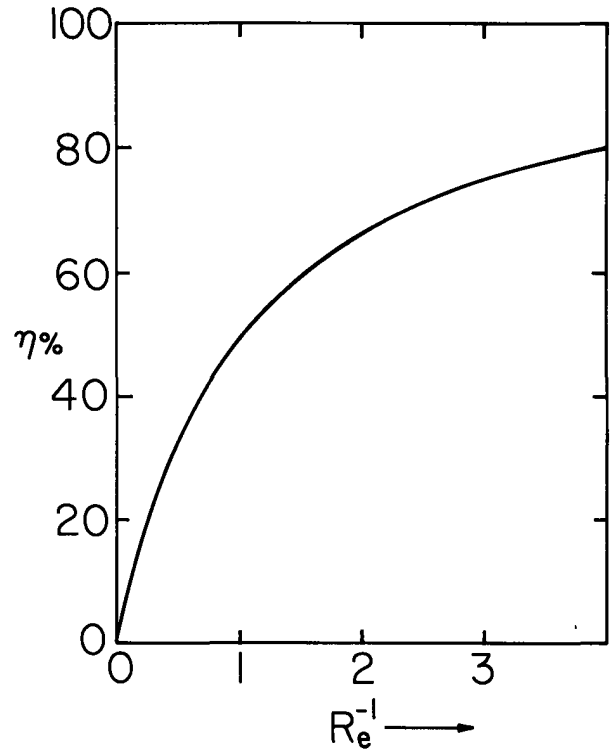


Fig. 5.6.5. Efficiency of space-charge precipitator as function of reciprocal electric Reynolds number, the ratio of residence time to τ_e .

Thus, the time is eliminated as a parameter to obtain an equation for the characteristic line in the (r,z) plane. Integration of Eqs. 18 and 19 gives

$$\frac{r}{r_0} = \sqrt{1 + \frac{z}{\ell} R_e^{-1}} \quad (20)$$

Which trajectory is considered is determined by r_0 , the radial position at which a particle enters where $z = 0$. A sketch of the characteristic lines is included with Fig. 5.6.4.

5.7 Collinear Unipolar Conduction and Convection: Steady D-C Interactions

The electrohydrodynamic coupling undertaken in this section illustrates the electromechanical energy conversion processes that can take place if the space charge density is large enough to provide a significant contribution to the electric field. In the configuration shown in Fig. 5.7.1, a pair of electrically conducting grids at $z = 0$ and $z = \ell$ provide electrical "terminals" through which the fluid can pass and by which entrained charge particles are either injected or collected. The grids have the potential difference v . Charged particles are injected with zero potential at $z = 0$ and collected at potential v on the grid at $z = \ell$. Hence, with a load attached to the terminals, the charge carried by the fluid results in a current through the load, so that the configuration converts mechanical energy to electrical form. In this case, the fluid plays the role of the belt in a Van de Graaff generator. In fact, as for the Van de Graaff machine described in Sec. 4.14, it will be seen that generator, pump (motor) and brake operation are all possible.

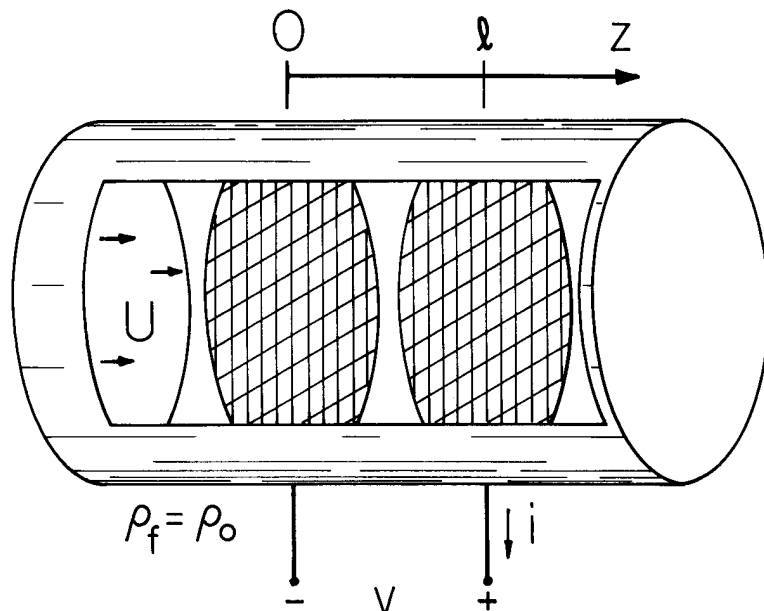


Fig. 5.7.1
One-dimensional unipolar
d-c pump, generator or
brake.

There is an important difference between the collinear configuration considered here and the Van de Graaff machine. In the latter, the generated field is orthogonal to the field associated with the charge carried by the belt. Here, transverse dimensions are very large and the charge entrained in the fluid produces a field that is collinear with the "generated" or "imposed" field associated with charges on the grids. Thus, $\vec{E} = i_z E(z)$. As a result, the electromechanical energy conversion is through normal stresses, rather than shear stresses. The volume between the grids can be identified with the volume shown in the abstract by Fig. 4.15.1, or specifically by Fig. 5.7.2.

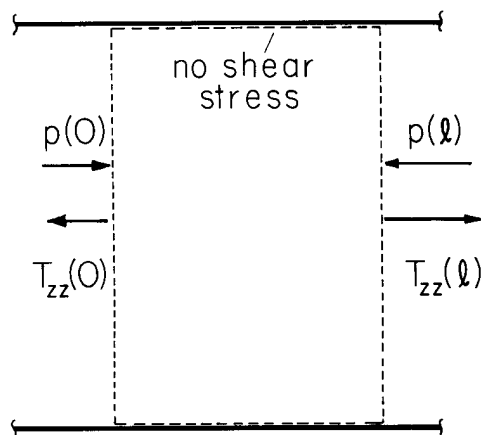


Fig. 5.7.2

The fluid volume between the grids is subject to the mechanical normal stresses (pressure) p defined as positive if acting inward.

Interest is confined to steady-state conditions, so conservation of charge, represented by Eq. 5.2.2 with $G-R = 0$ and $(\partial\rho/\partial t) = 0$, requires that the current density be solenoidal. The fluid is incompressible, so that \vec{v} is also solenoidal. It follows from the one-dimensional model that the fluid velocity $\vec{v} = U\hat{i}_z$ and the current density $\vec{J} = \hat{i}_z J$, where U and J are independent of z :

$$J = \frac{i}{A} = \rho(bE + U) \quad (1)$$

The scale of interest is presumed large enough that effects of diffusion are negligible.

In addition to Eq. 1, Gauss' law relates ρ to $\vec{E} = \hat{i}_z E(z)$. Elimination of E between these equations gives

$$\rho^{-1} d\rho^{-1} = \frac{b}{\epsilon J} dz \quad (2)$$

If the charge is injected with density $\rho(0) = \rho_0$, Eq. 2 is integrated to give

$$\frac{\rho}{\rho_0} = \left(1 + \frac{2}{R_e} \frac{i_0}{i} \frac{z}{\ell} \right)^{-1/2} \quad (3)$$

where $i_0 \equiv \rho_0 UA$ and the electric Reynolds number $R_e \equiv U\epsilon/b\rho_0 \ell$. Note that R_e is the ratio of the charge relaxation time $\epsilon/b\rho_0$ (based on the charge density at the entrance) to the fluid transport time ℓ/U . Hence, if R_e is large, convection plays a dominant role in determining the charge distribution.

Now, if Eq. 3 is used with Eq. 1, the electric field intensity is known:

$$E \equiv \frac{U}{b} \left\{ \frac{i}{i_0} \left[1 + \frac{2}{R_e} \frac{i_0}{i} \frac{z}{\ell} \right]^{1/2} - 1 \right\} \quad (4)$$

and integration of E in turn gives the potential distribution

$$\Phi = \frac{U\ell}{b} \left\{ \frac{z}{\ell} - \frac{R_e}{3} \left(\frac{i}{i_0} \right)^2 \left[\left(1 + \frac{2}{R_e} \frac{i_0}{i} \frac{z}{\ell} \right)^{3/2} - 1 \right] \right\} \quad (5)$$

Thus, because $\Phi(\ell)$ is the terminal voltage v , the "volt-ampere" characteristic of the device has been obtained.

The pressure rise $\Delta p \equiv p(\ell) - p(0)$ is balanced by the net electrical force on the fluid. Hence it is simply the difference in the normal electric stresses evaluated at the outlet and inlet. From Eq. 4,

$$\Delta p = \frac{\epsilon}{2} [E^2(\ell) - E^2(0)] = \frac{\epsilon U^2}{2b^2} \left\{ \left[\frac{i}{i_0} \left(1 + \frac{2i_0}{R_e i} \right)^{1/2} - 1 \right]^2 - \left[\frac{i}{i_0} - 1 \right]^2 \right\} \quad (6)$$

The pump, brake and generator energy conversion regimes can be identified by considering the dependence of the electrical power out, $P_e = vi$, and of the mechanical power in, $P_m = -\Delta pUA$, on the normalized current i/i_0 . These dependences are shown in Fig. 5.7.3 with the electric Reynolds number, R_e , as a parameter. Note that as R_e is raised, the $v-i$ relationship approaches that of a current source with $i = i_0$ (a vertical line through $i/i_0 = 1$ on the plot). The short-circuit current i_{sc} , normalized to i_0 , is determined by R_e . From Eq. 5 evaluated at $z = \ell$ and with $v = 0$,

$$R_e = \frac{3(4r^2 - 3) + [9(4r^2 - 3)^2 - 192r^3(r - 1)]^{1/2}}{12r^2(1 - r)} ; \quad r \equiv \frac{i_{sc}}{i_0} \quad (7)$$

For convenience, R_e is expressed here as a function of i_{sc}/i_0 . The current i_{bp} (at which the pressure rise is zero) follows from Eq. 6:

$$i_{bp}/i_0 = 2R_e/(2R_e + 1) \quad (8)$$

These currents i_{sc} and i_{bp} are sketched as a function of R_e in Fig. 5.7.4. They demark the extremes of the brake regime of operation, and hence also define the upper and lower currents, respectively, of

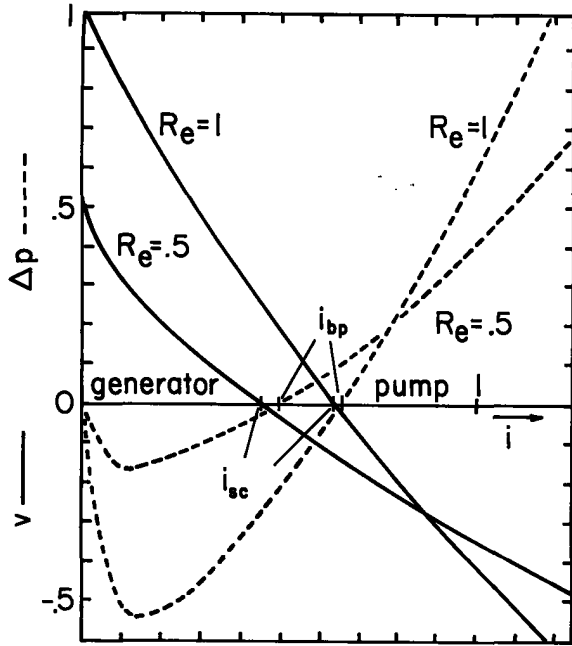


Fig. 5.7.3. Electrical and mechanical terminal characteristics as a function of the normalized terminal current with the electric Reynolds number R_e as a parameter. v is normalized to $\rho_0 l^2 / \epsilon$, Δp is normalized to $(\rho_0 l)^2 / 2\epsilon$, and i to i_0 .

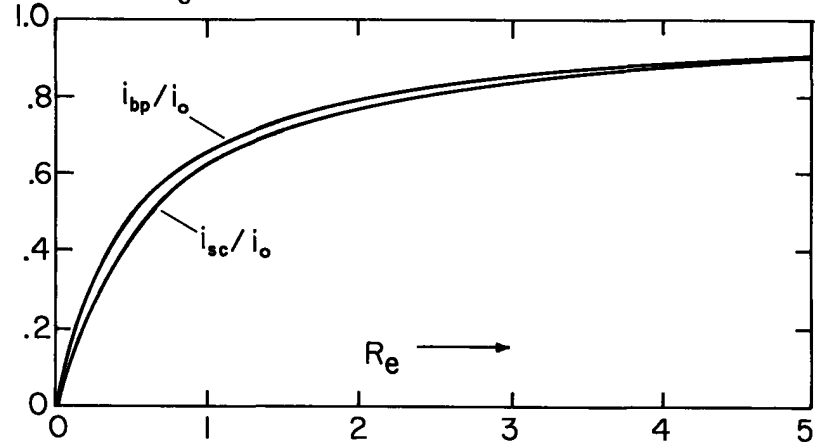


Fig. 5.7.4. Dependence of the normalized short-circuit and zero-pressure-drop currents on the electric Reynolds number R_e .

the generator and pump regimes.

The Generator Interaction: The optimum generator performance, from the point of view of electrical breakdown, is obtained by making $E(l) = 0$, so that the maximum pressure change is obtained for a given maximum E . In this case, it follows from Eq. 4 that i/i_0 should be adjusted to make

$$\frac{i}{i_0} = -\frac{1}{R_e} + [(1/R_e)^2 + 1]^{1/2} \quad (9)$$

In any case, the electrical power output is given by Eq. 5 as

$$P_e = vi = \frac{\rho_0 AU^2 l}{b} \left(\frac{i}{i_0}\right) \left\{ 1 - \frac{R_e}{3} \left(\frac{i}{i_0}\right)^2 \left[\left(1 + \frac{2}{R_e} \frac{i_0}{i}\right)^{3/2} - 1 \right] \right\} \quad (10)$$

For this particular case, the mechanical power input follows from Eqs. 6 and 9 as

$$P_m = -\Delta p UA = \frac{U^3 A \epsilon}{2b^2} \left(\frac{i}{i_0} - 1\right)^2 \quad (11)$$

From these last two expressions, an electromechanical energy conversion efficiency is determined as a function of R_e or i/i_0 :

$$\frac{P_e}{P_m} = \frac{1}{3} \left(1 + 2 \frac{i}{i_0}\right) = \frac{1}{3} \left\{ 1 - \frac{2}{R_e} + 2[(1/R_e)^2 + 1]^{1/2} \right\} \quad (12)$$

The dependences of the energy conversion efficiency and i/i_0 on R_e are summarized in Fig. 5.7.5.

The Pump Interaction: Consider now the distribution of fields that gives rise to the greatest pressure rise for a given maximum electric field intensity within the flow. From Eq. 6, in this case $E(0) = 0$: a condition obtained by making $i = i_0$. That is, at the entrance current is entirely carried by the convection, there being no slip velocity between the charge carriers and the neutral fluid. The electrical power P_e is again given by Eq. 10, but now $i/i_0 = 1$. The mechanical power P_m follows from Eq. 6 and the current condition as

$$P_m = -\frac{U^3 A \epsilon}{2b^2} [(1 + 2/R_e)^{1/2} - 1]^2 \quad (13)$$

The efficiency of the electrical to mechanical energy conversion is then fully determined by the

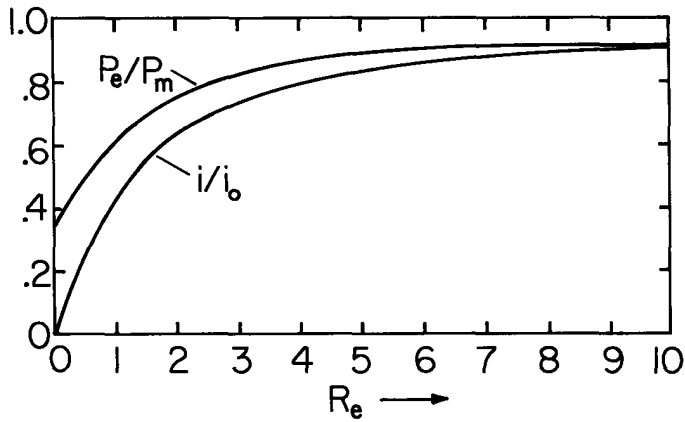


Fig. 5.7.5

Dependence of generator electromechanical energy conversion efficiency P_e/P_m and normalized terminal current i/i_0 on the electric Reynolds number R_e .

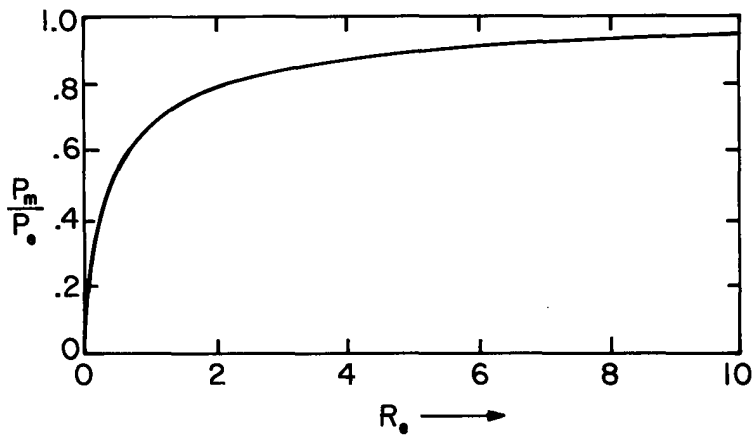


Fig. 5.7.6

Efficiency of electrical to mechanical energy conversion for unipolar one-dimensional interaction with current $i=i_0$ so that the entrance electric field intensity is zero.

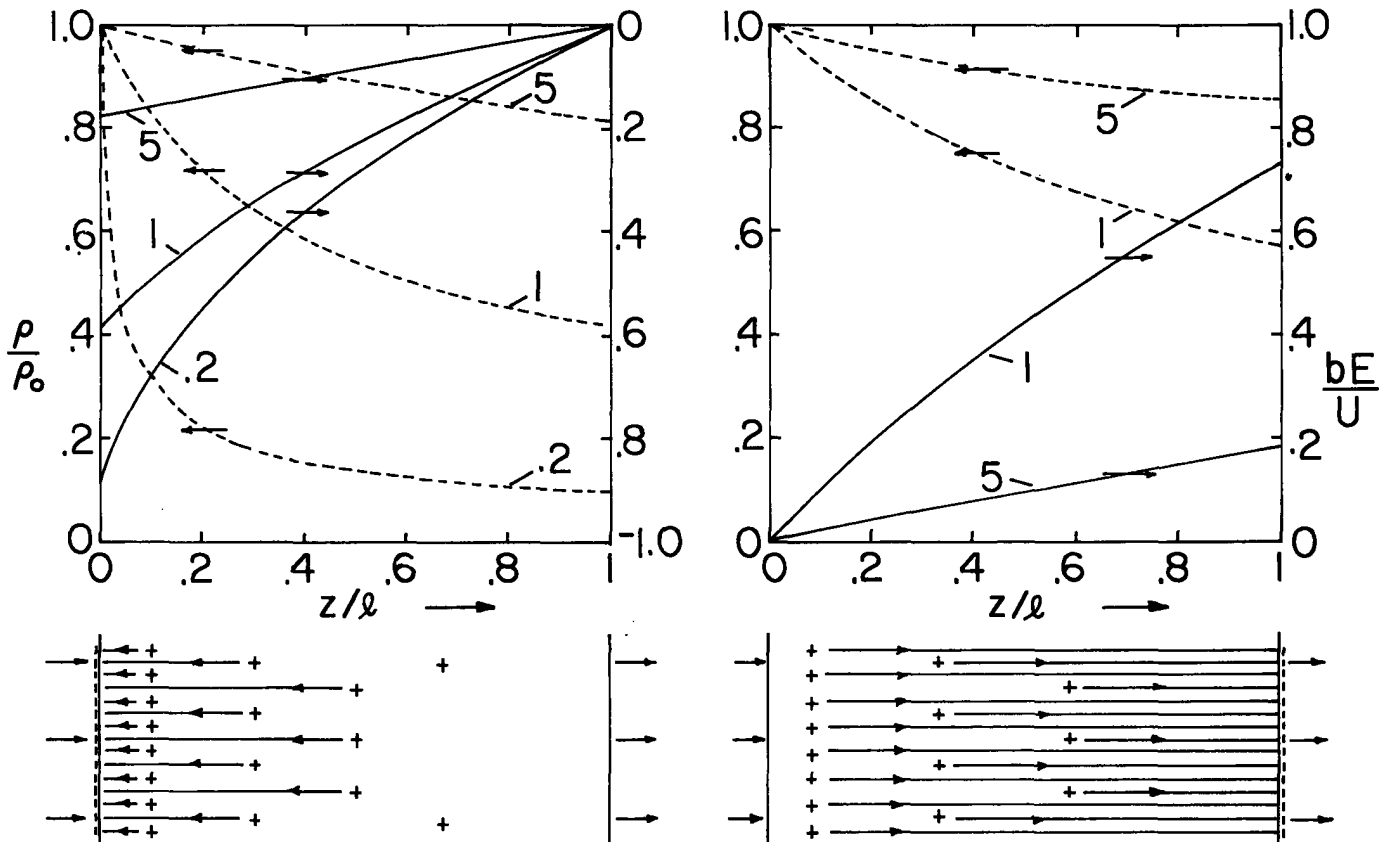


Fig. 5.7.7. Distribution of charge density and electric field intensity for generator and pump. The parameter $R_e \equiv (\epsilon/b\rho_0)/(l/U)$ can be regarded as a normalized velocity.

electric Reynolds number

$$\frac{P_m}{P_e} = 3[2(1 + 2/R_e)^{1/2} + 1]^{-1} \quad (14)$$

The dependence on R_e is summarized in Fig. 5.7.6.

For both the generator and pump under these idealized conditions, the charge and electric field distributions are illustrated in Fig. 5.7.7. Because the relationship between $1/i_0$ and R_e is determined by the operating conditions (Eq. 9 for the generator and $1/i_0 = 1$ for the pump) the only parameter is R_e .

In this steady-state interaction, characteristics, emphasized in Sec. 5.6, still offer an alternative point of view. In the neighborhood of a given charged particle as it passes through the interaction region, the charge density must decay in accordance with Eq. 5.6.2. The spatial rate of decay shown in Fig. 5.7.7 decreases with increasing electric Reynolds number because the particle then spends less time in the interaction region.

5.8 Bipolar Migration with Space Charge

Common conduction phenomena involve more than one charge species. Media supporting one positive and one negative species are used here to illustrate interactions between carriers caused by space-charge fields, recombination and generation. The method of characteristics is further developed as a means of understanding the evolution of the charge distributions. Based on the bipolar model of this section, the limit of ohmic conduction is examined in the next section.

Each of the charge species is governed by a conservation equation taking the form of Eq. 5.2.3:

$$\frac{\partial \rho_{\pm}}{\partial t} + \nabla \cdot (\rho_{\pm} \vec{v}_{\pm} + \vec{J}'_{\pm}) = G_{\pm} - R_{\pm} \quad (1)$$

where the current density relative to the moving material is

$$\vec{J}'_{\pm} = b_{\pm} \rho_{\pm} \vec{E} \mp K_{\pm} \nabla \rho_{\pm} \quad (2)$$

Consider some physical situations to which these expressions pertain. Because pairs of charged particles are generated and recombined, $G_+ = G_- \equiv G$ and $R_+ = R_- \equiv R$.

Positive and Negative Ions in a Gas: Perhaps by means of a corona discharge, a flame or a radioactive source, ion pairs are created and then carried into the region of interest by a gas flow or by an electric field. With the proviso that the charge per particle of each species has the same magnitude, $q_+ = q$, recombination results in the creation of a neutral particle. Carriers can recombine at a rate that is proportional to the product of the charge densities:¹

$$R = \frac{\alpha \rho_+ \rho_-}{q} \quad (3)$$

One recombination results in the loss of one particle from each of the species, so R_{\pm} is the same in the two equations summarized by Eq. 1.

At pressures somewhat exceeding atmospheric, the recombination coefficient α can be computed by picturing the process as one of oppositely charged particles being attracted to each other with a Coulomb force that is retarded by collisions between the ions and the neutral gas molecules. This results in the Langevin recombination coefficient:

$$\alpha = \frac{q(b_+ + b_-)}{\epsilon_0} \quad (4)$$

A radioactive source of α or β particles could be used to create a generation term, G_{\pm} , that would then be dependent on the density of neutral particles at not only the point in question, but points in the gas between the radioactive source and the point of interest, since these could contribute to the slowing and hence final absorption of the ionizing particle.

¹S. C. Brown, "Conduction of Electricity in Gases," in Handbook of Physics, E. U. Condon and H. Odishaw, eds., McGraw-Hill Book Company, New York, Toronto, London, 1958, pp. 4-166.

Aerosol Particles: Submicron particulate products of combustion are an example of macroscopic particles that often carry a natural charge of both signs. Self-agglomeration of overtly charged particles is also of interest in air pollution control.² In these cases, the charge per particle can be many electronic charges, and so electrically induced agglomeration of oppositely charged particles does not necessarily result in a neutral particle. Rather, with the assumption that the agglomeration is stable (the particles stick), yet another species of charged particles is created and the situation is generally much more complicated than can be described by the bipolar model. But, for a mixture of uniformly charged particles, the model applies with $G_{\pm} = 0$ and the self-agglomeration represented by the recombination term of Eq. 3.

Intrinsically Ionized Liquid: In liquids, thermal processes result in dissociation (ionization) of constituent molecules. For example, in pure water, a small fraction of the H_2O molecules disassociate into H^+ and OH^- ions. With these constituting the positive and negative species, there is a local thermal generation of ion pairs that is proportional to the number density, n , of neutral molecules:

$$G = \beta n \quad (5)$$

and a recombination rate given by Eq. 3 with $\epsilon_0 \rightarrow \epsilon$. In the terminology of chemical kinetics, the recombination process would be regarded as a second order rate process.³

Partially Dissociated Salt in Solvent: When dissolved, materials such as NaCl or KCl tend to disassociate into positive and negative ions, Na^+Cl^- and K^+Cl^- . These then contribute to the conduction and, in this regard, can dominate over the intrinsic ionization. In that case, the conduction is represented in terms of just the two species, but it is also important to recognize that the unionized neutral molecules represent a third species. The number density, n , of this species is now, like the ion number densities n_+ and n_- , a function of space and time.

To describe the evolution of the neutral particles, a conservation equation is written much as for the ions, Eq. 1. However, because these particles are not charged, the only particle current density is due to diffusion. The migration term in Eq. 2 is absent. Also, generation of ion pairs now means that neutral particles are lost, and recombination means that neutrals are gained. Hence, terms on the right-hand side of the conservation equation are the negatives of those on the right in Eq. 1:

$$\frac{\partial n}{\partial t} + \nabla \cdot (n\vec{v} - K_D \nabla n) = -\frac{G}{q} + \frac{R}{q} \quad (6)$$

Summary of Governing Laws: Each of the illustrative situations that have been outlined can be described by deleting the inappropriate terms from the laws now summarized. The two charge densities contribute to Gauss' law:

$$\nabla \cdot \epsilon \vec{E} = \rho_+ - \rho_- \quad (7)$$

where polarization is modeled as being linear and hence represented by the permittivity ϵ . In the following discussions, ϵ is taken as being uniform. The electric field is irrotational, and so

$$\vec{E} = -\nabla \phi \quad (8)$$

With the understanding that the given material deformations are incompressible (that $\nabla \cdot \vec{v} = 0$), the carrier evolutions are represented by Eqs. 1 and 2, which in view of Gauss' law, Eq. 7, combine to become the two equations

$$\frac{\partial \rho_{\pm}}{\partial t} + (\vec{v} \pm b_{\pm} \vec{E}) \cdot \nabla \rho_{\pm} = \mp \rho_{\pm} b_{\pm} \frac{(\rho_+ - \rho_-)}{\epsilon} + \beta n - \frac{\alpha \rho_+ \rho_-}{q} + K_{\pm} \nabla^2 \rho_{\pm} \quad (9)$$

Here, Eqs. 3 and 5 are used to represent the recombination and generation. If n is a constant, or the generation term is absent, then the law governing the neutrals is not required; but if the neutral evolution is also part of the story, then Eq. 6 is added to the list:

$$\frac{\partial n}{\partial t} + \vec{v} \cdot \nabla n = -\frac{\beta n}{q} + \frac{\alpha}{2} \rho_+ \rho_- + K_D \nabla^2 n \quad (10)$$

Equations 7 - 10 constitute one vector and 4 scalar equations in the unknowns \vec{E} , ϕ , ρ_+ , ρ_- and n .

2. J. R. Melcher, K. S. Sachar and E. P. Warren, "Overview of Electrostatic Devices for Control of Submicrometer Particles," Proc. IEEE 65, 1659 (1977).

3. K. J. Laidler, Chemical Kinetics, McGraw-Hill Book Company, New York, 1965, p. 535.

Characteristic Equations: With the understanding that lengths of interest are large enough to justify ignoring the diffusion contributions to Eqs. 9 and 10 (typically, the ratio given by Eq. 5.2.12 is small), Eqs. 9 can be written in the characteristic form introduced in Sec. 5.3:

$$\frac{d\rho_{\pm}}{dt} = \mp \rho_{\pm} b_{\pm} \frac{(\rho_{+} - \rho_{-})}{\epsilon} + \beta n - \frac{\alpha}{q} \rho_{+} \rho_{-} \quad (11)$$

Here, the time rate of change is measured by an observer moving respectively with the \pm ions, on the characteristic lines

$$\frac{d\vec{r}}{dt} = \vec{v}_{\pm} + b_{\pm} \vec{E} \quad (12)$$

Similarly, Eq. 10 becomes

$$\frac{dn}{dt} = -\frac{\beta n}{q} + \frac{\alpha}{2} \rho_{+} \rho_{-} \quad (13)$$

on the characteristic lines that are physically the particle lines for the neutrals

$$\frac{d\vec{r}}{dt} = \vec{v} \quad (14)$$

Following a particle of the neutral material, the neutral number density changes with time in accordance with the local balance between generation and recombination. What makes the bipolar situation more complex than for unipolar migration is that not only are the positive and negative species described by Eqs. 11 along different characteristic lines, but the space-charge term on the right has an effect that is proportional to the net charge, generally with contributions from both species.

One-Dimensional Characteristic Equations: Consider the one-dimensional configuration, illustrated by Fig. 5.8.1, in which densities and fields are independent of (y, z) , with $\vec{E} = E(x, t)\hat{i}_x$ and $\vec{v} = U(t)\hat{i}_x$. Because \vec{v} is solenoidal, U is at most a function of time only. Then, Eqs. 11-14 reduce to the first six ordinary differential equations summarized by Eq. 15:

$$\frac{d}{dt} \begin{bmatrix} \rho_{+} \\ \rho_{-} \\ x_{+} \\ x_{-} \\ n \\ x_n \\ E_{+} \\ E_{-} \\ E_n \end{bmatrix} = \begin{bmatrix} -\frac{b_{+}}{\epsilon} \rho_{+} (\rho_{+} - \rho_{-}) + \beta n - \frac{\alpha}{q} \rho_{+} \rho_{-} \\ \frac{b_{-}}{\epsilon} \rho_{-} (\rho_{+} - \rho_{-}) + \beta n - \frac{\alpha}{q} \rho_{+} \rho_{-} \\ U + b_{+} E_{+} \\ U - b_{-} E_{-} \\ -\frac{\beta}{q} n + \frac{\alpha}{2} \rho_{+} \rho_{-} \\ U \\ -\frac{(b_{+} + b_{-})}{\epsilon} \rho_{-} E_{+} + \frac{C(t)}{\epsilon} \\ -\frac{(b_{+} + b_{-})}{\epsilon} \rho_{+} E_{-} + \frac{C(t)}{\epsilon} \\ -\frac{1}{\epsilon} (b_{+} \rho_{+} + b_{-} \rho_{-}) E_n + \frac{C(t)}{\epsilon} \end{bmatrix} \quad (15)$$

where

$$\frac{C(t)}{\epsilon} \equiv \frac{1}{d} \left\{ \frac{dv}{dt} + \frac{1}{\epsilon} \int_0^d [\rho_{+}(U + b_{+}E) - \rho_{-}(U - b_{-}E)] dx \right\}$$

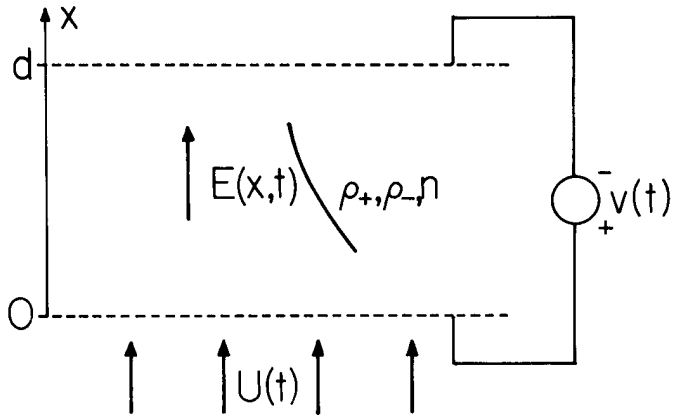


Fig. 5.8.1. One-dimensional bipolar migration configuration.

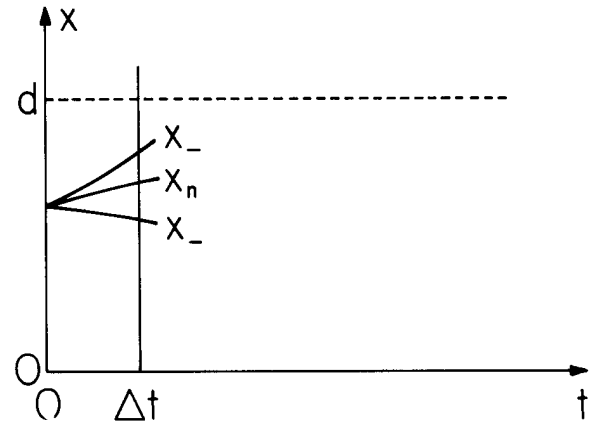


Fig. 5.8.2. Characteristic lines in (x-t) plane.

Here, subscripts are used to distinguish the characteristic lines. Thus the first two equations respectively apply along lines in the (x-t) plane represented respectively by the third and fourth expressions. Similarly, the fifth equation applies along the lines defined by the sixth expression.

In numerically integrating these equations it is convenient to take account of Gauss' law, Eq. 7, by having equations for the time rates of change of the electric field for an observer moving along each of the respective characteristic lines.⁴ To this end, the time rate of change of Eq. 7 is written as

$$\frac{\partial}{\partial x} \left(\frac{\partial E}{\partial t} \right) = \frac{1}{\epsilon} \frac{\partial}{\partial t} (\rho_+ - \rho_-) \quad (16)$$

The difference between Eqs. 9 becomes

$$\frac{\partial}{\partial t} (\rho_+ - \rho_-) + \frac{\partial}{\partial x} [\rho_+(U + b_+E) - \rho_-(U - b_-E)] = 0 \quad (17)$$

Elimination of the term in $\rho_+ - \rho_-$ between these equations leads to the conclusion that

$$\frac{\partial}{\partial x} \left\{ \epsilon \frac{\partial E}{\partial t} + [\rho_+(U + b_+E) - \rho_-(U - b_-E)] \right\} = 0 \quad (18)$$

The quantity in brackets, the sum of the displacement current and the migration currents, is defined as $C(t)$. Integration of $C(t)$ from $x = 0$ to $x = d$ results in the expression given with Eq. 15. The voltage v , defined as the integral of E between the planes $x = 0$ and $x = d$, brings in the remaining field law, Eq. 8.

Gauss' law can be used to eliminate the net charge $\rho_+ - \rho_-$ from $C(t)$, the quantity in brackets in Eq. 18, to obtain

$$\frac{\partial E}{\partial t} + U \frac{\partial E}{\partial x} = \frac{C(t)}{\epsilon} - \frac{1}{\epsilon} (b_+\rho_+ - b_-\rho_-)E \quad (19)$$

What is on the left is the time rate of change of E for an observer moving on the neutral characteristic lines. Thus, Eq. 19 is the last of Eqs. 15. To obtain the time rates of change of E on the charged particle characteristic lines, add to both sides of Eq. 19 $\pm b_{\pm}E\partial E/\partial x$. On the left is then the time rate of change of E for an observer moving on the respective characteristic lines x_{\pm} . With Gauss' law used to replace $\partial E/\partial x$ on the right with $(\rho_+ - \rho_-)/\epsilon$, these equations become the seventh and eighth expressions of Eq. 15.

The functions $E_+(t)$, $E_-(t)$ and $E_n(t)$ are numerically the same as $E(x,t)$. Each is now regarded as solely a function of time because it is understood that the respective functions are measured by an observer moving along the lines $x_+(t)$, $x_-(t)$, and $x_n(t)$, respectively.

Numerical Solution: A beauty of the method of characteristics is that it reduces partial differential equations to a system of ordinary differential equations, Eqs. 15. Many numerical techniques

4. M. Zahn, "Transient Electric Field and Space Charge Behavior for Drift Dominated Bipolar Conduction," in Conduction and Breakdown in Dielectric Liquids, J. M. Goldschvartz, ed., Delft University Press, 1975, pp. 61-64.

exist for integrating nonlinear equations in this form, e.g., Runge-Kutta or predictor-corrector.⁵

The region of interest in the (x-t) plane is bounded by x = 0 and x = d, where screen electrodes are respectively constrained to potential v(t) and 0. These planes define two sides of a "U" shaped region, sketched in Fig. 5.8.2, with the initial line t = 0 the third side. Wherever one of the characteristic lines (x₊, x₋, x_n) enters this region, there must be a condition on the associated density ρ₊, ρ₋ or n. In addition, the potential of the boundaries at x = 0 and x = d is constrained. Thus, when t = 0, characteristic lines enter the region with the initial values of ρ₊, ρ₋ and n. Taken with the constraint on the potential difference between the screens, this determines the initial distribution of E(x,0), because at any time, Gauss' law can be integrated to obtain

$$E(x) = \int_0^x \frac{(\rho_+ - \rho_-)}{\epsilon} dx' + E_0 \quad (20)$$

The constant of integration, E₀, is determined by integrating E from x = 0 to x = d and requiring that the result be v. If the resulting value of E₀ is substituted back into Eq. 20, an expression is obtained for E(x,t) in terms of ρ₊ and ρ₋ when t = t:

$$E(x,t) = \int_0^x \frac{(\rho_+ - \rho_-)}{\epsilon} dx' - \frac{1}{d} \int_0^d dx \int_0^x \frac{(\rho_+ - \rho_-)}{\epsilon} dx' + \frac{v}{d} \quad (21)$$

With the initial values of all quantities on the right in Eq. 15 established, it is now possible to begin marching forward in time.

In the integration scheme used to generate the distributions shown, a predictor-corrector subroutine is used which calls a user-written subroutine for evaluation of derivatives (Eqs. 15) after each prediction or correction step. Because Eqs. 15 are a set of coupled ordinary nonlinear differential equations, there are readily available routines for carrying out the main integration (compiled subroutines for predictor-corrector integration are available, for example, in the International Mathematical & Statistical Library).

Note that the derivatives are not entirely determined by quantities naturally evaluated on the same characteristic line. For example, dρ₊/dt is determined by not only ρ₊, but by ρ₋ and n as well, and these quantities are naturally found along their respective characteristic lines. If the distance d is broken into (i - 1) segments, there are (i) characteristic lines of each family emanating from the t=0 line into the region of interest. Equations 15 comprise (9i) coupled ordinary differential equations. The equations for values on a (+) characteristic line are coupled to those on neighboring characteristic lines by Eqs. 15b and 15e, and coupled to all the other characteristic lines thru C(t). Thus, at each step in time, values of ρ₋ and n on the x₊ characteristic must be interpolated from values on the neighboring characteristics x₋ and x_n. Similarly, values of ρ₊ and n must be interpolated from their respective characteristic lines onto the x₋ lines for use in the equation for ρ₋, and values of ρ₊ and ρ₋ must be interpolated onto the neutral characteristics in order to compute dn/dt. The interpolation for the examples illustrated here are done with a four-point Lagrangian formula. This fits a cubic equation to the nearest two data points on both sides of the interpolation point.

The charge and neutral density profiles are conveniently initiated with step singularities. In order to prevent the smearing out of these step edges, a two-point (linear) interpolation is used when near these edges, so that the data on one side of the edge does not influence the interpolated values on the other side.

The integration in C(t) is carried out in two parts: the ρ₊(U₊ + b₊E) term is integrated over the (irregular) set of x₊ points using the readily available values of ρ₊ and E₊ on these points, and the ρ₋(U₋ - b₋E) term is similarly integrated over the x₋ points.

Numerical Example: (The numerical analysis of this section was carried out by R. S. Withers) A situation which is the basis for gaining physical insights in this and the next section is sketched in Fig. 5.8.3. When t = 0, equal amounts of positive and negative charge uniformly occupy the region next to the lower screen, with the region above initially free of charge. Initially, neutral particles are absent throughout and there is no generation at any time. Because the effect of the convection in one dimension is to translate the material in the x direction, the material velocity U is taken as zero. Hence, the model is appropriate to describing what might be considered a "conducting layer" adjacent to an insulating layer of material sandwiched between plane-parallel electrodes. It is assumed that charged particles leaving the region by arriving at one or the other of the electrodes are neutralized and removed from the volume. Further, charged particles cannot be generated at the electrode

5. F. S. Acton, Numerical Methods that Work, Harper & Row, Publishers, New York, 1970.

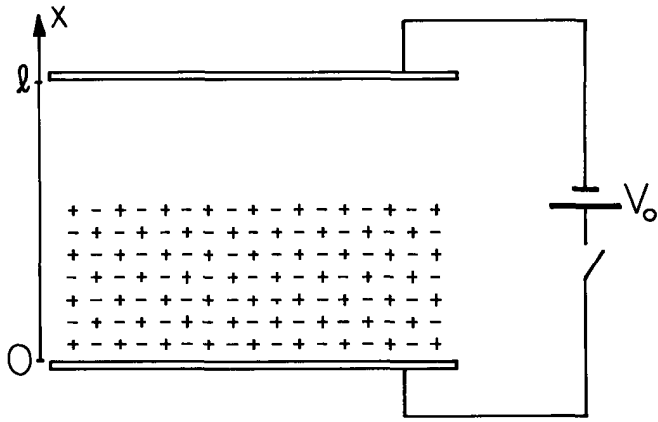


Fig. 5.8.3

When $t=0$, voltage is applied to plates. Initially, lower half of region between is filled with equal densities of positive and negative charges. Figure 5.8.4 shows evolution with time if there is no generation. Figure 5.9.3 illustrates what happens with generation.

surfaces, and hence characteristic lines emanating from the electrodes carry no associated particle density.

The evolution of electric field and net charge are displayed in Fig. 5.8.4a, where the $x-t$ plane forms the "floor." Similarly, the $x-t$ dependence of the particle densities is shown in Fig. 5.8.4b. The critical characteristic lines, x_+ and x_- , are also shown in these plots. (The neutral characteristics, x_n , are simply lines running parallel to the t axis.)

Considerable insight can be extracted from this example by identifying the dominant processes in each of the regions demarked in Fig. 5.8.5 by critical characteristic lines. In region I, bounded by x_+ originating at the lower electrode and x_- originating at the initial interface between the charged layer and the region above, the initial charge densities at A, A', and A'' are the same. It follows that these initial points can be chosen such that B and B' occur at the same time (on the same line $t = \text{constant}$). Also, the initial conditions are the same so the values of ρ_+ and of ρ_- at the points B and B' are the same. In turn, the value of the charge densities at C are the same as at other positions in region I at this same time. It is concluded that Eqs. 15a and 15b describe the time dependence at any given fixed location x in region I. In the example, initial conditions set $\rho_+ = \rho_-$ and these equations reduce to the same equation for subsequent times. Thus, the net charge density $\rho_+ - \rho_-$ is zero in region I, and, through recombination alone, the individual charge species decay according to the law

$$\rho_+ = \frac{\rho_0}{1 + t/\tau}; \quad \tau = \frac{\epsilon_0}{\rho_0(b_+ + b_-)} \quad (22)$$

where Eq. 5.8.4, the Langevin recombination coefficient, has been used.

Because there is no generation, the recombination simply feeds the neutral equation, and Eq. 15e shows that in region I

$$n = \int_0^t \frac{\rho_0}{q} \frac{d(t'/\tau)}{(1 + t'/\tau)^2} = \frac{\rho_0}{q} \frac{t/\tau}{(1 + t/\tau)} \quad (23)$$

Region II, like region I, has uniform initial conditions, so the same arguments apply. But, the initial conditions on (ρ_+, ρ_-, n) are all zero, and so these quantities remain zero throughout. It follows from the characteristic electric field equations, Eqs. 15g-15j, that E is uniform in this region.

In region III, the x_+ characteristics enter from the lower electrode carrying no ρ_+ . At a point like D, Eq. 15a establishes $\rho_+ = 0$, and a step-by-step march into this region shows that at each point $\rho_+ = 0$. Hence, Eq. 15b applies with $\rho_+ = 0$ and it is concluded that along x_- in this region the charge evolution is as though the process were the unipolar self-precipitation process discussed in Sec. 5.6. Because there are only negative charges, there is no recombination.

Region IV, where the positive charges are moving upward along the E lines but the negative charges have been swept downward, is of essentially the unipolar character of region III. Because charges do not originate on the upper electrode, region VII is also unipolar.

Finally, it can be argued that in regions V, VI and VIII, $\rho_+ = 0$ and $\rho_- = 0$.

The neutral characteristics, x_n , do not enter into the classification of regimes because the coupling to n is "one-way." But, neutrals created by recombination remain behind the x_- wavefront defining the demarcation of regions IV and I. As a result, the distribution of n at a given time is uniform in region I (with amplitude given by Eq. 23) and makes a smooth transition to zero at the

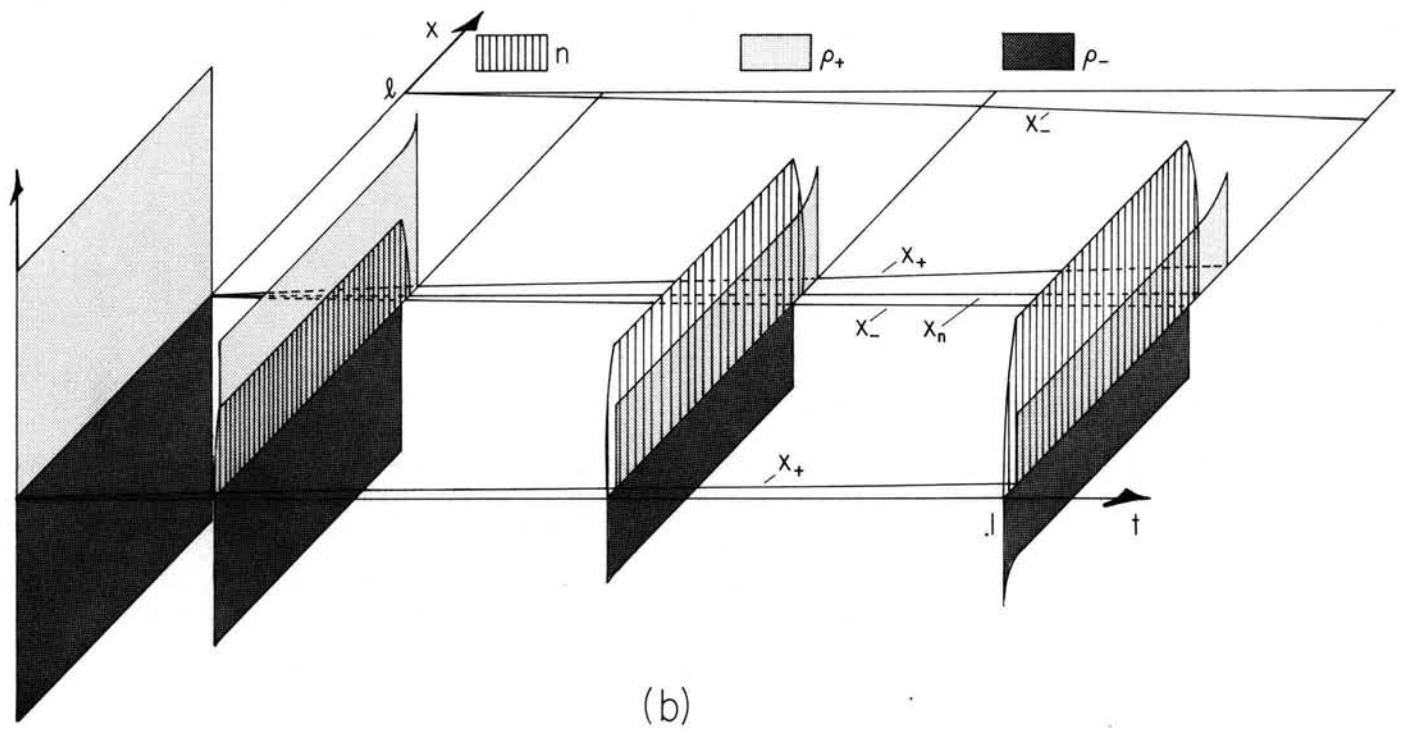
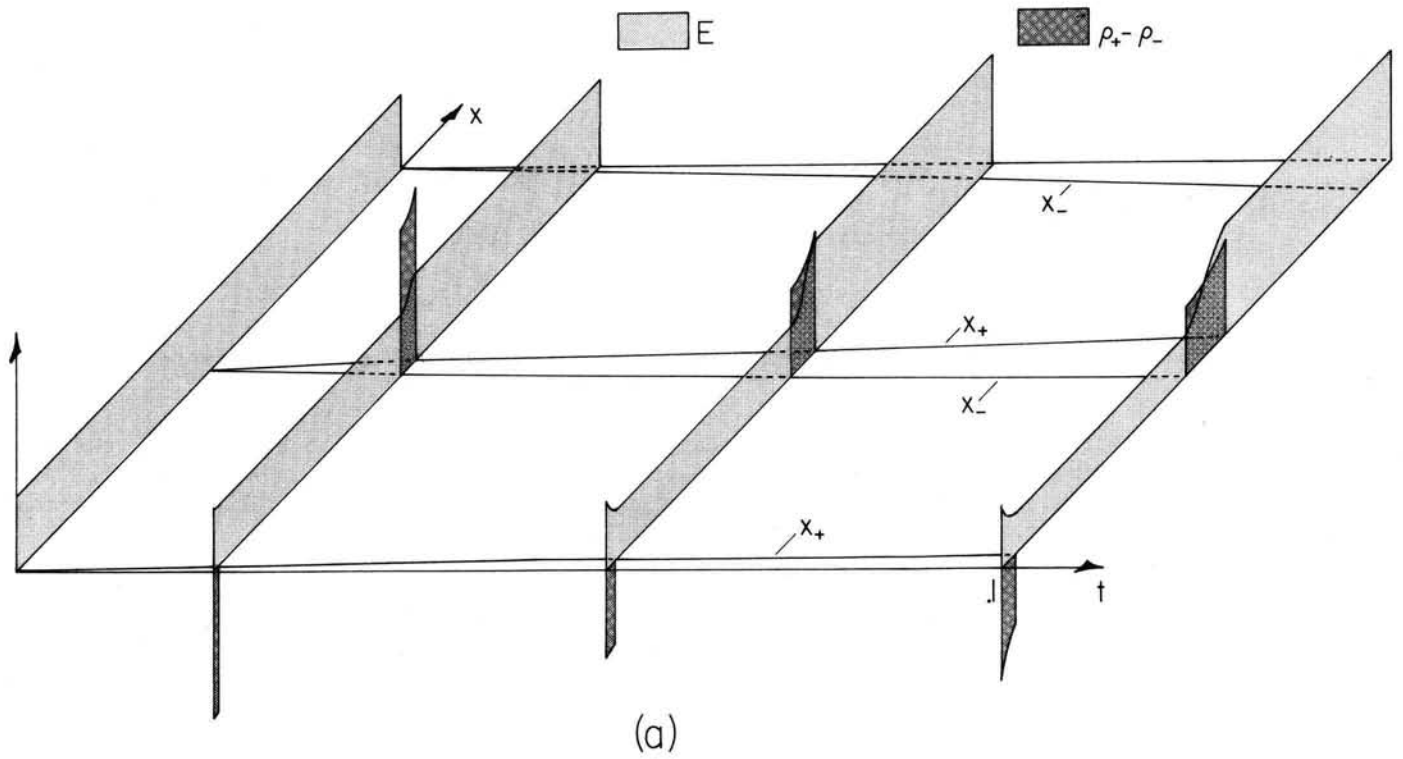


Fig. 5.8.4. Evolution of layer composed of equal densities of positive and negative carriers occupying lower half of region between capacitor plates. Initially there are no neutrals. Generation is absent ($\beta = 0$) so recombination results in neutrals. For the case shown, $t = \underline{t} [l/\mathcal{E}(b_+ + b_-)]$, where $\mathcal{E} \equiv V_0/l$. Also, $b_+ = b_-$ and the initial charge densities are such that $\rho_+ = \rho_- = 30(\epsilon V_0/l^2)^0$. (a) Electric field and net charge density; (b) neutral density and positive and negative charge densities.

initial location of the region IV-I interface.

At a given instant, the net charge in region IV increases with x . The reason for this is apparent from following the x_+ characteristic originating at A in Fig. 5.8.5. At first, ρ_+ decays by recombination, with a time constant $\tau = \epsilon_0/\rho_0(b_+ + b_-)$, until x_+ passes from regime I to region IV. The subsequent decay is due to self-precipitation and occurs with the larger (slower) unipolar time constant $\epsilon_0/\rho_0 b_+$. Thus, at G in Fig. 5.8.5, particles have spent more time in the unipolar regime and less time in the recombination regime than those at G'. This is why, at a given instant in Fig. 5.8.4a, the net charge at the x_+ wavefront of the regime IV (which is decaying at the unipolar rate) is greater than behind the front. (Note, however, that the ρ_0 used in evaluating this latter time constant is the value of ρ_+ when the characteristic line enters region IV, which is not the same for points G and G'.)

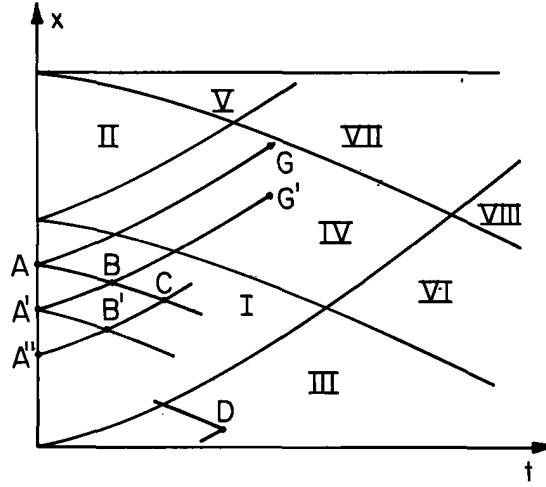


Fig. 5.8.5. Regions are delimited by x_+ and x_- characteristics emanating from interface and electrodes.

5.9 Conductivity and Net Charge Evolution with Generation and Recombination: Ohmic Limit

The net free charge density and conductivity for the bipolar systems treated in Sec. 5.8, defined as

$$\rho_f = \rho_+ - \rho_-; \quad \sigma = b_+ \rho_+ + b_- \rho_- \quad (1)$$

are natural variables for understanding the relationship between charge migration and relaxation. In terms of (ρ_f, σ) , the charge densities ρ_+ and ρ_- are found by inverting Eqs. 1:

$$\rho_{\pm} = \frac{\sigma \pm b_{\mp} \rho_f}{b_+ + b_-} \quad (2)$$

With the objective of casting the charge evolution in terms of ρ_f and σ , the difference is taken between the conservation equations for + and - species, Eqs. 5.8.9, and ρ_+ and ρ_- are replaced on the right using Eqs. 2:

$$\frac{D\rho_f}{Dt} = -\vec{E} \cdot \nabla \sigma - \frac{\sigma \rho_f}{\epsilon} + \left(\frac{K_+ - K_-}{b_+ + b_-} \right) \nabla^2 \sigma + \left(\frac{K_+ b_- + K_- b_+}{b_+ + b_-} \right) \nabla^2 \rho_f \quad (3)$$

To similarly obtain an expression for σ , Eqs. 5.8.9 are respectively multiplied by b_+ and summed to obtain

$$\begin{aligned} \frac{D\sigma}{Dt} = & -\vec{E} \cdot \nabla [(b_+ - b_-)\sigma + b_+ b_- \rho_f] - [(b_+ - b_-)\sigma + b_+ b_- \rho_f] \frac{\rho_f}{\epsilon} + (b_+ + b_-) \beta n \\ & - \frac{\alpha}{q(b_+ + b_-)} [\sigma^2 - (b_+ - b_-)\sigma \rho_f - b_+ b_- \rho_f^2] + \left(\frac{K_+ b_+ + K_- b_-}{b_+ + b_-} \right) \nabla^2 \sigma + \frac{b_+ b_-}{b_+ + b_-} (K_+ - K_-) \nabla^2 \rho_f \quad (4) \end{aligned}$$

To complete the description, Eqs. 2 are used to write Eq. 10 as

$$\frac{Dn}{Dt} = \frac{-\beta}{q} n + \frac{\alpha}{q^2 (b_+ + b_-)^2} [\sigma^2 - (b_+ - b_-)\sigma \rho_f - b_+ b_- \rho_f^2] + K_D \nabla^2 n \quad (5)$$

These last three expressions are an alternative to Eqs. 5.8.9 and 5.8.10 in describing the migration and diffusion of the carriers in a deforming material. The method of characteristics could be used to solve these expressions, much as illustrated in Sec. 5.8. But the objective in this section is to identify the rate processes encapsulated by these laws and hence to discern the dominant

contributions to the equations. Limiting forms of the equations, for example the ohmic model emphasized here and used in the remainder of this chapter, are necessary if the conduction laws are to be embodied in models that bring in still other dynamical processes.

The approach now used is similar to that introduced in Sec. 2.3, where the quasistatic limits of the electrodynamic laws are recognized by using a normalization of the laws to discern the critical characteristic times. Given that dynamical times of interest are characterized by τ , what are the times characterizing the processes represented by Eqs. 3-5?

Variables are normalized such that

$$t = \underline{t}\tau, \quad (x, y, z) = (\underline{x}, \underline{y}, \underline{z})\ell, \quad \vec{v} = \underline{\vec{v}}\ell/\tau, \quad \sigma = \underline{\sigma}\Sigma, \quad \vec{E} = \underline{\vec{E}}\mathcal{E}, \quad \rho_f = \underline{\rho}_f\epsilon\mathcal{E}/\ell \quad (6)$$

Thus, Σ is a typical electrical conductivity and \mathcal{E} is a typical electric field intensity. The free charge density is normalized so that it is typically the charge density that would "shield out" the field \mathcal{E} in the distance ℓ . In the state of equilibrium where the charge density is zero, while σ and n are uniform and constant, the generation and recombination terms balance. Thus, at each point

$$\frac{\beta}{q} = \frac{\alpha\sigma^2}{q^2(b_+ + b_-)^2 n} \quad (7)$$

This expression makes it possible to use equilibrium data to evaluate the generation coefficient, given the parameters on the right. It also suggests that the neutral number density be normalized such that

$$n = \underline{n} \frac{\alpha\Sigma^2}{q(b_+ + b_-)^2\beta} \quad (8)$$

Introduction of these normalizations into Eqs. 3-5 results in the expressions

$$\frac{D\rho_f}{Dt} = \frac{\tau}{\tau_e} (-\underline{\vec{E}} \cdot \nabla \sigma - \sigma \rho_f) + \frac{\tau}{\tau_e} \frac{\tau_{mig}}{\tau_D} \frac{(K_+ - K_-)(b_+ + b_-)}{(K_+ b_- + K_- b_+)} \nabla^2 \sigma + \frac{\tau}{\tau_D} \nabla^2 \rho_f \quad (9)$$

$$\begin{aligned} \frac{D\sigma}{Dt} = & -\frac{\tau}{\tau_{mig}} \frac{(b_+ - b_-)}{(b_+ + b_-)} (\underline{\vec{E}} \cdot \nabla \sigma + \sigma \rho_f) - \frac{\tau}{\tau_{mig}} \frac{\tau_e}{\tau_{mig}} \frac{b_+ b_-}{(b_+ + b_-)^2} (\underline{\vec{E}} \cdot \nabla \rho_f + \rho_f^2) \\ & + \frac{\tau}{\tau_e} \left[\frac{\epsilon\alpha}{(b_+ + b_-)q} \right] n - \frac{\tau}{\tau_e} \left[\frac{\epsilon\alpha}{(b_+ + b_-)q} \right] \sigma^2 + \frac{\tau}{\tau_{mig}} \left[\frac{\epsilon\alpha}{(b_+ + b_-)q} \right] \left(\frac{b_+ - b_-}{b_+ + b_-} \right) \sigma \rho_f \\ & + \frac{\tau}{\tau_{mig}} \frac{\tau_e}{\tau_{mig}} \left[\frac{\epsilon\alpha}{(b_+ + b_-)q} \right] \frac{b_+ b_-}{(b_+ + b_-)^2} \rho_f^2 + \frac{(K_+ b_+ + K_- b_-)}{(K_+ b_- + K_- b_+)} \nabla^2 \sigma \\ & + \frac{\tau}{\tau_{mig}} \frac{\tau_e}{\tau_D} \frac{b_+ b_-}{(b_+ + b_-)^2} \frac{(K_+ - K_-)(b_+ + b_-)}{(K_+ b_- + K_- b_+)} \nabla^2 \rho_f \end{aligned} \quad (10)$$

$$\frac{Dn}{Dt} = -\frac{\tau}{\tau_{th}} n + \frac{\tau}{\tau_{th}} \left[\sigma^2 - \frac{(b_+ - b_-)}{(b_+ + b_-)} \frac{\tau_e}{\tau_{mig}} \sigma \rho_f - \frac{b_+ b_-}{(b_+ + b_-)^2} \left(\frac{\tau_e}{\tau_{mig}} \right)^2 \rho_f^2 \right] + \frac{\tau}{\tau_D} \frac{K_D(b_+ + b_-)}{(K_+ b_- + K_- b_+)} \nabla^2 n \quad (11)$$

where the following characteristic times have been identified

$$\tau_e \equiv \frac{\epsilon}{\Sigma}, \quad \tau_{mig} \equiv \frac{\ell}{\mathcal{E}(b_+ + b_-)}, \quad \tau_D \equiv \frac{\ell^2}{\frac{K_+ b_- + K_- b_+}{\left[\frac{b_+ + b_-}{\tau_{mig}} \right]}}, \quad \tau_{th} = \frac{q}{\beta} \quad (12)$$

The other dimensionless coefficients in Eqs. 9-11 are typically of the order of unity. (Note that at least for Langevin recombination, where α is given by Eq. 5.8.4, the coefficient $\epsilon\alpha/(b_+ + b_-)q$ is unity).

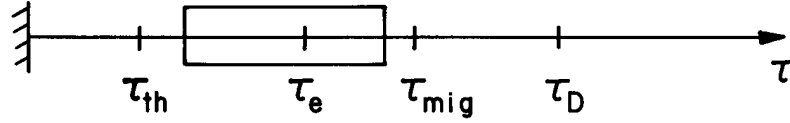


Fig. 5.9.1. Hierarchy of characteristic times and range of dynamical times appropriate to the use of an ohmic model.

With the objective of ordering the time constants of Eq. 13, τ_{th} is estimated by substituting the equilibrium values given by Eq. 7, α from Eq. 5.8.4 and $\sigma = (n_+ b_+ + n_- b_-)q$:

$$\tau_{th} \equiv \frac{q}{\beta} \approx \frac{q^2 (b_+ + b_-)^2 n}{\alpha \sigma^2} = \tau_e \frac{n}{(n_+ b_+ + n_- b_-) / (b_+ + b_-)} \quad (13)$$

Thus, τ_{th} is essentially τ_e multiplied by the ratio of the neutral to the charged particles. If β is large enough that essentially all of the particles available are ionized, then τ_{th} is a small fraction of the charge relaxation time τ_e .

The ordering of characteristic times shown in Fig. 5.9.1 is typical if a configuration is to be appropriately modeled as "ohmic." Because lengths of interest are relatively large, the diffusion time is extremely long. That the migration time τ_{mig} is also long compared to times of interest is also a matter of the length scale of interest, and is justified if the typical electric field intensities are not too large. Times of interest in the ohmic model are arbitrary relative to τ_e . They can be long or short compared to the charge relaxation time.

With the understanding that the equations are valid for processes in this dynamic range, Eqs. 9-11 are approximated by

$$\frac{D\rho_f}{Dt} = \frac{\tau}{\tau_e} (-\vec{E} \cdot \nabla \sigma - \rho_f \sigma) \quad (14)$$

$$\frac{D\sigma}{Dt} = \frac{\tau}{\tau_e} \left[\frac{\epsilon \alpha}{(b_+ + b_-)q} \right] (n - \sigma^2) \quad (15)$$

$$\frac{Dn}{Dt} = -\frac{\tau}{\tau_{th}} (n - \sigma^2) \quad (16)$$

By multiplying Eq. 16 by $(\tau_{th}/\tau_e)[\epsilon \alpha / (b_+ + b_-)q]$ and adding it to Eq. 15, it follows that

$$\frac{D}{Dt} \left[\sigma + \frac{\tau_{th}}{\tau_e} \frac{\epsilon \alpha}{(b_+ + b_-)q} n \right] = 0 \quad (17)$$

Now, if τ_{th} is short compared to times of interest, as depicted by Fig. 5.9.1, this expression becomes (with variables written in dimensional form),

$$\frac{D\sigma}{Dt} = 0 \quad (18)$$

For an observer attached to a given particle of the material, the conductivity is constant. In this limit, the conductivity can be regarded as a property of the material.

In unnormalized form, Eq. 14 is

$$\frac{D\rho_f}{Dt} = -\frac{\rho_f}{(\epsilon/\sigma)} - \vec{E} \cdot \nabla \sigma \quad (19)$$

In this charge relaxation expression, σ can now be regarded as a given parameter. These last two expressions constitute the "ohmic" model.

Maxwell's Capacitor: In terms of an ohmic model, the bipolar migration with generation and recombination is the two-region lossy capacitor of Fig. 5.9.2. The lower region is a fixed material, which according to Eq. 18 conserves its initially uniform conductivity. The upper region is of the same permittivity, but is insulating.

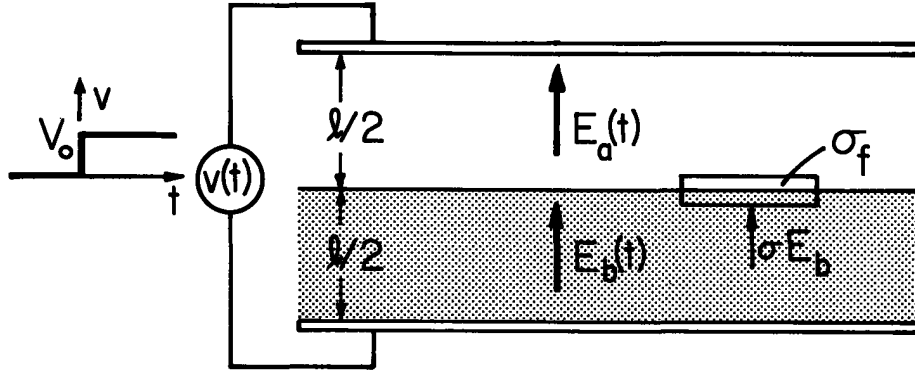


Fig. 5.9.2. Maxwell capacitor model for bipolar migration of Fig. 5.8.6.

As will be shown in the next section, with the application of a constant voltage V_0 to the electrodes, there is never a net free charge density in the material. Hence, fields in each region are uniform, $E_a(t)$ and $E_b(t)$. Because of the voltage constraint,

$$E_a \frac{l}{2} + E_b \frac{l}{2} = v \quad (20)$$

Accumulation of surface charge $\sigma_f = \epsilon E_a - \epsilon E_b$ at the interface between the lossy material and the insulating upper region is caused by the conduction current σE_b feeding the interface. (This boundary condition is considered in general terms in Sec. 5.11). Thus,

$$\frac{d}{dt} (\epsilon E_a - \epsilon E_b) = \sigma E_b \quad (21)$$

These two expressions combine to give a differential equation for the field inside the lossy material with the applied voltage as a drive:

$$\frac{dE_b}{dt} + \frac{\sigma}{2\epsilon} E_b = \frac{1}{l} \frac{dv}{dt}; \quad E_a = \frac{2v}{l} - E_b \quad (22)$$

It follows that the transient resulting from the application of a step in voltage to the amplitude V_0 is

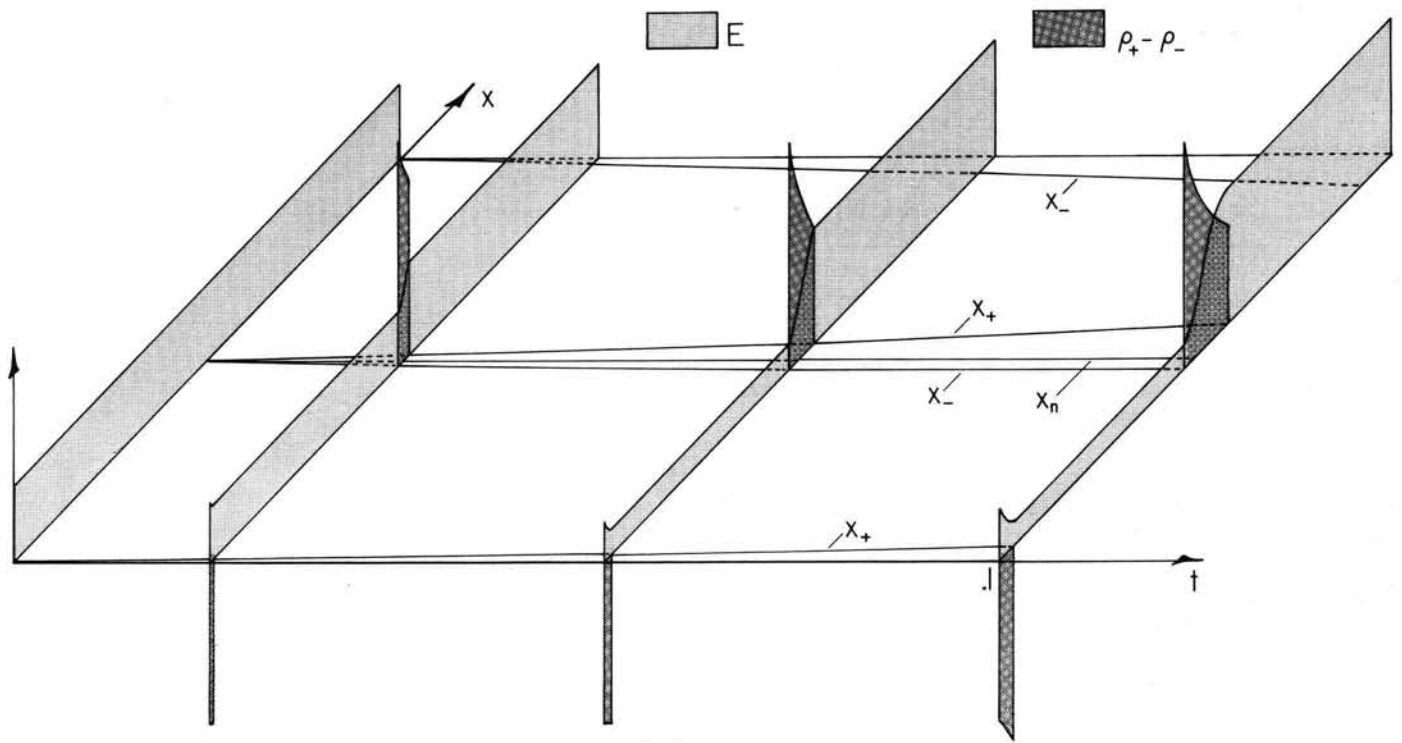
$$E_b = \frac{V_0}{l} e^{-t/\tau_e}; \quad \sigma_f = \frac{2\epsilon V_0}{l} [1 - e^{-t/\tau_e}]; \quad \tau_e \equiv 2\epsilon/\sigma \quad (23)$$

Numerical Example: (The numerical analysis of this section was carried out by R. S. Withers) Now, by comparing the predictions of the ohmic model to the "exact" solution afforded by the numerical scheme described in Sec. 5.8, consider the response of the Maxwell capacitor to a step in applied voltage. The configuration, shown in Fig. 5.8.3, is initially with the lower half of the region between the electrodes uniformly filled with positive and negative charge densities. In this lower region, generation and recombination are initially in equilibrium, as represented by Eq. 7. Thus, there is also an initial uniform distribution of n in the lower region.

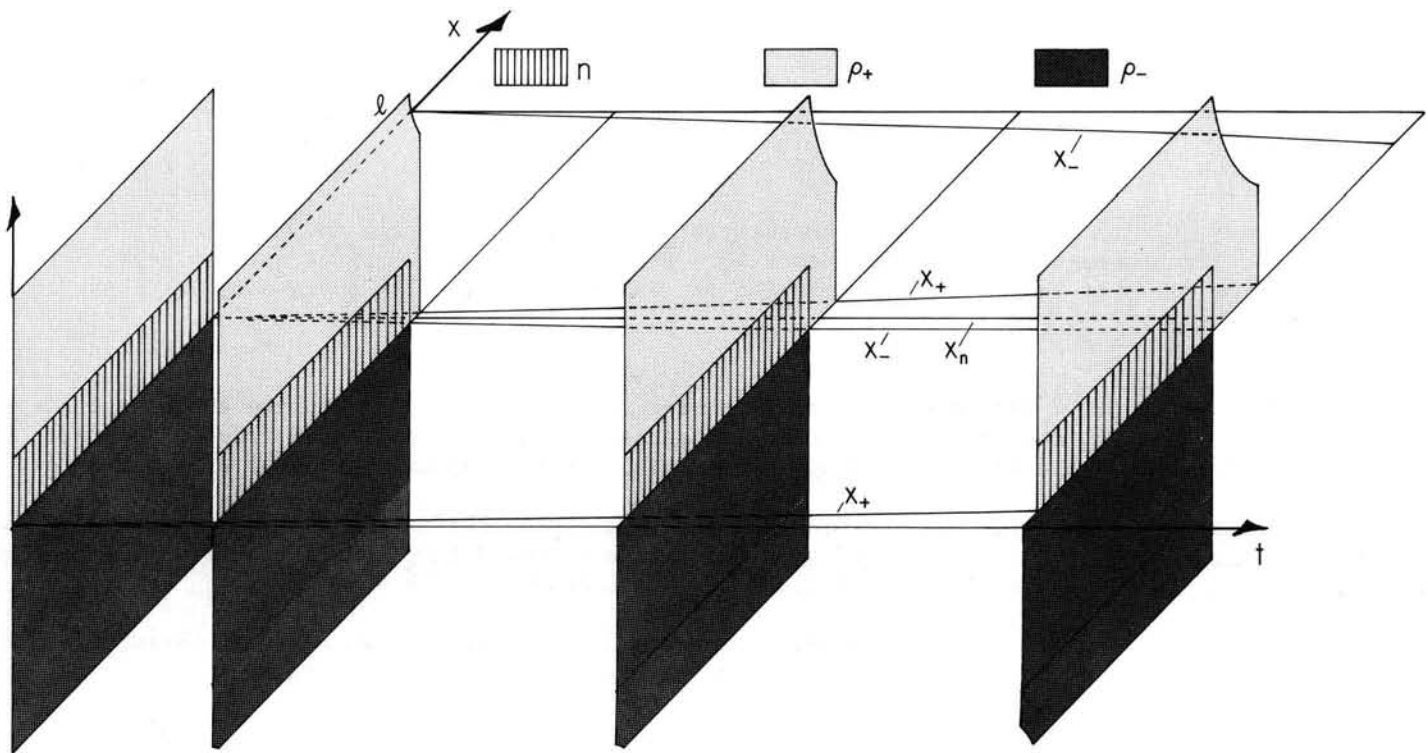
With parameters arranged so that the characteristic times have the ordering shown in Fig. 5.9.1, the response to a step in applied voltage is displayed by Fig. 5.9.3. As would be expected from the ohmic Maxwell capacitor model, the electric field in the conducting region, shown by Fig. 5.9.3a, decays exponentially with the time constant τ_e , while the surface charge "density" builds up with a similar time constant (Eqs. 23).

Figure 5.9.4 identifies some of the regions demarked by the three families of characteristics, particularly those emanating from the initial position of the interface. Regions I and IV are described by the Maxwell capacitor model. This means that the electric field on the demarking characteristics x_+ and x_- is known. For example, on x_- , \vec{E} is given by Eq. 23. Thus, the characteristic equation, Eq. 5.8.15c, can be integrated to delimit region I. In region I, charge neutrality prevails and generation is in equilibrium with recombination.

To further refine the picture, the role of the neutrals in determining the generation of new charged particle pairs must be recognized. Because region III is "ahead" of the neutral characteristic originating at the interface, this region is one where neutrals can only be created by recombination,



(a)



(b)

Fig. 5.9.3. Evolution of (a) field and free charge density and (b) charged particles and neutrals, with recombination and generation in the Maxwell capacitor configuration of Fig. 5.9.2. When $t = 0$, voltage is turned on. Characteristics x_+ and x_- are in the x - t plane. Neutral characteristics are $x_n = \text{constant}$. For the case shown, $b_+ = b_-$, $t = \frac{t}{\tau_{\text{mig}}}$, where τ_{mig} is given by Eq. 12 with $\mathcal{E} = V_0/l$. Also, initially $\rho_+ = \rho_- = 30\epsilon_0 V_0/l^2$, $n = \epsilon V_0/ql^2$ (i.e., 30 ion pairs for each neutral so that according to Eq. 13, $\tau_{\text{th}} = \tau_e/30$ and β is equilibrium value given by Eq. 7. Recombination is Langevin (Eq. 5.8.4).

Because there are no negative charges in this region, there is no recombination and hence no neutrals. Initially, in region II, there are neutrals. However, because of the high degree of ionization intrinsic to the ohmic model ($\tau_{th} \ll \tau_e$), the generation in this region (which for lack of negative charges is not balanced by recombination) quickly depletes the neutrals. Essentially, the neutral density in region II is zero. Thus, in both regions II and III, essentially unipolar dynamics prevail, with the positive charge density decaying in accordance with Eq. 5.6.6 and the initial charge density, essentially determined by ρ_+ where the characteristic enters region II from region I, equal to ρ_+ in the equilibrium region.

This unipolar picture of the charge density decay along an x_+ characteristic in regions II and III explains why ρ_+ decays with increasing x at any given time. Characteristics x_+ entering region II at A and A' (Fig. 5.9.4) carry the same equilibrium charge density. Thus there is more time for decay of ρ_+ at point B than there is at B', even though B and B' are at the same instant in time.

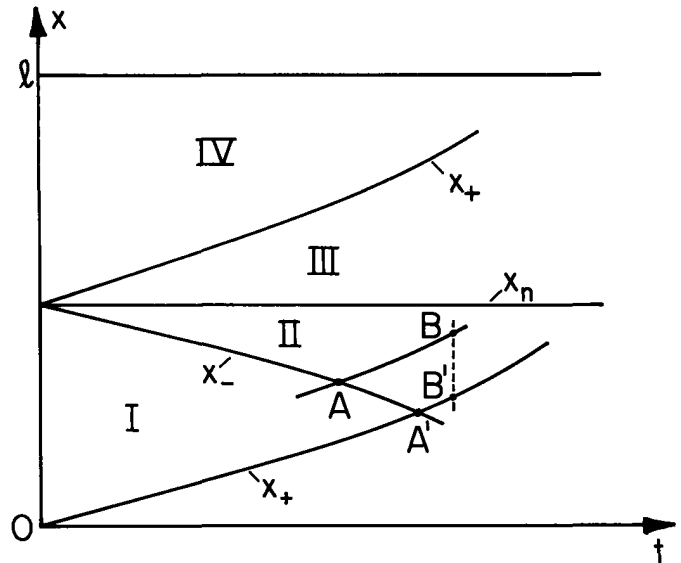


Fig. 5.9.4. Regions in $x-t$ plane delimited by characteristic lines emanating from initial interface position.

DYNAMICS OF OHMIC CONDUCTORS

5.10 Charge Relaxation in Deforming Ohmic Conductors

If it is taken as an empirically substantiated fact that a material at rest is an ohmic conductor, then, moving in an inertial (primed) frame of reference, it is described by the constitutive law

$$\vec{J}'_f = \sigma \vec{E}' \quad (1)$$

The conductivity, $\sigma(\vec{r}, t)$, is a parameter characterizing (and hence tied to) the material. The electroquasistatic transformation laws require that $\vec{E}' = \vec{E}$ but that $\vec{J}'_f = \vec{J}_f - \rho_f \vec{v}$ (Eqs. 2.5.9a and 2.5.12a) and show that in terms of laboratory-frame variables, the constitutive law implied by Eq. 1 is

$$\vec{J}_f = \sigma \vec{E} + \rho_f \vec{v} \quad (2)$$

With the use of Eq. 2 to describe an accelerating material goes the postulate that the conduction process is not altered by material accelerations. Because of the high collision frequency between charge carriers and the molecules comprising the material, this is usually an excellent assumption.

In this section, it is further assumed that polarization can be modeled in terms of a permittivity $\epsilon(\vec{r}, t)$, in general a function of space and time. Like the conductivity, ϵ is a property tied to the material. Also, the given material deformations are incompressible: $\nabla \cdot \vec{v} = 0$.

The fundamental laws required to define the relaxation process picture \vec{E} as irrotational, relate ρ_f to \vec{E} through Gauss' law ($\nabla \cdot \epsilon \vec{E} = \epsilon \nabla \cdot \vec{E} + \vec{E} \cdot \nabla \epsilon$) and invoke conservation of charge:

$$\vec{E} = -\nabla \phi \quad (3)$$

$$\nabla \cdot \vec{E} = \frac{\rho_f}{\epsilon} - \frac{\vec{E} \cdot \nabla \epsilon}{\epsilon} \quad (4)$$

$$\nabla \cdot \vec{J}_f + \frac{\partial \rho_f}{\partial t} = 0 \quad (5)$$

The charge relaxation equation is obtained by entering \vec{J}_f from Eq. 2 into Eq. 5, using Eq. 4 to replace the divergence of \vec{E} and remembering that \vec{v} is solenoidal,

$$\frac{\partial \rho_f}{\partial t} + \vec{v} \cdot \nabla \rho_f = -\frac{\sigma}{\epsilon} \rho_f - \vec{E} \cdot \nabla \sigma + \frac{\sigma}{\epsilon} \vec{E} \cdot \nabla \epsilon \quad (6)$$

For a material of uniform permittivity, this is the same expression as Eq. 5.9.19, a fact that emphasizes the multispecies contribution to the conduction process necessary to justify the use of the ohmic model.

If characteristic lines are defined as the trajectories of fluid elements, then

$$\frac{d\vec{r}}{dt} = \vec{v} \quad (7)$$

and time is measured for an observer moving along a line satisfying Eq. 7, the charge relaxation equation, Eq. 6, becomes

$$\frac{d\rho_f}{dt} = -\frac{\sigma}{\epsilon} \rho_f - \vec{E} \cdot \nabla \sigma + \frac{\sigma}{\epsilon} \vec{E} \cdot \nabla \epsilon \quad (8)$$

For an observer moving with the material, the three terms on the right are the possible contributors to a time rate of change of the charge density. Respectively, they represent the relaxation of the charge due to its self-field, the possible accumulation of charge where the electrical conductivity varies, and where the permittivity is inhomogeneous. Typically, these latter two terms are at interfaces, and hence are singular.

Region of Uniform Properties: In this case, the last two terms in Eq. 8 are zero, and the equation can be integrated without regard for details of geometry and boundary conditions:

$$\rho_f = \rho_0(\vec{r}) e^{-t/\tau_e}; \quad \tau_e \equiv \epsilon/\sigma \quad (9)$$

For the neighborhood of a given material particle, ρ_0 is the charge density when $t = 0$. With Eq. 9, it has been deduced that at a given location within a deforming material having uniform conductivity and permittivity, the free charge density is zero unless that point can be traced backward in time along a particle line to a source of free charge density.

The general solution summarized by Eq. 9 has a physical significance which is best emphasized by considering two typical situations, one where the initial charge distribution is known, and the other involving a condition on the charge density where characteristic lines enter the volume of interest.

Suppose that the charge distribution is to be determined in an ohmic fluid as it passes between plane-parallel walls in the planes $x = 0$ and $x = d$. The flow is in the steady state with a velocity profile that is consistent with fully developed laminar flow:

$$\vec{v} = \frac{4x}{d} \left(1 - \frac{x}{d}\right) U \vec{i}_z \quad (10)$$

Initial Value Problem: When $t = 0$, the charge distribution throughout the flow is known to be

$$\rho_f(x, 0) = \rho_t \sin(kz) \quad (11)$$

This distribution is sketched in Fig. 5.10.1a. For the given steady velocity distribution, it is simple to integrate Eq. 7 to find the characteristic lines $x = x_0$, $y = y_0$ and

$$z = \frac{4x}{d} \left(1 - \frac{x}{d}\right) Ut + z_0 \quad (12)$$

The integration constant, z_0 , is the z intercept of the characteristic line with the $t = 0$ plane. Figure 5.10.1b represents these characteristic lines in the x - z - t space. In the channel center, the characteristic line has its greatest slope (U) in the z - t plane, while at the channel edges the slope is zero. The lines take the same geometric shape regardless of z_0 , and therefore other families of lines are generated by simply translating the picture shown along the z axis.

Now according to Eq. 9, the charge density at any time $t > 0$ is found by evaluating the initial charge density at the root of a characteristic line, when $t = 0$, and following that line to the point in question. The charge decays along this line by an amount predicted by the exponential equation using the elapsed time. If (x, z, t) represent the coordinates where the solution is required at some later time, then these coordinates are related to z_0 through Eq. 12, and the initial charge density appropriate to the point in question is given by Eq. 11 with $z \rightarrow z_0$. Thus, the required solution is

$$\rho_f(x, z, t) = \rho_t \sin k \left[z - \frac{4x}{d} \left(1 - \frac{x}{d}\right) Ut \right] e^{-t/\tau_e} \quad (13)$$

This distribution is the one sketched in Fig. 5.10.1c.

The consequences of a boundary-value transient serve to provide further background for establishing the point of this section.

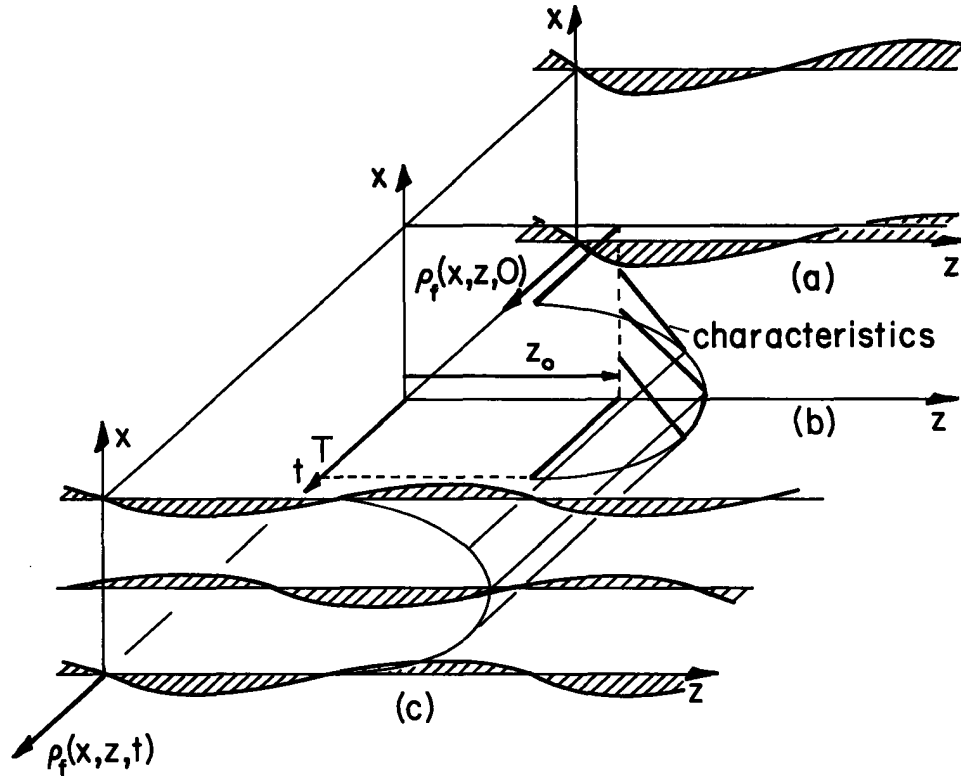


Fig. 5.10.1. (a) The initial distribution of charge density as a function of (x,z) . (b) Characteristic lines in (x,z,t) space. Those lines originating along the cross section $z = z_0$ when $t = 0$ are shown. (c) Distribution of charge density by the time $t = T$. Charge is transported downstream in proportion to the stream velocity, and decays as $\exp(-t/\tau_e)$.

Injection from a Boundary: It is possible to inject charge into the bulk of an ohmic fluid so that a steady-state condition can be established with a space charge in the material volume. However, the position of interest in the material bulk must then be joined by a characteristic line to a source of charge. As an illustration, consider the case where, initially, there is no charge in the material. Again, the fluid flow of Eq. 10 is considered. However, now charge is introduced by a source in the plane $z = 0$. When $t = 0$, this source is turned on and provides a volume charge density ρ_s henceforth at $z = 0$. The problem is then one of finding the resulting downstream charge distribution. The boundary condition is shown graphically in Fig. 5.10.2a.

For this type of problem, the characteristic lines of Eq. 12 are more conveniently used if written in terms of the time $t = t_a$ when a given characteristic intercepts the $z = 0$ plane, where the source of charge is located, and it is known that for $t > 0$, the charge density is ρ_s . Then

$$z = \frac{4x}{d} \left(1 - \frac{x}{d}\right) U(t - t_a) \quad (14)$$

The family of characteristics having roots in the $z = 0$ plane when $t = t_a$ is sketched in Fig. 5.10.2b.

From the characteristic lines of the sketch, Fig. 5.10.2b, it follows that the distribution of charge can be divided into two regions, the surface of demarcation between the two being the surface formed by the characteristic lines with $t_a = 0$. For z greater than the envelope of these characteristic

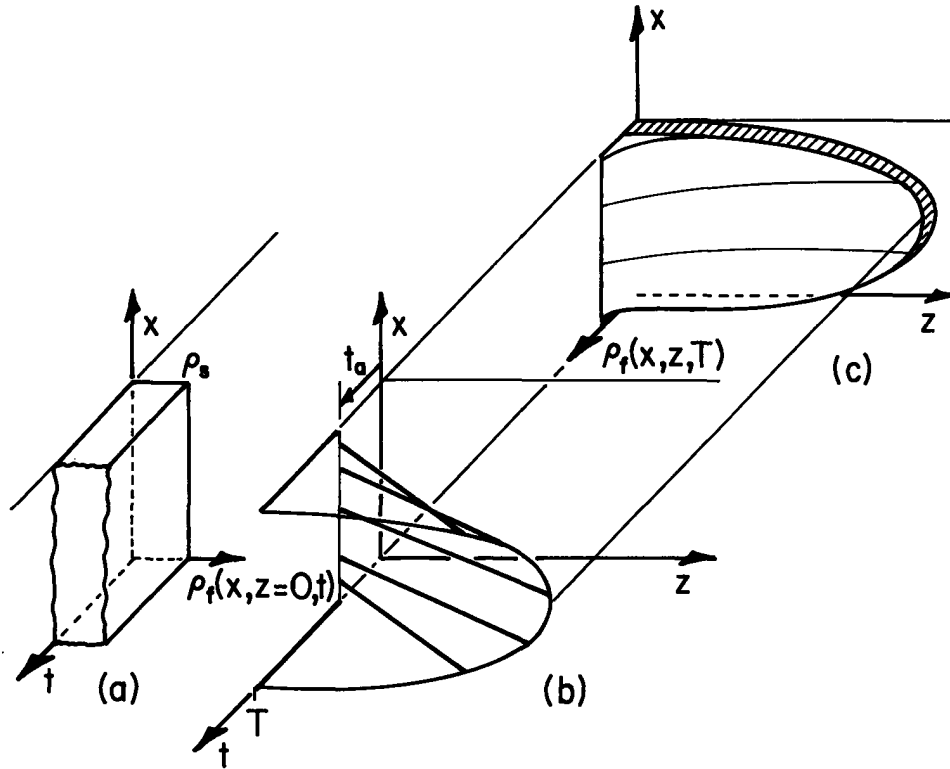


Fig. 5.10.2. (a) When $t = 0$, a uniform and henceforth constant source of charge is turned on at $z = 0$. (b) Characteristic lines. (c) Later distribution of charge density.

lines there is no response, because the characteristic lines originate from the $z = 0$ plane at a time when the charge density is constrained to be zero. For z less than the envelope, the initial charge distribution at $z = 0$ is the constant ρ_s . Thus, there is a wavefront between the two regions, as sketched in Fig. 5.10.2c. The charge density at any point behind the wavefront is determined by multiplying $\exp[-(t-t_a)/\tau_e]$ times the charge density at $z=0$. That is, the appropriate evaluation of Eq. 9 is \times

$$\rho_f = \rho_s e^{-(t-t_a)/\tau_e} \quad (15)$$

and in view of the relation between a point in question (x,z,t) and the time of origination from the $z = 0$ plane, t_a (given by Eq. 14), the charge distribution of Eq. 15 can be written in terms of (x,z,t) as

$$\rho_f = \rho_s e^{-z/[v(x)\tau_e]} ; \quad v(x) = \frac{4x}{d} \left(1 - \frac{x}{d}\right)U \quad (16)$$

This stationary distribution of charge is shown in Fig. 5.10.2c.

Because of the dependence of the velocity on x , the spatial rate of decay behind the front depends on the transverse position x . At the center of the channel, where the velocity is U , the spatial rate of decay is determined by the ratio of the relaxation time to the time required for the material to transport the charge to the given z position in question. This ratio is a measure of the influence of the material motion on the charge distribution: for a characteristic length ℓ in the z direction, it is convenient to define the electric Reynolds number of an ohmic conductor as

$$R_e \equiv (\epsilon/\sigma)/(\ell/U) = \frac{\epsilon U}{\sigma \ell} \quad (17)$$

and Eq. 16, written for the channel center where $x = d/2$, becomes

$$\rho_f\left(\frac{d}{2}, z, t\right) = \rho_s e^{-\frac{z}{\ell} (1/R_e)} \quad (18)$$

At a given location z , once the wavefront has passed, the response represented in general by Eq. 9 is independent of time.

5.11 Ohmic Conduction and Convection in Steady State: D-C Interactions

The one-dimensional configuration of Fig. 5.7.1 is revisited in this section using an ohmic rather than a unipolar model. This gives the opportunity to exemplify the role of the electric field and boundary conditions while making a contrast between the ohmic model, introduced in Sec. 5.10 and the unipolar model of Sec. 5.7. As in Sec. 5.7, the model is used to demonstrate a type of "d-c" pump or generator exploiting longitudinal stresses. Again, screen electrodes are used to charge a uniform z -directed flow: $\vec{v} = U\vec{i}_z$.

Because the fluid has uniform properties, the steady one-dimensional form of Eq. 5.10.6 is

$$\frac{d\rho_f}{dz} + \frac{\sigma}{U\epsilon} \rho_f = 0 \quad (1)$$

and it follows directly that the space-charge distribution is exponential:

$$\rho_f = \rho_o e^{-z/R_e \ell}; \quad R_e \equiv \frac{\epsilon v}{\sigma \ell} \quad (2)$$

The electric Reynolds number R_e is introduced at this point because it reflects such attributes of the flow as the efficiency of energy conversion.

Conservation of charge requires that in the steady state $\vec{J}_f = J\vec{i}_z$ is a constant: the total current I divided by the area A . Thus the constitutive law, Eq. 5.10.2, can be solved for $\vec{E} = E(z)\vec{i}_z$ with ρ_f substituted from Eq. 2:

$$E = \frac{i}{\sigma A} - \frac{\rho_o U}{\sigma} e^{-z/R_e \ell} \quad (3)$$

In turn, the terminal potential is determined,

$$v = -\int_0^\ell E dz = -\frac{i\ell}{\sigma A} + \frac{\rho_o \ell U}{\sigma} R_e (1 - e^{-1/R_e}) \quad (4)$$

This is the electrical terminal relation for the interaction: a "volt-ampere" characteristic sketched in Fig. 5.11.1.

The electrical force on the charged particles is fully transmitted to the vehicle fluid, and hence the pressure rise between inlet and outlet is simply the difference in electric stresses at $z = \ell$ and $z = 0$, evaluated using Eq. 3:

$$\Delta p = p_o - p_i = \frac{1}{2} \epsilon [E^2(\ell) - E^2(0)] = \frac{1}{2} \epsilon \left[\left(\frac{i}{\sigma A} - \frac{\rho_o U}{\sigma} e^{-1/R_e} \right)^2 - \left(\frac{i}{\sigma A} - \frac{\rho_o U}{\sigma} \right)^2 \right] \quad (5)$$

This mechanical "terminal relation" has a dependence on the terminal current i summarized by Fig. 5.11.1. Observe that $i_{sc} < i_{bp}$, where the short-circuit and zero pressure-rise currents follow from setting Eqs. 4 and 5 to zero:

$$I_{sc} = A \rho_o U R_e (1 - e^{-1/R_e}) \quad (6)$$

$$I_{bp} = A \rho_o U (1 + e^{-1/R_e})/2 \quad (7)$$

Three energy conversion regimes are defined by recognizing that the electrical power out is $P_e = VI$, while the mechanical power in is $P_m = -\Delta pUA$. Each of these quantities must be positive to give a generator function. Similarly, if both P_e and P_m are negative, energy is converted from electrical to mechanical form and the device is a pump. There is a midregion, which tends to vanish as R_e is increased, wherein both electrical and mechanical energy are absorbed. This region gives a braking effect at the expense of electrical energy. These three regimes are summarized by Fig. 5.11.1.

The Generator Interaction: A primary limitation on electrohydrodynamic energy conversion devices is the relatively small electric pressure that can be obtained without incurring electrical breakdown. Difficulties in making an efficient converter are amplified by the extremely small fraction of the available mechanical energy that is altered by the electric coupling. It is clear from Eq. 5 that any electric stress at the outlet detracts from the total pressure change. To take the greatest advantage of the available electric stress, $E(\ell)$ should be adjusted to vanish. This can be done, according to Eq. 3, by operating with the space-charge density

$$\rho_0 v = \frac{I}{A} e^{1/R_e} \tag{8}$$

It follows from Eq. 4 that (use upper sign):

$$P_e = -\frac{I^2 \ell}{\sigma A} [1 \pm R_e (1 - e^{+1/R_e})] \tag{9}$$

while Eq. 5 shows that (upper sign)

$$P_m = \pm \frac{UAE}{2} \left(\frac{I}{\sigma A}\right)^2 (1 - e^{+1/R_e})^2 \tag{10}$$

The efficiency of energy conversion from mechanical to electrical form is then only a function of the electric Reynolds number (upper sign)

$$P_e/P_m = 2[+R_e (e^{+1/R_e} - 1) - 1]/[+R_e (1 - e^{+1/R_e})^2] \tag{11}$$

Of course, the conversion becomes perfectly efficient as $R_e \rightarrow \infty$. The detailed dependence is shown in Fig. 5.11.2.

The Pump Interaction: If it is a pumping function that is desired, Eq. 5 makes it clear that the space charge should be adjusted so that $E(0) = 0$, and it follows from Eq. 3 that

$$\frac{I}{A} = \rho_0 v \tag{12}$$

The electrical and mechanical powers are now given by Eqs. 9 and 10 using the lower signs. In turn, the efficiency of electrical to mechanical conversion is the reciprocal of Eq. 11, using the lower signs. This pumping efficiency is summarized also in Fig. 5.11.2.

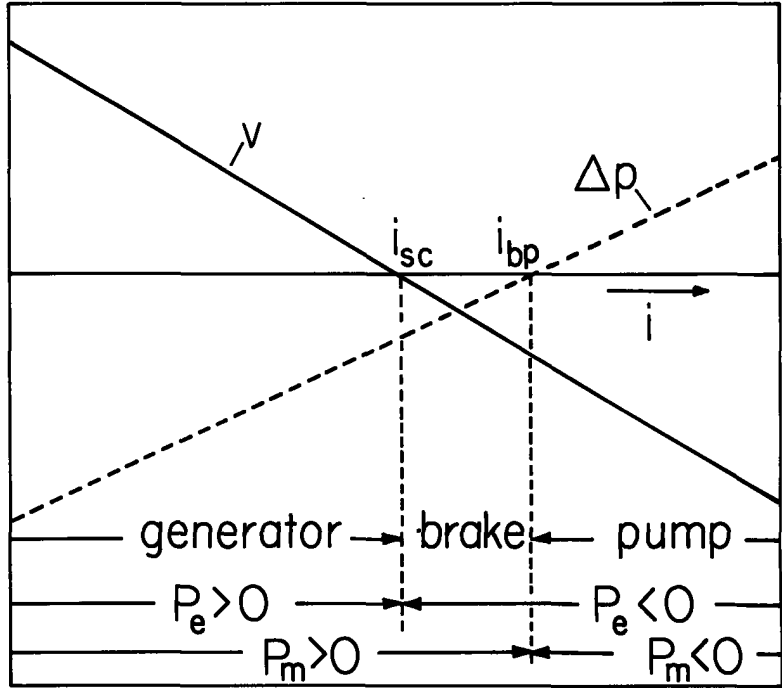


Fig. 5.11.1. Dependence of terminal voltage and pressure rise on terminal current i . Energy conversion regimes are as indicated.

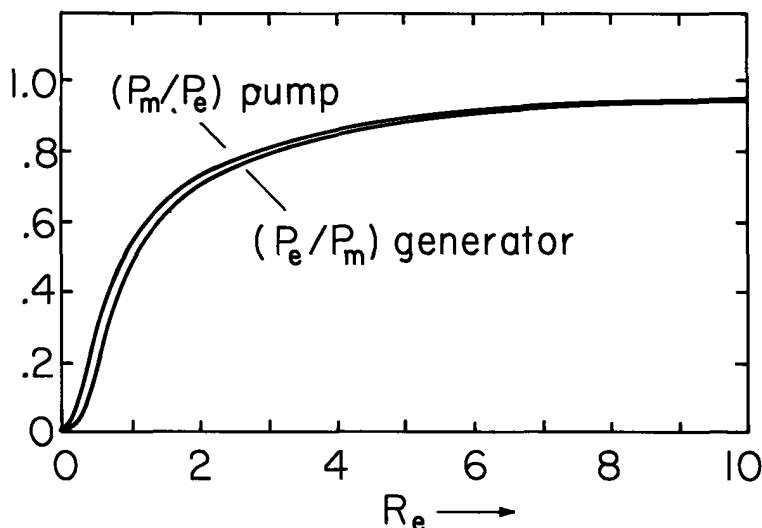


Fig. 5.11.2

Energy conversion efficiency of one-dimensional flow with ohmic fluid and immobile charged particles.

5.12 Transfer Relations and Boundary Conditions for Uniform Ohmic Layers

Transport Relations: In a region having uniform conductivity and permittivity, the free charge density is zero unless the material occupying the region can be traced back along a particle line to a source of charge. With the understanding that charge-free bulk regions are being described, it follows from either Gauss' Law or conservation of charge (Eqs. 5.10.4 or 5.10.5) that \vec{E} is solenoidal in the bulk of such regions. Because \vec{E} is also irrotational (Eq. 5.10.3), it follows that the distribution of potential Φ is governed by Laplace's equation. To describe the volume field distributions, the same relations are applicable as used to derive the flux-displacement relations of Sec. 2.16. The transfer relations for planar layers, cylindrical annuli and spherical shells summarized in Sec. 2.16 are also applicable to regions having uniform conductivity. Because the effect of material motion on the fields comes from the convection of the free charge density, and ρ_f is zero in the material, these relations hold even if the material is moving. For example, the planar layer of Table 2.16.1 could be moving in the z direction with an arbitrary velocity profile.

In conjunction with the transfer relations, the conduction currents normal to the bounding surfaces (α, β) are of interest, and these are simply

$$\begin{bmatrix} \tilde{j}_n^\alpha \\ \tilde{j}_n^\beta \end{bmatrix} = \sigma \begin{bmatrix} \tilde{E}_n^\alpha \\ \tilde{E}_n^\beta \end{bmatrix} \quad (1)$$

where n signifies a coordinate normal to the (α, β) surfaces and σ has the value appropriate to the region between.

Conservation of Charge Boundary Condition: A typical model involves two or more materials having uniform properties and separated by interfaces. The boundary condition implied by the requirement that charge be conserved is given with some generality by Eq. 2.10.16. With the proviso that the regions neighboring the interface have the nature described in the previous paragraph, the volume current densities are simply $\vec{j}_f = \sigma \vec{E}$. In certain situations, the interface is itself comprised of a thin region over which the conductivity is appreciably greater than in the bulk. Then, a surface conductivity σ_s is used to model a surface conduction and the surface current density is

$$\vec{k}_f' = \sigma_s \vec{E}_t \Rightarrow \vec{k}_f = \sigma_s \vec{E}_t + \vec{v}_t \sigma_f \quad (2)$$

where the subscript t means that only components of the vector tangential to the interface contribute and σ_f is the surface charge density. Incorporating the appropriate values of \vec{j}_f and \vec{k}_f , the required boundary condition, Eq. 2.10.16, becomes

$$\frac{\partial \sigma_f}{\partial t} + \nabla_\Sigma \cdot (\sigma_s \vec{E}_t + \vec{v}_t \sigma_f) + \vec{n} \cdot [\sigma \vec{E}] = 0 \quad (3)$$

The tangential component of \vec{E} is continuous at the interface, and so \vec{E}_t or the potential can be evaluated on either side of the interface.

As an example used in subsequent sections, suppose that the interface is planar (in the y-z plane) and moves with the uniform velocity U in the z direction. Then, for $\vec{n} = \vec{i}_x$, Eq. 3 becomes

$$-\left(\frac{\partial \sigma_f}{\partial t} + U \frac{\partial \sigma_f}{\partial z}\right) = \sigma_s \left(\frac{\partial E_y}{\partial y} + \frac{\partial E_z}{\partial z}\right) + \llbracket \sigma E_x \rrbracket \quad (4)$$

Physically, this expression states that, for an observer moving with the material, the rate of decrease of σ_f with respect to time is proportional to the conduction current flowing out of the interfacial region in the plane of the interface and to the disparity between volume conduction currents leaving and entering from the bulk regions to either side of the interface.

5.13 Electroquasistatic Induction Motor and Tachometer

A configuration for establishing basic notions concerned with electric induction interactions is shown in Fig. 5.13.1, where a thin sheet having surface conductivity σ_s moves uniformly in the z-direction with the velocity U.¹ At a distance d above the sheet, a traveling wave of potential is imposed by means of electrodes, while the potential a distance d below is constrained by a solid electrode to be constant. The objective in this section is to determine the dependence of the electrical shear force tending to carry the sheet in the z direction on the frequency ω , the relative material and wave velocities, and the electrical surface conductivity. Later, the configuration is used to make a tachometer. In actual construction, the sheet might be wrapped around on itself to form a rotating shell.

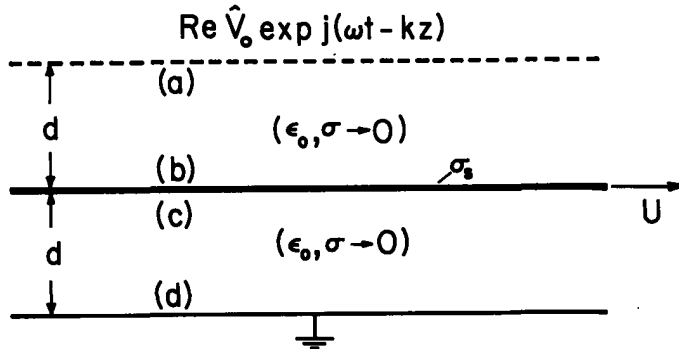


Fig. 5.13.1

A conducting sheet moves with velocity U and interacts with traveling waves of potential imposed on adjacent electrodes.

The active volume breaks into two regions joined by the conducting sheet. Thus, an analytical model simply involves the combination of transfer relations for the free space regions, and the boundary conditions for the sheet. The transfer relations of Table 2.16.1, Eqs. (a), become

$$\begin{bmatrix} \hat{D}_x^a \\ \hat{D}_x^b \end{bmatrix} = \begin{bmatrix} -\epsilon_0 k \coth(kd) & \frac{\epsilon_0 k}{\sinh(kd)} \\ \frac{-\epsilon_0 k}{\sinh(kd)} & \epsilon_0 k \coth(kd) \end{bmatrix} \begin{bmatrix} \hat{V}_0 \\ \hat{\phi}^b \end{bmatrix} \quad (1)$$

where the surface potentials have been identified as those of the electrodes and sheet, and the variables refer to the upper region with superscripts as defined in Fig. 5.13.1. From Eq. 5.12.4 with $\partial(\)/\partial y = 0$ and $\llbracket J_x \rrbracket = 0$ (the regions adjacent to the sheet are insulating),

$$\sigma_s k^2 \hat{\phi}^b + j(\omega - kU)(\hat{D}_x^b - \hat{D}_x^c) = 0 \quad (2)$$

where it is recognized that the net surface charge density on the sheet is $(\hat{D}_x^b - \hat{D}_x^c)$. Finally, the description is completed by the transfer relations for the lower region, again provided by Table 2.16.1:

$$\begin{bmatrix} \hat{D}_x^c \\ \hat{D}_x^d \end{bmatrix} = \begin{bmatrix} -\epsilon_0 k \coth(kd) & \frac{\epsilon_0 k}{\sinh(kd)} \\ \frac{-\epsilon_0 k}{\sinh(kd)} & \epsilon_0 k \coth(kd) \end{bmatrix} \begin{bmatrix} \hat{\phi}^b \\ 0 \end{bmatrix} \quad (3)$$

1. For description of a somewhat similar device, see S. D. Choi and D. A. Dunn, "A Surface-Charge Induction Motor," Proc. IEEE 59, No. 5, 737-748 (1971).

Incorporated in the potentials on the right are the boundary conditions that $\phi^b = \phi^c$ and $\phi^d = 0$. These three expressions can be viewed as five equations for the unknowns ϕ^b and $(D_x^a, D_x^b, D_x^c, D_x^d)$. Before further manipulation is undertaken, it is advisable to look forward to the required variables.

Induction Motor: Summation of shear stresses on the sheet (see Eq. 4.2.2) shows that the space-average force density in the z direction is

$$\langle T_z \rangle_z = \frac{1}{2} \text{Re} j k \hat{\phi}^b [\hat{D}_x^b - \hat{D}_x^c]^* \quad (4)$$

The total complex surface charge density required in Eq. 4 follows from the subtraction of Eqs. 1b and 3a:

$$\hat{D}_x^b - \hat{D}_x^c = \frac{-\epsilon_o k}{\sinh(kd)} \hat{V}_o + 2\epsilon_o k \coth(kd) \hat{\phi}^b \quad (5)$$

and substitution of this expression into Eq. 4 further reduces the surface force density to

$$\langle T_z \rangle_z = \frac{-\epsilon_o k^2}{2 \sinh(kd)} \text{Re} j \hat{\phi}^b \hat{V}_o^* \quad (6)$$

The complex sheet potential is found by again using Eq. 5, but this time to eliminate $\hat{D}_x^b - \hat{D}_x^c$ from Eq. 2:

$$\hat{\phi}^b = \frac{j S_e \hat{V}_o}{2 \sinh kd (1 + j S_e \coth kd)} \quad (7)$$

where S_e is product of the angular frequency $(\omega - kU)$ measured by an observer moving with the material velocity U and the relaxation time constant $2\epsilon_o/k\sigma_s$:

$$S_e = \frac{2\epsilon_o (\omega - kU)}{k\sigma_s} \quad (8)$$

The surface force density follows by substituting Eq. 7 into 6:

$$\langle T_z \rangle_z = \frac{\epsilon_o k^2 \hat{V}_o \hat{V}_o^*}{4 \sinh^2(kd)} \frac{S_e}{(1 + S_e^2 \coth^2 kd)} \quad (9)$$

This result is analogous to one obtained for a magnetic induction machine in Sec. 6.4. It exhibits a maximum which is determined by the frequency in the frame of the moving sheet relative to the effective relaxation time. That is, the optimum or largest electric surface force density is

$$\langle T_z \rangle_z = \frac{\epsilon_o k^2 \hat{V}_o \hat{V}_o^* \tanh(kd)}{8 \sinh^2(kd)} ; S_e = \tanh(kd) \quad (10)$$

Again, this result fits the general description of a "shearing" type of electromechanical energy converter given in Sec. 4.15. The surface force density takes the form of an electric stress $\epsilon_o (kV_o)^2/2$ multiplied by factors reflecting the geometry and charge relaxation phenomena. The factor $(\sinh kd)^{-2}$ represents the Laplacian decay of the fields from the excitation to the sheet and then back again.

A sketch of the dependence of $\langle T_z \rangle_z$ on S_e is shown in Fig. 5.13.2. The physical origins of this curve are understood by interpreting Eq. 7. At very low material-frame frequencies, $S_e \rightarrow 0$ and $\hat{\phi}^b \rightarrow 0$. The sheet behaves as a perfect conductor, supports no tangential electric field intensity, and hence no electrical force in the z direction.

In the opposite extreme, the frequency is large compared to the reciprocal relaxation time for the system of sheet and adjacent regions of free space, and the amount of surface charge induced on the sheet becomes small. This follows from Eqs. 5 and 7. The optimum of Fig. 5.13.2 represents the compromise between the extremes of S_e small, and hence the wrong lag angle, and S_e large and hence reduced sheet surface charge.

Electroquasistatic Tachometer: It is the induced force upon the moving, semi-insulating sheet that is emphasized so far. The reverse effect of the motion on the field is emphasized by the slightly

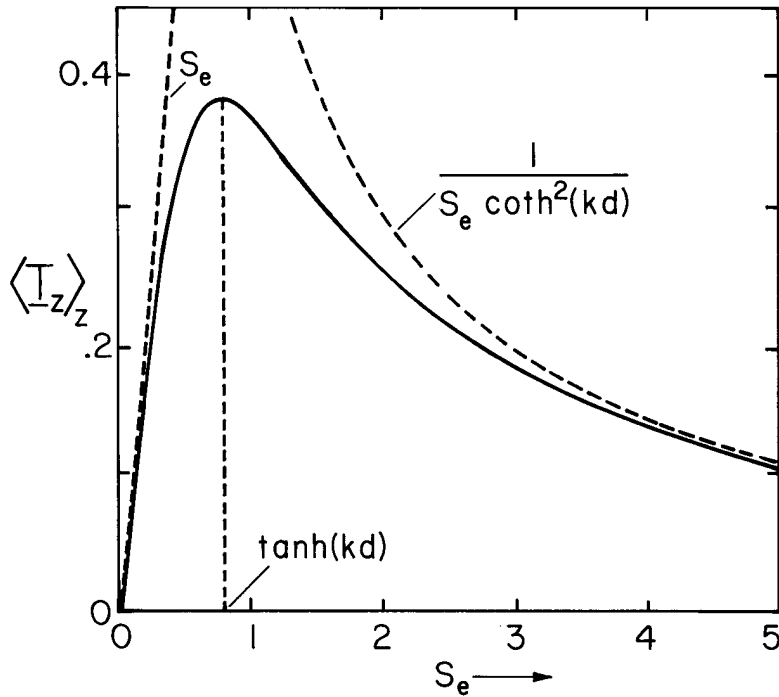


Fig. 5.13.2

Dependence of time-average surface force density normalized to $(\epsilon_0 |kV_0|^2 / 4 \sinh^2 kd)$ as a function of frequency in moving frame of reference, normalized to relaxation time. S_e is defined by Eq. 8 ($kd = 1$).

revised configuration of Fig. 5.13.3. Instead of a traveling wave, the imposed potential is now a standing wave. Points of zero amplitude retain fixed positions along the z axis. For the purpose of detecting the material velocity U , a pair of electrode segments is positioned in the grounded wall just below the moving sheet. The time variation of charge induced on these segments gives rise to a current, i , which is measured by means of external circuitry. Each segment is one half-wavelength, and positioned so that, in the absence of material motion, there is as much positive as negative surface charge induced on a segment surface. Thus, the electrodes are designed so that there is no output current in the absence of a material motion. But, with motion, the fields are skewed so that there is a net charge induced on each output segment. The result, an output signal v_o reflecting the material velocity U , is now going to be computed.

There is considerable analogy between the interaction studied here in the context of charge relaxation, and the magnetic diffusion example of Sec. 6.4. To make a practical device for measuring the rotational velocity of a shaft, the sheet pictured in Fig. 5.13.3 would be closed on itself, with the standing wave of imposed potential and the output segments perhaps arranged as in Fig. 5.13.4. By contrast with the conventional drag-cup tachometer, the sheet material in the device studied in this section would be made from semi-insulating material, rather than a metal.

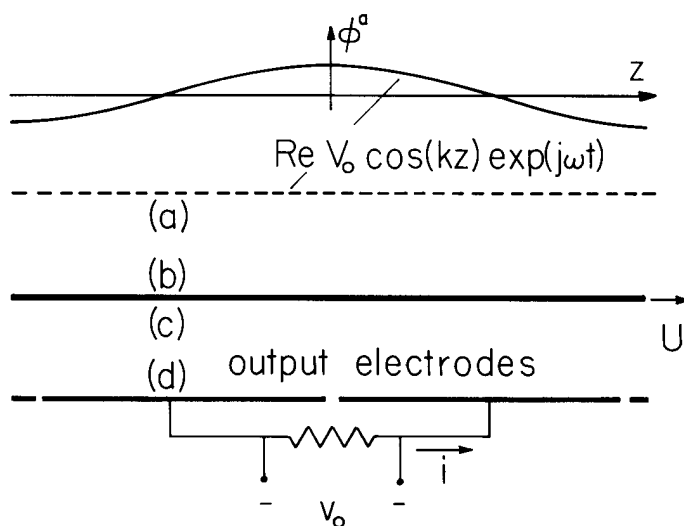


Fig. 5.13.3. A device for measuring the velocity U is made by exciting from above with a standing wave of potential and measuring the induced current on an electrode pair below the sheet.

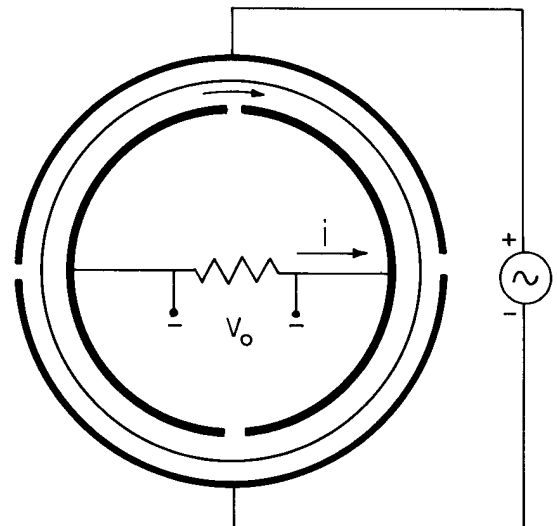


Fig. 5.13.4. Adaptation of the planar configuration of Fig. 5.13.3 to measure rotational velocity of shell of slightly conducting material.

The fields from a standing wave of excitation potential are simply the superposition of two of the traveling waves analyzed already. That is, the excitation can be written as

$$\hat{\phi}^a = \text{Re} \hat{V}_o \cos(kz) e^{j\omega t} = \text{Re} \frac{\hat{V}_o}{2} (e^{-jkz} + e^{jkz}) e^{j\omega t} \quad (11)$$

The surface charge induced on the equipotential plane below the moving sheet is desired. It is assumed that the current, i , is measured through a sufficiently small resistance that the output electrodes remain at essentially zero potential. Thus, the output electrode surface charge is simply D_x^d and is found from Eq. 3b, as the superposition of the responses to the two traveling-wave components of the drive identified by Eq. 11:

$$D_x^d = \frac{-\epsilon_o k}{\sinh(kd)} (\hat{\phi}_+^b + \hat{\phi}_-^b) \quad (12)$$

The potential amplitudes called for with Eq. 12 are given by evaluating Eq. 7 with $\hat{V}_o \rightarrow \hat{V}_o/2$ and k first positive and then negative:

$$\hat{\phi}_\pm = j S_{e\pm} \hat{V}_o / 4 \sinh(kd) [1 + j S_{e\pm} \coth(kd)] \quad (13)$$

$$S_{e\pm} \equiv 2\epsilon_o (\omega \mp kU) / k\sigma_s$$

The combination of Eqs. 12 and 13 give the space-time dependence of the charge induced on the lower surface:

$$D_x^d = -\text{Re} j \frac{\epsilon_o k \hat{V}_o}{4 \sinh^2(kd)} \left\{ \frac{S_{e+} e^{-jkz}}{1 + j S_{e+} \coth(kd)} + \frac{S_{e-} e^{jkz}}{1 + j S_{e-} \coth(kd)} \right\} e^{j\omega t} \quad (14)$$

The net charge on the right electrode is now computed by integrating the surface charge over its area, from $z = 0$ to $z = \pi/k$ and over the width w of the electrode in the y direction. The required current is the time rate of change of the net charge on the electrode, and therefore given by

$$\hat{i} = j\omega \hat{q} = - \frac{j\omega w \epsilon_o V_o}{2 \sinh^2(kd)} \left[\frac{S_{e+}}{1 + j S_{e+} \coth(kd)} - \frac{S_{e-}}{1 + j S_{e-} \coth(kd)} \right] \quad (15)$$

As required, the net charge on the electrode vanishes in the absence of a material motion. To see the dependence of the output current on the material velocity, Eq. 15 is expanded, using the definition of $S_{e\pm}$ from Eq. 13:

$$|\hat{i}| = I_o \frac{\left[\frac{2\epsilon_o \omega}{k\sigma_s} \coth(kd) \right] (kU/\omega)}{\sqrt{[1 + S_{e+}^2 \coth^2(kd)][1 + S_{e-}^2 \coth^2(kd)]}} \quad (16)$$

where

$$I_o \equiv \frac{\omega \epsilon_o |\hat{V}_o| w}{\sinh(kd) \cosh(kd)}; \quad S_{e\pm} \equiv \frac{2\epsilon_o \omega}{k\sigma_s} (1 \mp \frac{kU}{\omega})$$

With the excitation frequency large compared to kU , the dependence of $S_{e\pm}$ on U is weak, and Eq. 16 shows that the output current is then a linear function of the material velocity. The general dependence of $|\hat{i}|$ on the ratio of sheet velocity to wave phase velocity, ω/k , is illustrated in Fig. 5.13.5.²

2. For a similar approach to measuring fluid velocity, see J. R. Melcher, "Charge Relaxation on a Moving Liquid Interface," *Phys. Fluids* 10, 325-331 (1967).

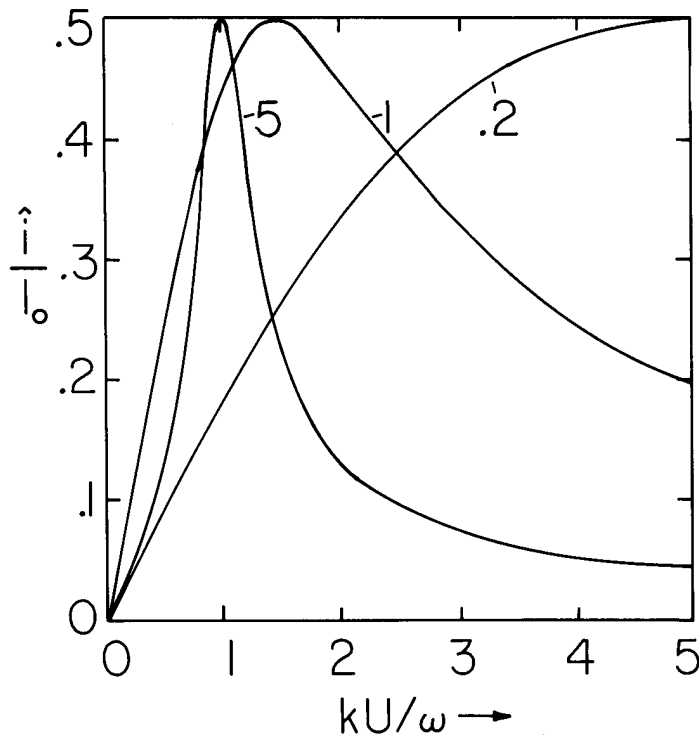


Fig. 5.13.5.

Dependence of output signal on material velocity U relative to phase velocity (ω/k) for tachometer of Fig. 5.13.3. Parameter is $2\epsilon_0\omega\coth(kd)/k\sigma_s$.

5.14 An Electroquasistatic Induction Motor; Von Quincke's Rotor

The configuration of Fig. 5.14.1 gives the opportunity to study charge relaxation for finite-thickness conductors. Regions (a) and (b) are each composed of homogeneous materials having uniform conductivity and permittivity. The b-c interface moves to the right with a uniform velocity, U . The materials may move as rigid bodies with this same velocity, or might be composed of fluids which have some unspecified velocity profile $\vec{v} = v_z(x)\hat{i}_z$. They are bounded from below by a constant-potential plane, and from above by a system of electrodes used to impose a traveling wave of potential.

An objective is to determine the fields and hence the electrical surface force density acting on the interface in the direction of motion. From Sec. 5.10 it is known in advance that the only charges within the moving materials exist where the conductivity and permittivity have a spatial variation, at the interface. The planar configuration could be a developed model for a system "closed on itself" so that the interaction considered would be between a system of rotating, semi-insulating materials and an imposed rotating electric field. Except for geometric factors, the torque on the semi-insulating rotor sketched in Fig. 5.14.2 depends on the physical parameters and the imposed fields in essentially the same way as for the planar case study (see Problem 5.14.1).

The potential is the given traveling wave at the boundary denoted by (a), is continuous at the interface, and must vanish at the lower boundary ($\hat{\phi}^a = V_0, \hat{\phi}^b = \hat{\phi}^c, \hat{\phi}^d = 0$). Thus, the transfer relations representing the field distributions in the bulk of each region, Eqs. (a) of Table 2.16.1, are

$$\begin{bmatrix} \hat{D}_x^a \\ \hat{D}_x^b \end{bmatrix} = \begin{bmatrix} -\epsilon_a k \coth(ka) & \frac{\epsilon_a k}{\sinh(ka)} \\ \frac{-\epsilon_a k}{\sinh(ka)} & \epsilon_a k \coth(ka) \end{bmatrix} \begin{bmatrix} \hat{V}_0 \\ \hat{\phi}^b \end{bmatrix} \tag{1}$$

$$\begin{bmatrix} \hat{D}_x^c \\ \hat{D}_x^d \end{bmatrix} = \begin{bmatrix} -\epsilon_b k \coth(kd) & \frac{\epsilon_b k}{\sinh(kb)} \\ \frac{-\epsilon_b k}{\sinh(kb)} & \epsilon_b k \coth(kb) \end{bmatrix} \begin{bmatrix} \hat{\phi}^b \\ 0 \end{bmatrix} \tag{2}$$

By contrast with the model used in Sec. 5.13, there is no surface conduction, but rather a volume conduction, so that the boundary condition implied by conservation of charge for the interface,

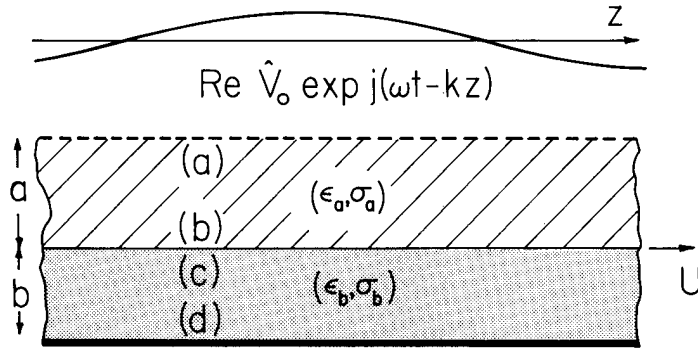


Fig. 5.14.1. Cross-sectional view of two planar layers of material having thicknesses a and b , respectively. The potential is constrained to be a traveling wave just above, and to be constant just below.

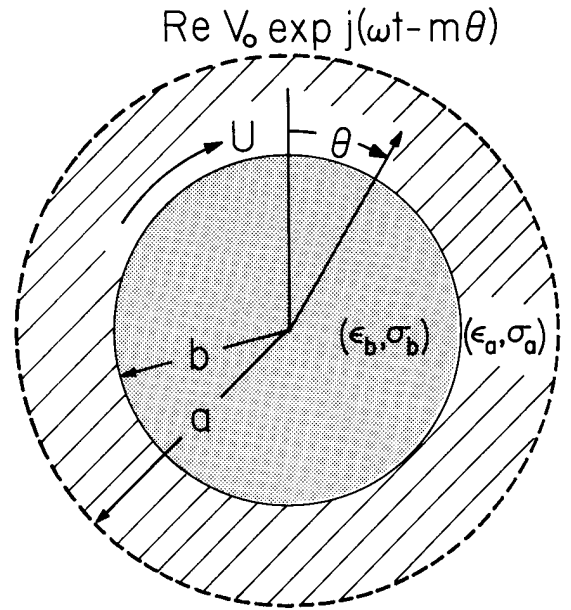


Fig. 5.14.2. Circular analog of the planar system of Fig. 5.14.1. Qualitatively, fields in the planar problem are the same as those in this circular configuration if the z axis of Fig. 5.14.1 is wrapped around on itself in an integral number of wavelengths.

and represented by Eq. 5.12.4, becomes

$$\left(\frac{\sigma_a}{\epsilon_a} \hat{D}_x^b - \frac{\sigma_b}{\epsilon_b} \hat{D}_x^c \right) + j(\omega - kU)(\hat{D}_x^b - \hat{D}_x^c) = 0 \quad (3)$$

The space average of the surface force density acting on the only charges within the volume of interest, those at the interface, is given by integrating the Maxwell stresses over an incremental volume enclosing the interface and having one wavelength in the z direction (see Sec. 4.2 for a similar calculation). Thus, the space-average force per unit area is

$$\langle T_z \rangle_z = \frac{1}{2} \text{Re} [(\hat{D}_x^b)^* \hat{E}_z^b - (\hat{D}_x^c)^* \hat{E}_z^c] = \frac{1}{2} \text{Re} jk \hat{\Phi}^b (\hat{D}_x^b - \hat{D}_x^c)^* \quad (4)$$

The jump in D_x called for with Eq. 4 is the surface charge density given by subtracting Eq. 2a from 1b:

$$\hat{D}_x^b - \hat{D}_x^c = \frac{-\epsilon_a k \hat{V}_0}{\sinh(ka)} + \hat{\Phi}^b k [\epsilon_a \coth(ka) + \epsilon_b \coth(kb)] \quad (5)$$

Then, substitution into Eq. 4 shows that it is the interfacial potential which determines the space-average of the surface force density

$$\langle T_z \rangle_z = - \frac{\epsilon_a k^2}{2 \sinh(ka)} \text{Re} j \hat{\Phi}^b \hat{V}_0^* \quad (6)$$

With the objective of finding $\hat{\Phi}^b$, the first quantity in brackets in Eq. 3 is found in terms of the potential $\hat{\Phi}^b$ by multiplying Eq. 1b by σ_a/ϵ_a and subtracting Eq. 2a multiplied by σ_b/ϵ_b :

$$\frac{\sigma_a \hat{D}_x^b}{\epsilon_a} - \frac{\sigma_b \hat{D}_x^c}{\epsilon_b} = \frac{-\sigma_a k}{\sinh(ka)} \hat{V}_0 + \hat{\Phi}^b k [\sigma_a \coth(ka) + \sigma_b \coth(kb)] \quad (7)$$

Then, substitution of Eqs. 5 and 7 into 3 gives the required surface potential in terms of the driving potential

$$\hat{\Phi}^b = \frac{[j(\omega - kU)\epsilon_a + \sigma_a] \hat{V}_0}{\sinh(ka) \{ [\sigma_a \coth(ka) + \sigma_b \coth(kb)] + j(\omega - kU)[\epsilon_a \coth(ka) + \epsilon_b \coth(kb)] \}} \quad (8)$$

For purposes of physical interpretation, it is helpful also to have the surface charge density given in terms of the driving potential by substituting Eq. 8 into Eq. 5:

$$\hat{D}_x^b - \hat{D}_x^c = \frac{-k\hat{V}_0 \coth(kb) (\epsilon_a \sigma_b - \epsilon_b \sigma_a)}{\sinh(ka) [\sigma_a \coth(ka) + \sigma_b \coth(kb)] (1 + jS_E)} \quad (9)$$

where

$$S_E = \omega \tau_E (1 - \frac{kU}{\omega}), \quad \tau_E = \frac{[\epsilon_a \coth(ka) + \epsilon_b \coth(kb)]}{[\sigma_a \coth(ka) + \sigma_b \coth(kb)]} \quad (10)$$

Finally, the electric surface force density is found by substituting Eq. 8 into Eq. 6:

$$\langle T_z \rangle_z = \frac{1}{2} \epsilon_a (k\hat{V}_0) (k\hat{V}_0)^* K (\epsilon_a \sigma_b - \epsilon_b \sigma_a) \frac{S_E}{1 + S_E^2} \quad (11)$$

where

$$K = \coth(kb) \sqrt{\sinh^2(ka) [\epsilon_a \coth(ka) + \epsilon_b \coth(kb)] [\sigma_a \coth(ka) + \sigma_b \coth(kb)]} \quad \}$$

What has been computed relates to a number of different physical situations. If the material layers are solid, then Eq. 11 represents the force per unit x-y area acting on the layers. Even though Eq. 11 came from an integration of the stresses over a volume enclosing only the interface, because there is no free charge density anywhere else in the volume of the materials, it includes all of the force on the material. It is possible that one or the other, or both, of the materials could be fluids, in which case Eq. 11 is the surface force density acting at the interface and U is the interfacial velocity. The calculation remains correct, even if the material to either side of the interface moves with some velocity other than U.

To examine the physical implications of Eq. 11, suppose that the traveling-wave frequency is fixed, and interest is in the dependence of the electrical surface force density on the material velocity. First, note that for a given kU/ω , the sign of the surface stress depends on the relative permittivities and conductivities. If the lower material is sufficiently more conducting than the upper one, so that $\sigma_b \epsilon_a > \sigma_a \epsilon_b$, then for $kU/\omega < 1$ the force is in the same direction as the wave velocity. As a function of S_E , this stress first rises linearly, reaches a peak, and then falls off, in a manner familiar from Sec. 5.13. The dependence on U has the same nature except that the point where S_E vanishes is at the synchronous velocity $U = \omega/k$, and increasing U is equivalent to decreasing S_E . Hence, a plot of $\langle T_z \rangle_z$ as a function of the normalized velocity kU/ω is as shown in Fig. 5.14.3. If the lower material is a conducting solid or fluid, and the intervening material an insulator, such as air, and the interface moves at a velocity less than synchronous, there is an induced electrical force tending to pull the material in the direction of wave propagation.

If the electrical force is retarded by one proportional to the velocity, as would be the case with viscous damping, then the velocity at which there would be an equilibrium between the electrical force and the retarding viscous force is the intersection (i) of Fig. 5.14.3a. The material tends to follow the traveling wave at a somewhat lesser velocity than the phase velocity ω/k . Note that, if a perturbing force makes the velocity decrease in magnitude slightly, the electrical force dominates the viscous force and tends to return the material to its steady equilibrium position. An experiment illustrating the force as it pumps a liquid is shown in Fig. 5.14.4a.

So far, there is little qualitative difference between what has been found for the finite-thickness slab and the results of Sec. 5.13 for the sheet conductor. But now, suppose that the material adjacent to the traveling-wave structure conducts sufficiently more than that below so that $\sigma_a \epsilon_b > \sigma_b \epsilon_a$. From Eq. 11, it is clear that the electrical force now acts in a direction which opposes the direction of relative propagation for the field. Even more, there are now three velocities at which the electrical force can be equilibrated by a viscous retarding force. At position (ii), the material is moving in a direction opposite to that of the wave.

Arguments similar to those given for equilibrium (i) can be used to see that (ii) is also stable. Two equilibria are possible with the material moving faster than the traveling wave. Of these, (iii) is unstable and (iv) is stable.

The example illustrates that there are exceptions to the intuitive notion that in an induction type of interaction, the material always tends to follow the traveling wave, and that under conditions of "motor" operation, the material velocity is less than the phase velocity of the wave.

The seemingly mysterious finding, with $\sigma_a \epsilon_b > \epsilon_a \sigma_b$, is explained first by considering why the material follows the traveling wave in the case of Fig. 5.14.3a. Equation 9 gives the surface charge

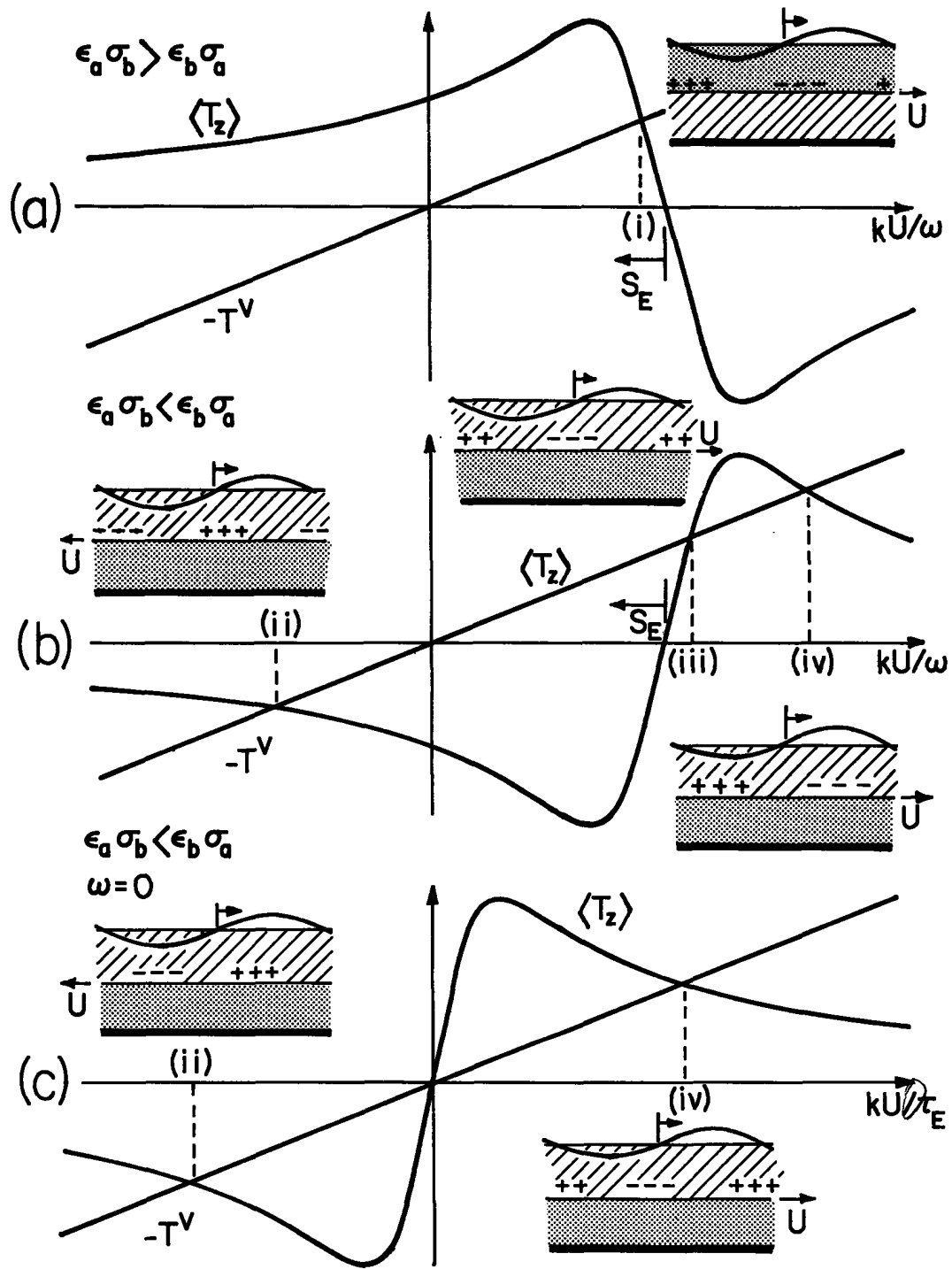
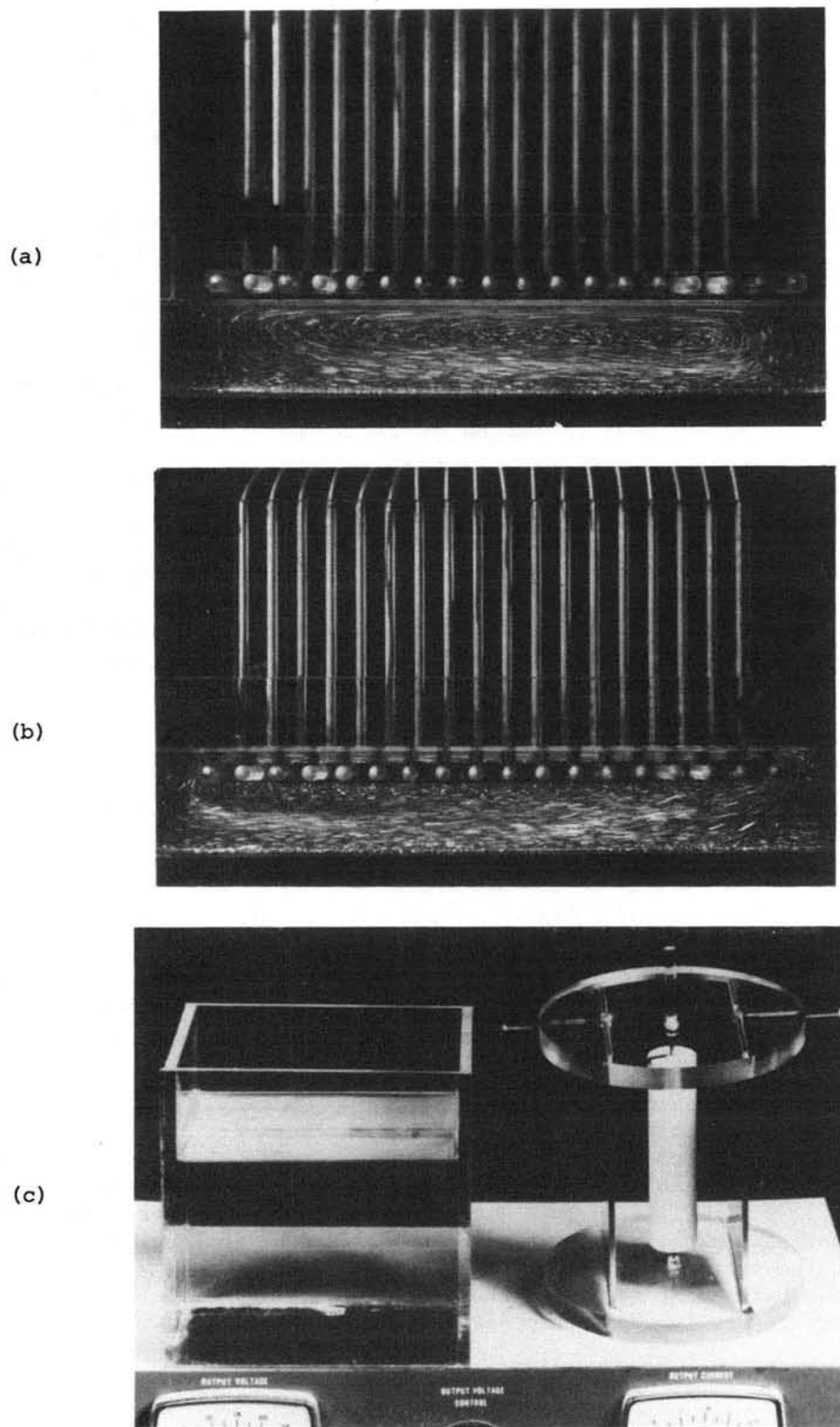


Fig. 5.14.3. Dependence of electric space-average surface force density on material velocity. (a) With the lower material more conducting, the material tends to follow the traveling wave. (b) With the conducting material next to the electrodes, the material can travel in a direction opposite to that of the imposed wave, or move faster than the traveling wave. (c) Applied frequency zero. Motion results from raising the applied field so that the slope of the curve exceeds that of the viscous force curve.



Courtesy of Education Development Center, Inc. Used with permission.

Fig. 5.14.4. (a) Electrodes embedded in a plastic sheet are driven by a 60-Hz 6-phase source so as to approximate a wave of potential traveling to the right. Separated from the electrode structure by an air gap, corn oil (doped to make $\omega\tau_E = 1$) has an interface that is pumped to the right, illustrating equilibrium (i) of Fig. 5.14.3a. To conserve mass, the liquid recirculates below the interface. (From film "Electric Fields and Moving Media," Reference 12, Appendix C.) (b) The traveling wave still propagates to the right but the electrode is immersed in the corn oil. The interface, which is now above, moves in the opposite direction of the wave. The configuration is Fig. 5.14.1 turned upside down, and the pumping illustrates equilibrium (ii) in Fig. 5.14.3b. (c) Von Quincke's rotor, consisting of a Teflon rotor immersed in a semi-insulating liquid. As a d-c potential applied between the electrodes is raised to about 20 kV, the rotor begins to rotate in either direction.

density, and shows that there is negative surface charge lagging the peak in potential on the electrode above by an angle less than 90° . The picture is one of a field axis on the fixed structure pulling along charges induced in the material. But, if the material adjacent to the electrodes is the conductor, so that $\sigma_a \epsilon_b > \epsilon_a \sigma_b$, then Eq. 9 shows that the sign of the charge at the interface is reversed. Regions of positive charge on the electrodes induce positive surface charge on the adjacent interface. What was a force of attraction in the case of Fig. 5.14.3a, becomes a force of repulsion in Fig. 5.14.3b. This is why the material can actually be repelled in a direction opposite to that of the traveling wave. An illustrative experiment is shown in Fig. 5.14.4b.

Equilibrium (iii) is best illustrated by considering the limit where the applied frequency vanishes. Thus, the applied potential is static. In the circular analog of Fig. 5.14.2 the applied field might be produced by a pair of parallel plates used to impose a field perpendicular to the z axis that, in the absence of the conducting materials, would be uniform. Such a configuration is Von Quincke's rotor, illustrated in Fig. 5.14.4c. The rotor is insulating relative to the corn oil in which it is immersed; hence $\epsilon_a \sigma_b < \epsilon_b \sigma_a$. The electrical force then depends on the material velocity, as sketched in Fig. 5.14.3c. If the applied field is raised, then there is a threshold value of field at which the slope of the electric force curve exceeds that of the viscous force. At that condition, equilibrium (iii) becomes unstable and the material spontaneously moves, in the developed model either to the right or left, in the circular geometry clockwise or counterclockwise, so as to establish a new equilibrium with a steady-state velocity either at (ii) or (iv). At the position (iii), the static field induces positive charges on the interface directly opposite positive charges on the electrodes. As a result, any small excursion of the material which tends to carry that charge distribution to the right or left is accompanied by a proportionate electric stress that tends to further the original deflection.

Spontaneous rotation of insulating objects immersed in somewhat conducting media and stressed by d-c fields are observed in seemingly unrelated situations. Examples are macroscopic particles in semi-insulating liquids and objects in ionized gases.

5.15 Temporal Modes of Charge Relaxation

Temporal Transients Initiated from State of Spatial Periodicity: The configurations of the two previous sections are typical of linear systems that are inhomogeneous in one direction only and excited from transverse boundaries. Pictured in the abstract by Fig. 5.15.1, the transverse direction, x , denotes the direction of inhomogeneity, while in the longitudinal (y and z) directions the system is uniform. In Secs. 5.13 and 5.14, it is at transverse boundaries (having x as the perpendicular) that driving conditions are imposed. In the picture, ϕ_d imposes a driving frequency ω and a spatial dependence on the longitudinal coordinates that is periodic, either a pure traveling wave with known wavenumbers (k_y, k_z) or a Fourier superposition of these waves. The most common configuration in which spatial periodicity is demanded is one in which y or z "closes on itself," for example becomes the θ coordinate in a cylindrical system.

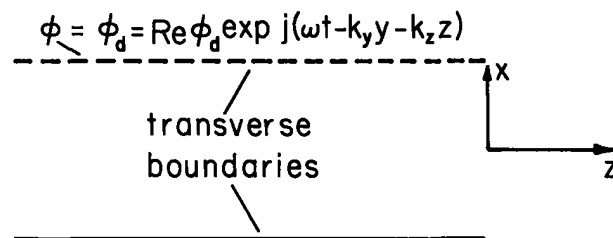


Fig. 5.15.1. Abstract view of systems that are inhomogeneous in a transverse direction, x , and uniform in longitudinal directions (y, z).

The temporal transient resulting from turning on the excitation when $t = 0$ with the system initially at rest can be represented as the sum of a particular solution (the sinusoidal steady-state driven response) and a homogeneous solution (itself generally the superposition of temporal modes having the natural frequencies s_n):

$$\phi(x, y, z, t) = \text{Re} \hat{\phi}(x) e^{j(\omega t - k_y y - k_z z)} + \sum_n \text{Re} \hat{\phi}_n(x) e^{s_n t - j(k_y y + k_z z)} \quad (1)$$

Turning off the excitation results in a response composed of only the temporal modes. The coefficients $\hat{\phi}_n(x)$ are adjusted to guarantee that the total response satisfy the proper initial conditions for all values of x . In some situations this may require only one mode, whereas in others an infinite set of modes is entailed.

Identification of the eigenfunctions and their associated eigenfrequencies is accomplished in one of two ways. First, if the driven response is known, its complex amplitude takes the form

$$\hat{\phi}(x) = \frac{\hat{\phi}_d}{D(\omega, k_y, k_z)} \quad (2)$$

By definition, the natural modes are those that can exist with finite amplitude even in the limit of zero drive. This follows from the fact that the particular solution in Eq. 1 satisfies the driving conditions, so the natural modes must vanish at the driven boundaries. Thus, for given wavenumbers

(k_y, k_z) of the drive, the frequencies s_n must satisfy the dispersion relation

$$D(-js_n, k_y, k_z) = 0 \quad (3)$$

Alternatively, if it is only the natural modes that are of interest, then the amplitudes are required to satisfy all boundary conditions, including those implied by setting the excitations to zero. In the abstract system of Fig. 5.15.1, $\hat{\phi}_d = 0$.

The natural modes identified in this way are only those that can be excited by means of the structure on the transverse excitation boundary. Thus, the implied distributions of sources within the volume are not arbitrary. The functions $\hat{\phi}_n(x)$ are complete only in the sense that they can be used to represent arbitrary initial conditions on sources induced in this way. They are not sufficient to represent any initial distribution of the fields set up by some other means within the volume. The remainder of this section exemplifies this subject in specific terms. Magnetic diffusion transients, considered in Chap. 6, broaden the class of example.

Transient Charge Relaxation on a Thin Sheet: The build-up or decay of charge on a moving conducting sheet excited by a sinusoidal drive can be described by revisiting the example treated in Sec. 5.13. In terms of the complex amplitude of the sheet potential, $\hat{\phi}^b$, and with $x=0$ at the sheet surface, the potential distributions above and below the sheet are (for a discussion of translating coordinate references to fit eigenfunctions to specific coordinates, see Sec. 2.20 in conjunction with Eq. 2.16.15)

$$\hat{\phi}(x) = \begin{cases} \hat{V}_o \frac{\sinh(kx)}{\sinh(kd)} - \hat{\phi}^b \frac{\sinh k(x-d)}{\sinh(kd)}; & x > 0 \\ \hat{\phi}^b \frac{\sinh k(x+d)}{\sinh(kd)}; & x < 0 \end{cases} \quad (4)$$

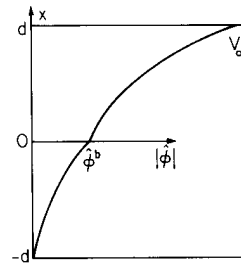


Fig. 5.15.2
Driven response

The eigenfrequency equation is the denominator of Eq. 5.13.7 set equal to zero and evaluated with $j\omega = s_n$:

$$\sinh(kd) + j \frac{2\epsilon_o}{k\sigma_s} (-js_n - kU) \cosh(kd) = 0 \quad (5)$$

This expression has only one root,

$$s_1 = jkU - \frac{k\sigma_s}{2\epsilon_o} \tanh(kd) \quad (6)$$

The one eigenfunction is determined by using the complex amplitudes of Sec. 5.13 with $j\omega = s_1$ and $\hat{V}_o = 0$. In this example, the eigenfunction has the distribution with x of Eq. 4 with $\hat{V}_o = 0$, and a complex amplitude $\hat{\phi}_1$ determined by the initial conditions:

$$\hat{\phi}_1(x) = \begin{cases} -\hat{\phi}_1^b \frac{\sinh k(x-d)}{\sinh(kd)}; & x > 0 \\ \hat{\phi}_1^b \frac{\sinh k(x+d)}{\sinh(kd)}; & x < 0 \end{cases} \quad (7)$$

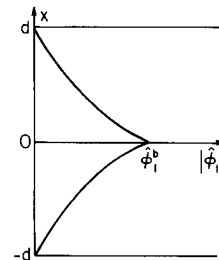


Fig. 5.15.3
Eigenfunction.

In general, the initial condition is on the charge distribution in the region $-d < x < d$. In this example, the charge is confined to the sheet and only the one eigenmode is needed to meet the initial condition.

Suppose that when $t = 0$ there is no sheet charge and the excitation is suddenly turned on. The total potential is given by Eq. 1 with $\hat{\phi}(x)$ and $\hat{\phi}_1(x)$ given by Eqs. 4 and 7. In terms of this potential, the surface charge is in general

$$\sigma_f(z, t) = D_x^b - D_x^c = -\epsilon_o k \text{Re} \left\{ \left[\frac{\hat{V}_o}{\sinh(kd)} - 2\hat{\phi}^b \coth(kd) \right] e^{j(\omega t - kz)} - 2\hat{\phi}_1^b \coth(kd) e^{s_1 t - jkz} \right\} \quad (8)$$

To make $\sigma_f(z,0) = 0$, the eigenfunction amplitude must be such that when $t = 0$, Eq. 8 vanishes for all z :

$$\hat{\phi}_1^b = -\hat{\phi}^b + \frac{\hat{v}_0}{2 \cosh(kd)} \quad (9)$$

When $t = 0^+$, the surface charge density is still zero, but the potential is finite over the entire region $-d < x < d$. It can be shown by using Eq. 9 in Eq. 1 (evaluated when $t = 0$ using Eqs. 4 and 7) that at this instant the potential is what it would be in the absence of the conducting sheet.

The surface charge builds up at a rate determined by s_1 , which expresses the natural frequency as seen from a laboratory frame of reference. The oscillatory part is what is observed in the fixed frame as a spatially periodic distribution moves with the velocity of the material. If the driving voltage were suddenly turned off, the fields would decay in a way characterized by the same natural frequencies, with an oscillatory part reflecting the spatial periodicity of the initial charge distribution as it decays with a relaxation time $2\epsilon_0/k\sigma_s \tanh kd$. Because the electric energy storage is in the free-space region, while the energy dissipation is within the sheet, this damping rate is not simply the bulk relaxation time of the conducting sheet.

In the long-wave limit, $kd \ll 1$, the relaxation in this inhomogeneous system can be largely attributed to energy storage in the transverse electric field and dissipation due to the longitudinal electric field. On a scale of the system as a whole, the charge actually diffuses rather than relaxes. This can be seen by taking the limit $kd \ll 1$ of Eq. 6:

$$s_1 + (-jk)U = \frac{\sigma_s d}{2\epsilon_0} (-jk)^2 \quad (10)$$

to obtain the dispersion equation for diffusion with convection. By inferring time and z derivatives from the complex frequency s and $-jk$ respectively, it can be seen from Eq. 10 that in the long-wave limit the surface charge density is governed by the equation

$$\left(\frac{\partial}{\partial t} + U \frac{\partial}{\partial z}\right)\sigma_f = \frac{\sigma_s d}{2\epsilon_0} \frac{\partial^2 \sigma_f}{\partial z^2} \quad (11)$$

This model is consistent with the distributed network shown in Fig. 5.15.4. The rigorous deduction of Eq. 11 would exploit the space-rate expansion introduced in Sec. 4.12. The dominant electric fields are $\vec{E} = E_x(z,t)\vec{i}_x$ in the air gaps and $\vec{E} = E_z(z,t)\vec{i}_z$ in the sheet. This model is embedded in the discussion of the Van de Graaff machine given in Sec. 4.14, Eqs. 4.14.9 and 4.14.10.

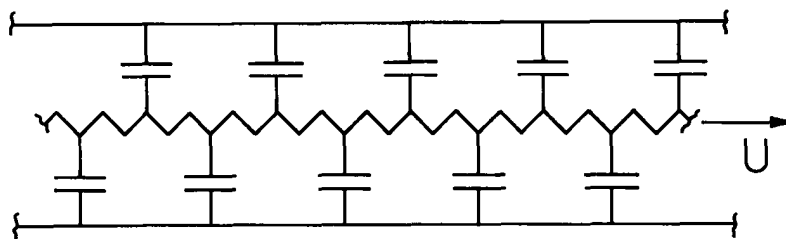


Fig. 5.15.4

Distributed network in the long-wave limit, equivalent to system of Fig. 5.13.1.

Heterogeneous Systems of Uniform Conductors: A generalization of the system of two uniformly conducting regions (the theme of Sec. 5.14) is shown in Fig. 5.15.5. Layers of material, each having the thickness d , have different conductivities and move to the right with the velocity profile $\vec{v} = U(x)\vec{i}_x$. Charge is confined to the interfaces, which have a negligible surface conductivity. Thus, the n th interface moves to the right with the velocity U_n and is bounded from above and below by regions having the uniform properties (ϵ_n, σ_n) and $(\epsilon_{n+1}, \sigma_{n+1})$ respectively. Variables evaluated just above and below the n th interface are denoted by n and n' respectively.

In the limit where the number of interfaces, N , becomes large, the "stair-step" conductivity distribution approaches that of a continuous distribution. The following illustrates the second method of determining the natural frequencies, while giving insight as to why an infinite number of natural modes exists in systems having a distributed conductivity.

The regions just above and just below the n th interface are described by the planar transfer relations representing Laplace's equation, Eq. (a) of Table 2.16.1:

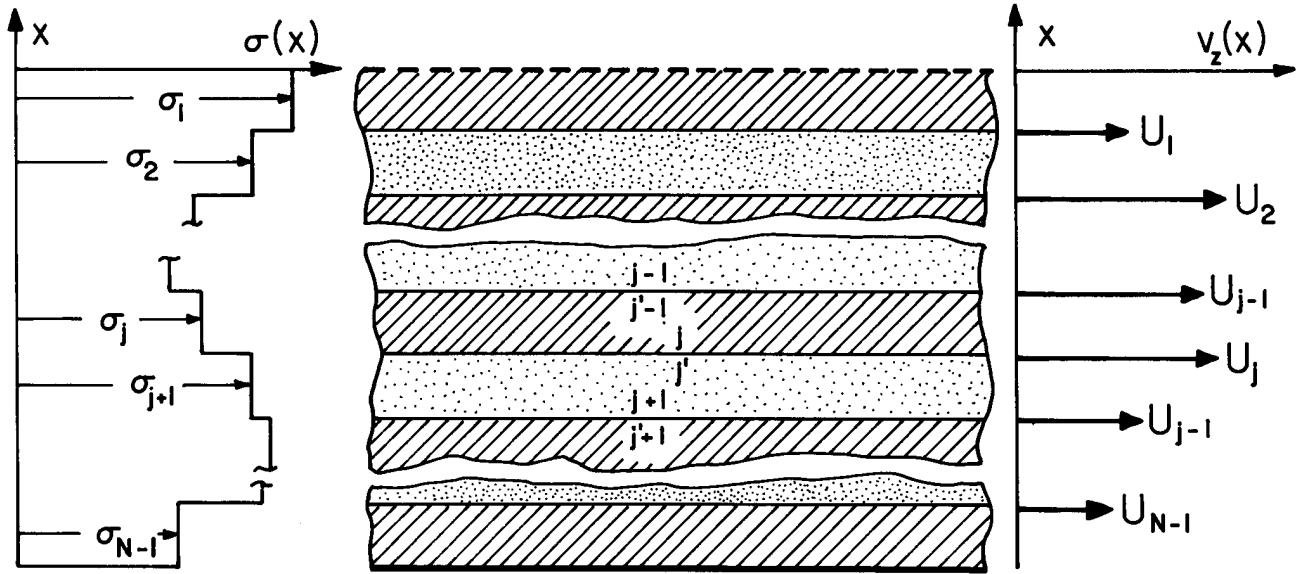


Fig. 5.15.5. A material having a conductivity that depends on x moves to the right with the velocity distribution $v_x = U(x)$.

$$\begin{bmatrix} \hat{D}_x^{n'-1} \\ \hat{D}_x^n \end{bmatrix} = \epsilon_n^k \begin{bmatrix} -\coth(kd) & \frac{1}{\sinh(kd)} \\ -\frac{1}{\sinh(kd)} & \coth(kd) \end{bmatrix} \begin{bmatrix} \hat{\phi}^{n'-1} \\ \hat{\phi}^n \end{bmatrix} \quad (12)$$

$$\begin{bmatrix} \hat{D}_x^{n'} \\ \hat{D}_x^{n+1} \end{bmatrix} = \epsilon_{n+1}^k \begin{bmatrix} -\coth(kd) & \frac{1}{\sinh(kd)} \\ -\frac{1}{\sinh(kd)} & \coth(kd) \end{bmatrix} \begin{bmatrix} \hat{\phi}^{n'} \\ \hat{\phi}^{n+1} \end{bmatrix} \quad (13)$$

At each interface, the potential is continuous:

$$\hat{\phi}^{n'-1} = \hat{\phi}^{n-1}; \quad \hat{\phi}^{n'} = \hat{\phi}^n \quad (14)$$

With the understanding that the natural modes now identified are associated with the response to potential constraints at the transverse boundaries, potentials at the upper and lower surfaces must vanish:

$$\hat{\phi}^0 = 0; \quad \hat{\phi}^{N+1} = 0 \quad (15)$$

On the n th interface, conservation of charge (Eq. 5.12.4) requires the additional boundary condition:

$$(-s + jkU_n)\hat{\sigma}_f^n = \frac{\sigma_n}{\epsilon_n} \hat{D}_x^n - \frac{\sigma_{n+1}}{\epsilon_{n+1}} \hat{D}_x^{n'} \quad (16)$$

At each interface, the surface charge is related to potentials at that and the adjacent interfaces, as can be seen by using Eqs. 12b, 13a and 14 to write

$$\hat{\sigma}_f^n = \hat{D}_x^n - \hat{D}_x^{n'} = k \left[\frac{-\epsilon_n \hat{\phi}^{n-1}}{\sinh(kd)} + (\epsilon_n + \epsilon_{n+1}) \coth(kd) \hat{\phi}^n - \frac{\epsilon_{n+1} \hat{\phi}^{n+1}}{\sinh(kd)} \right] \quad (17)$$

This expression holds at each of the N interfaces. In view of the boundary conditions at the transverse boundaries, Eqs. 15, Eqs. 17 are N equations for the N $\hat{\sigma}_f^n$'s in terms of the interfacial potentials $\hat{\phi}^n$:

$$\begin{bmatrix} \hat{\sigma}_f \end{bmatrix} = \begin{bmatrix} A \end{bmatrix} \begin{bmatrix} \hat{\phi} \end{bmatrix} \quad (18)$$

where $[\sigma_f]$ and $[\hat{\phi}]$ are Nth order column matrices and

$$[A] = \begin{bmatrix} k(\epsilon_1 + \epsilon_2) \coth(kd) & -k\epsilon_2 / \sinh(kd) & & 0 \\ -k\epsilon_2 / \sinh(kd) & k(\epsilon_2 + \epsilon_3) \coth(kd) & -k\epsilon_3 / \sinh(kd) & 0 \\ 0 & & & \\ 0 & & & \\ \cdot & & & \\ \cdot & & & \\ & & 0 & -k\epsilon_N / \sinh(kd) & k(\epsilon_N + \epsilon_{N+1}) \coth(kd) \end{bmatrix}$$

Equation 16 can similarly be written in terms of the potentials by using Eqs. 12b, 13a and 14:

$$(-s + jkU_n) \hat{\sigma}_f^n = \frac{-k\sigma_n}{\sinh(kd)} \hat{\phi}^{n-1} + k(\sigma_n + \sigma_{n+1}) \coth(kd) \hat{\phi}^n - \frac{k\sigma_{n+1}}{\sinh(kd)} \hat{\phi}^{n+1} \quad (19)$$

In view of Eq. 15, this expression, written with $n = 1, 2, \dots, N$, takes the matrix form

$$\begin{bmatrix} -s + jkU_1 & 0 & 0 \\ 0 & -s + jkU_2 & 0 \\ 0 & & \\ \cdot & & \\ \cdot & & -s + jkU_N \end{bmatrix} \begin{bmatrix} \hat{\sigma}_f^1 \\ \hat{\sigma}_f^2 \\ \cdot \\ \hat{\sigma}_f^N \end{bmatrix} = [B] [\hat{\phi}] \quad (20)$$

where

$$[B] = \begin{bmatrix} k(\sigma_1 + \sigma_2) \coth(kd) & \frac{-k\sigma_2}{\sinh(kd)} & & 0 \\ \frac{-k\sigma_2}{\sinh(kd)} & k(\sigma_2 + \sigma_3) \coth(kd) & \frac{-k\sigma_3}{\sinh(kd)} & 0 \\ 0 & & & 0 \\ \cdot & & & \\ \cdot & & & \\ & & 0 & \frac{-k\sigma_N}{\sinh(kd)} & k(\sigma_N + \sigma_{N+1}) \coth(kd) \end{bmatrix}$$

Now, if Eq. 18 is inverted, so that $[\hat{\phi}] = [A]^{-1} [\hat{\sigma}_f]$ and the column matrix $[\hat{\phi}]$ substituted on the right in Eq. 20, a set of equations are obtained which are homogeneous in the amplitudes $\hat{\sigma}_f^n$,

$$\begin{bmatrix} jkU_1 - C_{11} - s & -C_{12} & -C_{13} \\ -C_{21} & jkU_2 - C_{22} - s & -C_{23} \\ \cdot & & \\ \cdot & & \\ & & jkU_N - C_{NN} - s \end{bmatrix} \begin{bmatrix} \hat{\sigma}_f^1 \\ \hat{\sigma}_f^2 \\ \cdot \\ \hat{\sigma}_f^N \end{bmatrix} = 0 \quad (21)$$

where $[C] = [B] [A]^{-1}$.

For the amplitudes to be finite, the determinant of the coefficients must vanish, and this constitutes the eigenfrequency equation $D(s, k_x, k_y) = 0$. The determinant takes the standard matrix form for a characteristic value problem.¹ Expanded, it is an Nth order polynomial in s , and hence has N roots which are the natural frequencies.

As an example, suppose that there is a single interface, $N=1$. Then, from Eqs. 18 and 20,

$$A^{-1} = \frac{1}{k(\epsilon_1 + \epsilon_2)\coth(kd)} ; \quad B = k(\sigma_1 + \sigma_2)\coth(kd) \quad (22)$$

and it follows that $C_{11} = (\sigma_1 + \sigma_2)/(\epsilon_1 + \epsilon_2)$ so that Eq. 21 gives the single eigenfrequency

$$s_1 = jkU_1 - \left(\frac{\sigma_1 + \sigma_2}{\epsilon_1 + \epsilon_2} \right) \quad (23)$$

With $a = b = d$, this result is consistent with setting the denominator of Eq. 5.14.8 equal to zero and solving for $j\omega$.

With two interfaces, there are two eigenmodes, with frequencies determined from Eq. 21:

$$\begin{bmatrix} (jkU_1 - C_{11} - s) & -C_{12} \\ -C_{21} & (jkU_2 - C_{22} - s) \end{bmatrix} = 0 \quad (24)$$

The entries C_{ij} follow from $[C] = [B][A]^{-1}$

$$[C] = \begin{bmatrix} k(\sigma_1 + \sigma_2)\coth(kd) & \frac{-k\sigma_2}{\sinh(kd)} \\ \frac{-k\sigma_2}{\sinh(kd)} & k(\sigma_2 + \sigma_3)\coth(kd) \end{bmatrix} \begin{bmatrix} \frac{k(\epsilon_2 + \epsilon_3)\coth(kd)}{\text{DET}} & \frac{k\epsilon_2}{\text{DET} \sinh(kd)} \\ \frac{k\epsilon_2}{\text{DET} \sinh(kd)} & \frac{k(\epsilon_1 + \epsilon_2)\coth(kd)}{\text{DET}} \end{bmatrix} \quad (25)$$

$$= \frac{k^2}{\text{DET}} \begin{bmatrix} [(\sigma_1 + \sigma_2)(\epsilon_2 + \epsilon_3)\coth^2(kd) - \frac{\epsilon_2\sigma_2}{\sinh^2(kd)}] & [(\sigma_1\epsilon_2 - \sigma_2\epsilon_1) \frac{\coth(kd)}{\sinh(kd)}] \\ [(\sigma_3\epsilon_2 - \sigma_2\epsilon_3) \frac{\coth(kd)}{\sinh(kd)}] & [(\sigma_2 + \sigma_3)(\epsilon_1 + \epsilon_2)\coth^2(kd) - \frac{\sigma_2\epsilon_2}{\sinh^2(kd)}] \end{bmatrix}$$

where

$$\text{DET} \equiv k^2 [(\epsilon_1 + \epsilon_2)(\epsilon_2 + \epsilon_3)\coth^2(kd) - \epsilon_2^2/\sinh^2(kd)]$$

The eigenfrequency equation, Eq. 24, is quadratic in s , and can be solved to obtain the two eigenfrequencies

$$\begin{pmatrix} s_1 \\ s_2 \end{pmatrix} = \frac{1}{2} [jk(U_1 + U_2) - C_{11} - C_{22}] \pm \sqrt{\frac{1}{4} [jk(U_1 + U_2) - C_{11} - C_{22}]^2 - (jkU_1 - C_{11})(jkU_2 - C_{22}) - C_{12}C_{21}} \quad (26)$$

where the C_{ij} are given by Eq. 25.

The N eigenmodes can be used to represent the temporal transient resulting from turning on or turning off a spatially periodic drive. Although more complicated, the procedure is in principle much as illustrated in the sheet conductor example. As expressed by Eq. 1, the transient is in general a superposition of the driven response (for the turn on) and the natural modes. The N eigenmodes make it possible to satisfy N initial conditions specifying the surface charges on the N interfaces.

In the limit where N becomes infinite, the number of modes becomes infinite and the physical system is one having a smooth distribution of conductivity, $\sigma(x)$, and permittivity, $\epsilon(x)$. This infinite

1. F. E. Hohn, Elementary Matrix Algebra, 2nd ed., Macmillan Company, New York, 1964, p. 273.

set of internal modes can also be used to account for initial conditions. Such modes are encountered again in Sec. 6.10, in connection with magnetic diffusion, where an infinite number of modes are possible even with systems having uniform properties. What has been touched on here is the behavior of smoothly inhomogeneous systems, described by linear differential equations with space-varying coefficients. The finite mode model, implicit to approximating $\sigma(x)$ and $\epsilon(x)$ by the stair-step distributions, is one way to take into account the terms $\vec{E} \cdot \nabla \sigma$ and $\vec{E} \cdot \nabla \epsilon$ in the charge relaxation law, Eq. 5.10.6.

5.16 Time Average of Total Forces and Torques in the Sinusoidal Steady State

Two descriptions are used to generalize the complex amplitude representations describing the steady-state response to a sinusoidal drive having the angular frequency ω . If the system is spatially periodic, or can be modeled by a portion of a periodic system, a Fourier series generalization of the complex amplitude description is appropriate. If it extends to "infinity," a Fourier transform is conveniently made the complex amplitude. The conventions and formulas for computing the time-average of field products, for example of forces, are summarized in this section.

Fourier Series Complex Amplitudes: With a periodicity length ℓ in the z direction, the Fourier series becomes one of complex amplitudes:

$$A(z, t) = \text{Re} \hat{A}(z, \omega) e^{j\omega t}; \quad \hat{A} = \sum_{n=-\infty}^{+\infty} \hat{A}_n(k_n, \omega) e^{-jk_n z} \quad (1)$$

where $k_n \equiv 2n\pi/\ell$. The series, which determines the phase as well as amplitude of the field at any given point, is in general complex. Thus, \hat{A}_n is not necessarily equal to \hat{A}_{-n}^* . Each term in the series can be regarded as a traveling wave with phase velocity ω/k_n . The Fourier amplitudes are determined by multiplying both sides of Eq. 1b by $\exp(jk_m z)$, integrating both sides over the length ℓ and exploiting the orthogonality to solve for \hat{A}_m . With $m \rightarrow n$,

$$\hat{A}_n = \frac{1}{\ell} \int_0^\ell \hat{A} e^{jk_n z} dz \quad (2)$$

The time-average of a product of fields A and B , written in this form, is obtained by regarding each series as the complex amplitude (Eq. 2.15.14, with $k \rightarrow \omega$ and $z \rightarrow t$) to obtain

$$\langle AB \rangle_t = \frac{1}{2} \text{Re} \left[\sum_{n=-\infty}^{+\infty} \hat{A}_n e^{-jk_n z} \sum_{m=-\infty}^{+\infty} \hat{B}_m^* e^{jk_m z} \right] \quad (3)$$

The total time-average force (or some other physical quantity involving the product AB) is the space average of Eq. 3 multiplied by the length. To compute the space-average of the time average, think of writing out the first series in Eq. 3, and then successively multiplying it by each term from the second series and averaging over the length. Each term from the second series forms only one product having a finite integral over the length ℓ , the term with $m = n$. Thus, Eq. 3 becomes

$$\frac{1}{\ell} \int_z^{z+\ell} \langle AB \rangle_t dz = \frac{1}{2} \text{Re} \sum_{n=-\infty}^{+\infty} \hat{A}_n \hat{B}_n^* \quad (4)$$

Application of this expression is illustrated in Sec. 6.4. Its role with respect to Fourier series complex amplitudes is analogous to that of the formula developed next in connection with Fourier transform complex amplitudes.

Fourier Transform Complex Amplitudes: In a spatial transient situation, such as illustrated in Sec. 5.17, the complex amplitude takes the form of a Fourier superposition integral:

$$A(z, t) = \text{Re} \hat{A}(z, \omega) e^{j\omega t}; \quad \hat{A} = \frac{1}{2\pi} \int_{-\infty}^{+\infty} \hat{A} e^{-jkz} dk \quad (5)$$

The Fourier transform is found from the complementary integral

$$\hat{A} = \int_{-\infty}^{+\infty} \hat{A} e^{jkz} dz \quad (6)$$

and is not necessarily real. Hence, $\hat{A}(k)$ is not necessarily equal to $\hat{A}^*(-k)$.

To compute the total time-average force acting over the interval $-\infty < z < \infty$, use is first made of the complex amplitude theorem, Eq. 2.15.14, with $z \rightarrow t$ and $k \rightarrow \omega$:

$$\langle AB \rangle_t = \frac{1}{2} \text{Re} \hat{A} \hat{B}^* \quad (7)$$

The integral of this time average over z , perhaps the total time-average force, is

$$\int_{-\infty}^{+\infty} \langle AB \rangle_t dz = \frac{1}{2} \operatorname{Re} \int_{-\infty}^{+\infty} \hat{A}(z) \hat{B}^*(z) dz \quad (8)$$

With the objective a Fourier transform analogue of Eq. 4, a convolution integral is defined such that $f(0)$ is the integral required to evaluate Eq. 8:

$$f(\xi) \equiv \int_{-\infty}^{+\infty} \hat{A}(z) \hat{B}^*(z - \xi) dz \quad (9)$$

This function can be written as an integral on k (the equivalent of a summation on n in Eq. 4) by taking its Fourier transform. Then the inverse integral, Eq. 5, is the desired integration on k . Thus, the Fourier transform (defined by Eq. 6) is taken of Eq. 9, to obtain

$$\hat{f}(k) = \int_{-\infty}^{+\infty} \int_{-\infty}^{+\infty} \hat{A}(z) \hat{B}^*(z - \xi) e^{jk\xi} dz d\xi \quad (10)$$

Now, the substitution $z - \xi \rightarrow z'$ is made, so that, for an integration holding z fixed, $d\xi = -dz'$ and the limits of integration on ξ are reversed:

$$\hat{f}(k) = \int_{-\infty}^{+\infty} \int_{-\infty}^{+\infty} \hat{A}(z) \hat{B}^*(z') e^{jk(z-z')} dz dz' \quad (11)$$

Finally, this expression can be factored to make it clear that the transform of the integral defined with Eq. 9 is in fact the product of the individual transforms:

$$\hat{f}(k) = \left[\int_{-\infty}^{+\infty} \hat{A}(z) e^{jkz} dz \right] \left[\int_{-\infty}^{+\infty} \hat{B}^*(z') e^{-jkz'} dz' \right] = \hat{A}(k) \hat{B}^*(k) \quad (12)$$

Hence, by using the inverse integral, Eq. 5, it follows that

$$f(\xi) = \frac{1}{2\pi} \int_{-\infty}^{+\infty} \hat{A}(k) \hat{B}^*(k) e^{-jk\xi} dk \quad (13)$$

In summary, it has been found that the integration over z called for in Eq. 8 can alternatively be made an integration on k , because substitution of $f(0)$ from Eq. 13 into Eq. 8 gives

$$\int_{-\infty}^{+\infty} \langle AB \rangle_t dz = \frac{1}{4\pi} \operatorname{Re} \int_{-\infty}^{+\infty} \hat{A}(k) \hat{B}^*(k) dk \quad (14)$$

Application of this theorem is illustrated in Sec. 5.17.

5.17 Spatial Modes and Transients in the Sinusoidal Steady State

An abstract view of systems that are uniform in a longitudinal direction and inhomogeneous in a transverse direction is shown in Fig. 5.17.1. The thin sheet and finite conductor configurations of Secs. 5.13 and 5.14 are specific examples. In those sections, it is the spatially periodic sinusoidal steady-state response that is emphasized. In any real system, the excitation must be turned on, and so there is a temporal transient before this sinusoidal steady state is established. For spatially periodic systems, Section 5.15 introduced the temporal modes representing this turn-on transient. But, except for systems that are reentrant (for example rotating machines), the spatial extent of the excitation is also limited. In terms of Fig. 5.17.1, where the "system" extends over the length L , the excitation is applied to transverse boundaries of region II. Within this region, the excitation is spatially periodic. It might consist of a pure traveling wave having an "imposed" wavenumber β and frequency ω , or (by superposition) have an arbitrary periodic z - t dependence.

In terms of the longitudinal coordinate z and time t , the general response of the fields in some transverse plane can be pictured as shown in Fig. 5.17.2. When $t = 0$, the sinusoidal steady state excitation is turned on over region II. At any position along the z -axis, the response of a stable system consists of a transient beginning at the earliest when $t = 0$ and, as $t \rightarrow \infty$, approaching a temporal sinusoidal steady state with the same frequency ω as the drive. But at any given time $t > 0$, there is the possibility of a response outside the region l as well as within. In the limit where the driven region is long (or the system is reentrant so that the extremes of region II are in fact the same location), the response in the middle of region II can be expected to have the same spatial periodicity as the drive. This is the limit in which the temporal transient and sinusoidal steady state of Secs. 5.13 or 5.14 and Sec. 5.15 pertain.

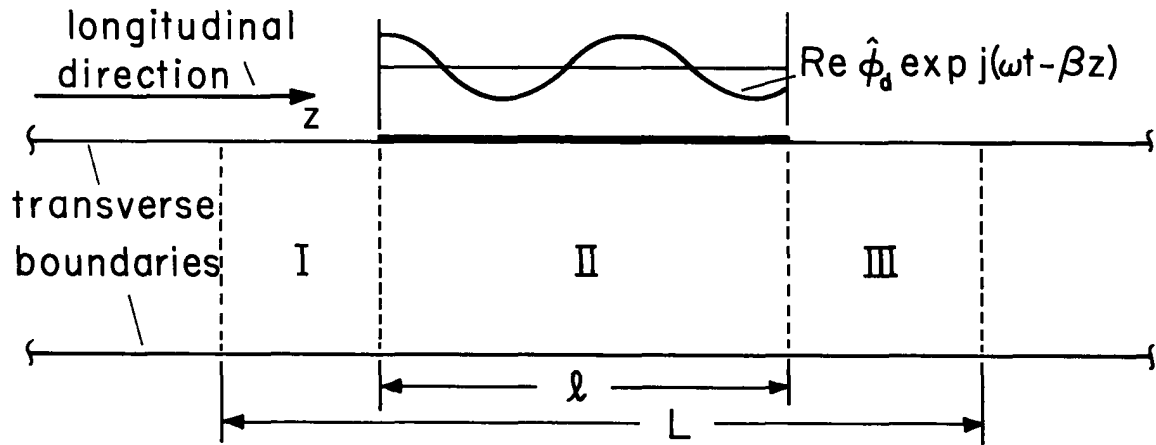


Fig. 5.17.1. Abstract view of systems having excitation on transverse boundaries which are in the temporal sinusoidal steady state but confined to the region ℓ .

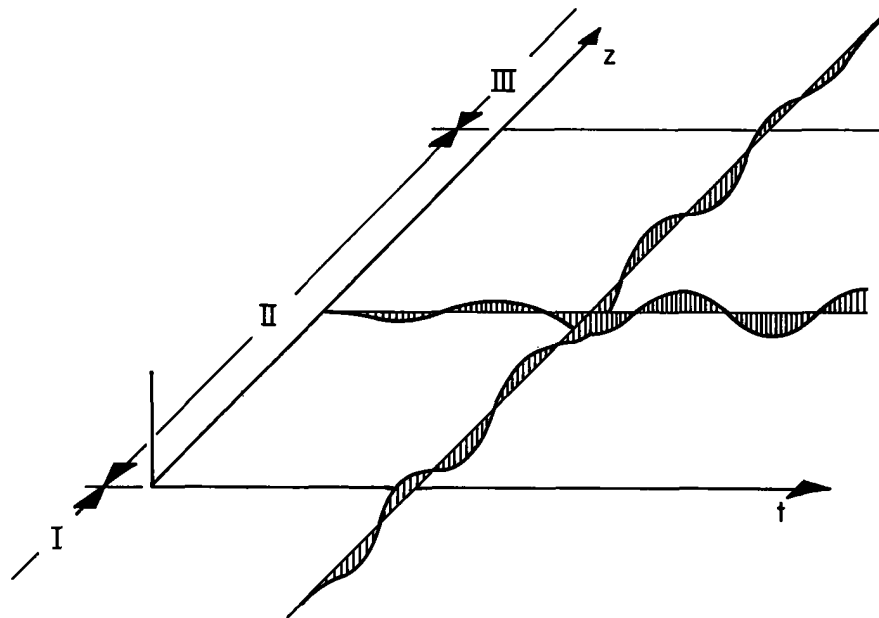


Fig. 5.17.2. Response in a given transverse plane of the system of Fig. 5.17.1 to a pure traveling wave turned on when $t=0$ and confined to the range $0 < z < \ell$.

In this section, a long enough time has elapsed that the temporal steady state has been established but the spatial extent of the excitation is not large enough to justify ignoring the end effects. A significant portion of region II is not in the spatial sinusoidal steady state. However, time has progressed to the point where the fields at any given location have the same temporal sinusoidal variation as the drive. Implicit to this section is the presumption of stability. If the turn-on transient gives rise to components that grow in time, then these will dominate the temporal sinusoidal steady state presumed to prevail as $t \rightarrow \infty$. A related question asks if the spatial transient in Regions I and III actually approaches zero far from the excitation. In this section, it is assumed that this is the case. It will be found in Chap.10 that to identify those systems where this assumption is not well founded it is necessary to consider the entire z - t transient.

Spatial Modes for a Moving Thin Sheet: The configuration shown in Fig. 5.17.3 is the same as that considered in Sec. 5.13, except that the excitation is confined to region II. A thin semi-insulating sheet, moving with velocity U , passes between electrodes constrained in potential as shown. In the range $0 < z < \ell$, the upper wall is excited with the traveling wave of potential. Elsewhere on the walls, both above and below, the potential is zero.

At every position in the system, fields have the same temporal frequency ω as the drive. Thus, at any location the temporal dependence is recovered by the operation

$$\Phi(x, z, t) = \text{Re } \hat{\Phi}(x, z, \omega) e^{j\omega t} \quad (1)$$

But then, the spatial Fourier transform of this complex amplitude is

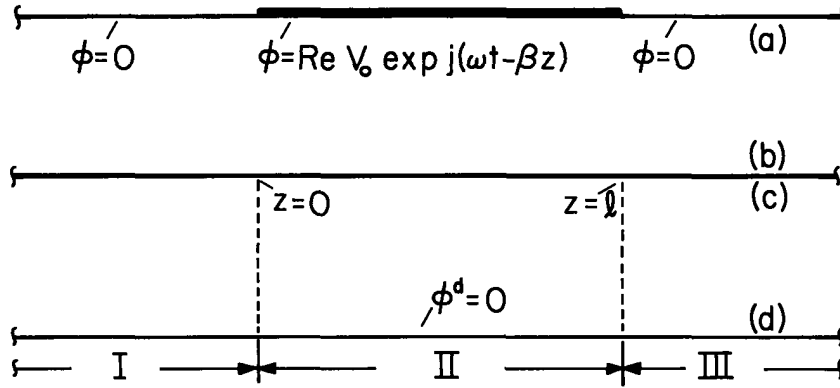


Fig. 5.17.3. A thin sheet moving with velocity U in the z direction enters the excitation region at $z = 0$ and leaves at $z = l$.

$$\hat{\phi}(x, k, \omega) = \int_{-\infty}^{+\infty} \hat{\phi}(x, z, \omega) e^{jkz} dz \quad (2)$$

with an inverse

$$\hat{\phi}(x, z, \omega) = \frac{1}{2\pi} \int_{-\infty}^{+\infty} \hat{\phi}(x, k, \omega) e^{-jkz} dk \quad (3)$$

Because the rule for taking the transform of a derivative with respect to z is the same as if a substitution of the form $\hat{\phi}e^{-jkz}$ is made, relations among complex amplitudes can now be regarded as relations among the Fourier transforms. For the specific problem at hand, these relations are developed in Sec. 5.13 where the Fourier transform of the sheet potential is given by Eq. 5.13.7:

$$\hat{\phi}^b = \frac{jS_e \hat{\phi}^a}{2 \sinh(kd) [1 + jS_e \coth(kd)]} \quad (4)$$

$$S_e \equiv \frac{2\epsilon(\omega - kU)}{k\sigma_s}$$

The fields are completely determined if the driving potential $\hat{\phi}^a$ is specified. For the traveling-wave driving potential of Fig. 5.17.3,

$$\hat{\phi}^a = \text{Re} \hat{V}_0 e^{-j\beta z} [u_{-1}(z) - u_{-1}(z - l)] e^{j\omega t} \quad (5)$$

where $u_{-1}(z)$ is the function; unity for $z > 0$, 0 for $z < 0$. From Eq. 2, the transform follows as

$$\hat{\phi}^a = \frac{\hat{V}_0}{j(k - \beta)} [e^{j(k - \beta)l} - 1] \quad (6)$$

Thus, Eqs. 3 and 4 give the complex amplitude of the sheet potential as

$$\hat{\phi}^b = \frac{1}{2\pi} \int_{-\infty}^{+\infty} \frac{\hat{V}_0 d\epsilon(\omega - kU) (e^{j(l-z)k} e^{-j\beta l} - e^{-jkz})}{\sigma_s (k - \beta) D(\omega, k)} dk \quad (7)$$

where $D(\omega, k)$ is the dispersion equation, Eq. 5.15.5, familiar from discussions of the temporal natural modes. In terms of normalized variables,

$$D(\omega, k) = k \sinh k + jU(\omega - k) \cosh k \quad (8)$$

where

$$\underline{k} \equiv kd, \quad \underline{\omega} \equiv \frac{\omega d}{U}, \quad \underline{U} \equiv \left(\frac{2\epsilon_0}{\sigma_s} \right) U$$

The integration called for in Eq. 7 is conveniently performed by closing the integration at infinity in the complex k plane and evaluating by Cauchy's integral theorem.¹ The contributions to the integration are then seen to be a sum of residues determined by the zeros of the denominator. One of these, $k = \beta$, is associated with the "driven response," while the others are residues from the poles:

$$D(\omega, k) = 0 \quad (9)$$

Remember, ω is a prescribed real number. The roots of Eq. 9, k_n , are in general complex and are each associated with an eigenfunction $\hat{\phi}_n(x)e^{-jk_n x}$ that satisfies all of the bulk conditions and boundary conditions in the interval $-d < x < d$ with the drive set equal to zero. Over the cross section, the eigenfunctions associated with a given root of Eq. 9 are

$$\hat{\phi}_n(x) = \begin{cases} -\hat{\phi}_n^b \frac{\sinh k_n(x-d)}{\sinh k_n d} & x > 0 \\ \hat{\phi}_n^b \frac{\sinh k_n(x+d)}{\sinh k_n d} & x < 0 \end{cases} \quad (10)$$

The complex roots of Eq. 9 must be found numerically. However, the dominant roots are easily identified in the long-wave limit $|kd| \ll 1$ because then Eq. 9 is quadratic in k and can be solved for the two roots,

$$k_{\pm 1} = \left[j \frac{U}{2} \pm \sqrt{\left(\omega^2 - \frac{1}{2}\right) \frac{U^2}{2} - j\omega U} \right] / \left(1 + \frac{j\omega U}{2}\right) \quad (11)$$

(Note that these are the same roots that would be determined from Eq. 5.15.10, with $s_1 \rightarrow j\omega$, and are therefore the only ones retained by a quasi-one-dimensional model.) Typical roots of Eq. 11, as a function of real ω , are shown in Fig. 5.17.4.

For kd not small compared to unity these roots retain the same qualitative nature. Thus k_{-1} and k_1 are respectively waves that have phase velocities in the $-$ and $+$ directions with the first decaying rapidly in the $-z$ direction and the second decaying slowly in the $+z$ direction. Although it is not in general possible to attribute certain of the modes to one aspect of the system or another, these two dominant modes are associated closely with the spectral build-up and decay of surface charge on the sheet.

The higher order modes are more closely connected with the fields that would exist in the free space regions in the absence of the sheet. In the limit where U is large enough that $U \gg \omega/k$, the term in ω in Eq. 8 is ignorable, so that approximately

$$1 = jU \coth k \quad (12)$$

This expression has an infinite number of purely imaginary solutions $k = jk_i$, as can be seen by substituting into Eq. 12 to obtain

$$\tan k_i = U \quad (13)$$

which can be solved graphically. In the limit $U \gg 1$, roots $k \rightarrow +j(2n' - 1)\pi/2$, where n' is an integer. Note that these are the eigenmodes that would be obtained if the sheet were absent. The x distribution of potential associated with these approximate eigenvalues is given by Eq. 10, and is sinusoidal. The associated pure decay in the $\pm z$ directions is typical of solutions to Laplace's equation that are periodic in x .

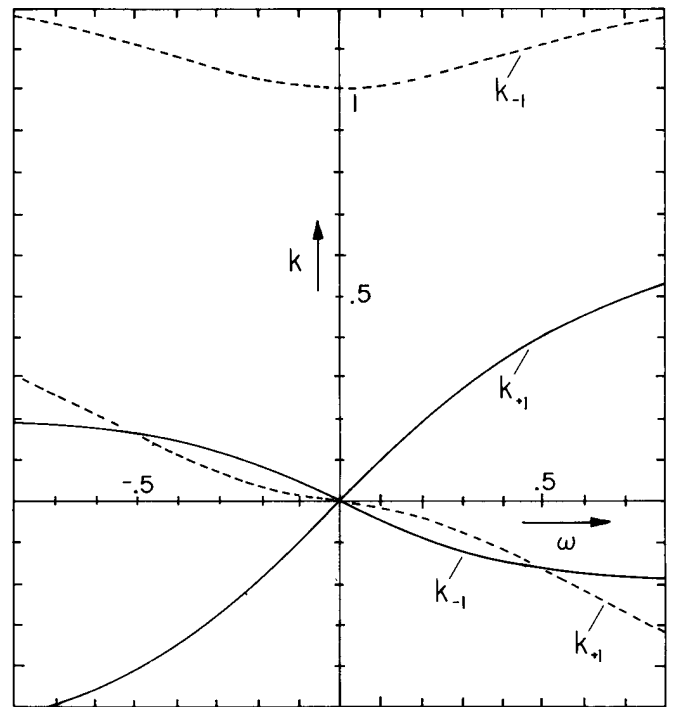


Fig. 5.17.4. Normalized complex wavenumber of lowest modes as function of normalized frequency.

1. F. B. Hildebrand, Advanced Calculus for Applications, Prentice Hall, Englewood Cliffs, N.J., 1962, p. 548.

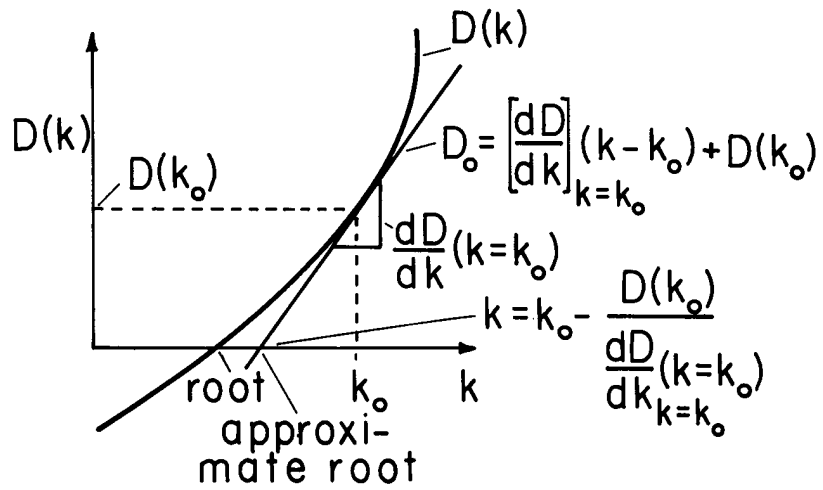


Fig. 5.17.5. Numerical solution illustrated graphically. The zero of the complex function $D(k)$ of the complex variable is approximated at the trial value k_0 by a straight line. The approximate root follows by setting $D_0(k) = 0$. This root can then be used as k_0 in refining the approximation and the process repeated until the desired accuracy is obtained. To obtain roots of Fig. 5.17.6, k_0 is first approximated by Eqs. 11 and 13.

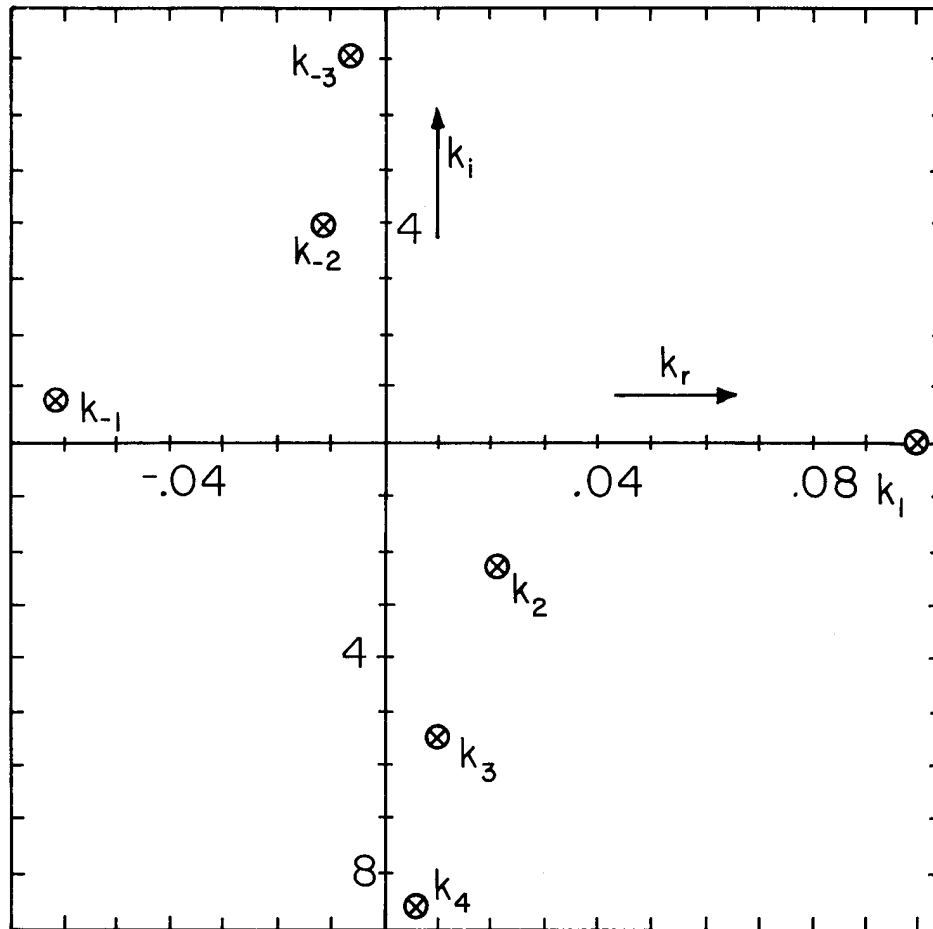


Fig. 5.17.6. Wavenumber eigenvalues given by Eqs. 8 and 9 for case $\omega \underline{U} = 0.1$, $\underline{U} = 1$.

The numerical solution of $D(\omega, k)$ is described in Fig. 5.17.5. Given in Fig. 5.17.6 are specific roots conveniently found by using the approximate roots given from Eqs. 11 and 13 as a first approximation. Roots are denoted by the integer n , which ranges from $-\infty$ to $+\infty$, with $n = 0$ omitted.

Spatial Transient on Moving Thin Sheet: Now that the spatial eigenmodes have been found, consider how the integral solution, Eq. 7, is tantamount to a superposition of these eigenmodes and, in region II, a "driven" response with wavenumber β of the drive.

Except at the poles $D(\omega, k) = 0$, the integrand of Eq. 7 is an analytic function. This is even true at $k = \beta$, because

$$\frac{e^{j(\ell-z)k} e^{-j\beta\ell} e^{-jkz}}{k - \beta} = j e^{-jkz} e^{j \frac{(k-\beta)\ell}{2}} \frac{\sin \left[\frac{(k-\beta)\ell}{2} \right]}{\left[\frac{(k-\beta)}{2} \right]} \quad (14)$$

is not singular at $k = \beta$.

To apply the Cauchy integral theorem, the integration of Eq. 7 is extended to an integration around a closed contour, with the closure defined such that there is no additional contribution to the integral. For integration around a contour C in the counterclockwise direction,

$$\oint_C \frac{N(k)}{D(k)} dk = 2\pi j [K_1 + K_2 + \dots] \quad (15)$$

where the residues K_n (at isolated singular points $k = k_n$) of a function $N(k)/D(k)$ are $N(k_n)/D'(k_n)$. Which of the contours shown in Fig. 5.17.7 is appropriate depends on the range of z of interest. With the three regions defined in Fig. 5.17.3, the appropriate contours are identified as follows. First, observe that with $k = k_r + jk_i$, the two z -dependent terms in Eq. 7 can be written as

$$e^{j(\ell-z)k} = e^{j(\ell-z)k_r} e^{-(\ell-z)k_i}; \quad e^{-jkz} = e^{-jk_r z} e^{k_i z} \quad (16)$$

Thus, in region I, $z < 0$ and $(\ell - z) > 0$, so both terms go to zero as $k_i \rightarrow \infty$ and C_1 is appropriate. In region II, $(\ell - z) > 0$, so the first term converges for $k_i \rightarrow \infty$ and C_1 is appropriate. Also in region II, $\ell < z$, so the second term converges for $k_i \rightarrow -\infty$ and C_2 is appropriate. Finally, in region III, $\ell < z$ and $(\ell - z) < 0$, so each term decays as $k_i \rightarrow -\infty$ and C_2 is appropriate.

It follows that in region I, integration of Eq. 7 gives

$$\hat{\phi}^b = \frac{j \hat{V}_0 d \epsilon}{\sigma_s} \sum_{n=-1}^{-\infty} \frac{(\omega - k_n U) [e^{j(k_n - \beta)\ell} - 1] e^{-jk_n z}}{(k_n - \beta) D'(\omega, k_n)} \quad (17)$$

In region II, the integration is broken into an integration of the first and second terms individually. Thus, for each of these integrations, $k = \beta$ becomes a singular point and $k - \beta$ must be included with $D(\omega, k)$ in determining the residues. This singular point can be regarded as being just below the axis, and hence as contributing to the integration on C_2 , but not on C_1 . Then, it follows that in region II

$$\hat{\phi}^b = \frac{j \hat{V}_0 d \epsilon}{\sigma_s} \left\{ \sum_{n=-1}^{-\infty} \frac{(\omega - k_n U) [e^{j(k_n - \beta)\ell} - 1] e^{-jk_n z}}{(k_n - \beta) D'(\omega, k_n)} + \frac{(\omega - \beta U) e^{-j\beta z}}{D(\omega, \beta)} + \sum_{n=1}^{\infty} \frac{(\omega - k_n U) e^{-jk_n z}}{(k_n - \beta) D'(\omega, k_n)} \right\} \quad (18)$$

Finally, in region III

$$\hat{\phi}^b = - \frac{j \hat{V}_0 d \epsilon}{\sigma_s} \left\{ \sum_{n=1}^{\infty} \frac{(\omega - k_n U) [e^{j(k_n - \beta)\ell} - 1] e^{-jk_n z}}{(k_n - \beta) D'(\omega, k_n)} \right\} \quad (19)$$

In regions I and III, the response is a superposition of the spatial modes that decay in the $-z$ and $+z$ directions, respectively. These are the bow and stern waves. In region II, all of the spatial modes are involved in accounting for the finite length of the traveling-wave excitation. In addition there is the "driven" response at the same wavenumber as the excitation, the second term in Eq. 18. Note that for positions z well away from both ends, for example at $z = \ell/2$, the sums over the natural modes in Eq. 18 approach zero while the driven response that remains is the spatial sinusoidal steady-state response found in Sec. 5.13.

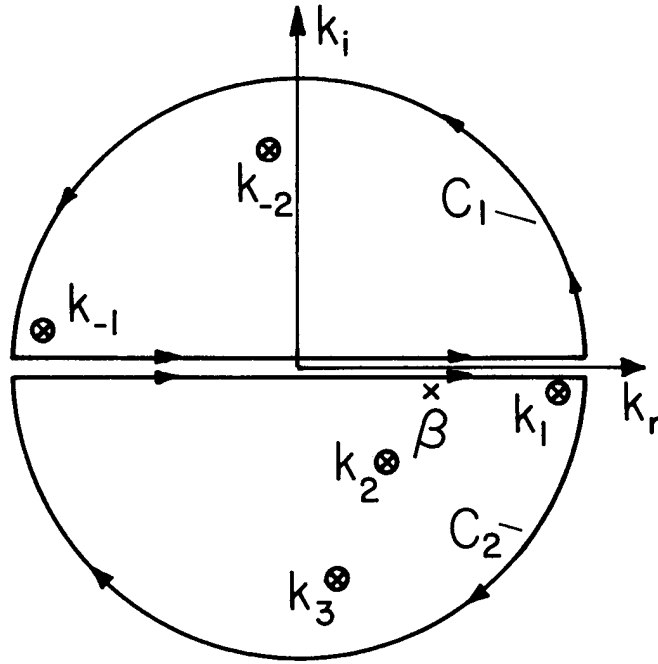


Fig. 5.17.7

Contours used to evaluate the integral of Eq. 7.

As a useful longwave approximation, only the two lowest spatial modes are used with k_1 and k_{-1} given by Eq. 11 and

$$D(\omega, k) \rightarrow d^2(k - k_1)(k - k_{-1}) \quad (20)$$

Then, Eqs. 17-19 reduce to:

$$\hat{\phi}^b = \frac{j\hat{V}_0 \epsilon}{\sigma_s d} \left\{ \frac{(\omega - k_{-1}U) (e^{j(k_{-1}-\beta)\ell} - 1) e^{-jk_{-1}z}}{(k_{-1}-\beta)(k_{-1}-k_1)} \right\}; \text{ region I} \quad (21)$$

$$\hat{\phi}^b = \frac{j\hat{V}_0 \epsilon}{\sigma_s d} \left\{ \frac{(\omega - k_{-1}U) e^{jk_{-1}(\ell-z)} e^{-j\beta\ell}}{(k_{-1}-\beta)(k_{-1}-k_1)} + \frac{(\omega - \beta U) e^{-j\beta z}}{(\beta - k_1)(\beta - k_{-1})} + \frac{(\omega - k_1U) e^{-jk_1z}}{(k_1-\beta)(k_1-k_{-1})} \right\}; \text{ region II} \quad (22)$$

$$\hat{\phi}^b = \frac{-j\hat{V}_0 \epsilon}{\sigma_s d} \left\{ \frac{(\omega - k_1U) (e^{j(k_1-\beta)\ell} - 1) e^{-jk_1z}}{(k_1-\beta)(k_1-k_{-1})} \right\}; \text{ region III} \quad (23)$$

The z - t dependence of the sheet potential, recovered by using these equations in Eq. 1, is illustrated in Fig. 5.17.8.

Time-Average Force: To compute the total time-average force acting on the sheet, the steps are the Fourier transform extension of those leading from Eq. 5.13.5 to Eq. 5.13.11. The total force is the integral over the length of the sheet of the time-average surface force density. This is in turn written as an integration over the wavenumbers, in accordance with Eq. 5.16.14:

$$\langle f_z \rangle_t = \frac{w}{2} \text{Re} \int_{-\infty}^{+\infty} \hat{E}_z^b (\hat{D}_x^b - \hat{D}_x^c)^* dz = w \text{Re} \frac{1}{2\pi} \int_{-\infty}^{+\infty} \frac{1}{2} \hat{E}_z^b (\hat{D}_x^b - \hat{D}_x^c)^* dk \quad (24)$$

Because $\hat{E}_z^b = jk\hat{\phi}^b$, the integrand of Eq. 24 is the same as Eq. 5.13.4. Thus, with $\hat{V}_0 \rightarrow \hat{\phi}^a$, steps paralleling those of Eqs. 5.13.5 and 5.13.6 give the total time-average force as simply

$$\langle f_z \rangle_t = \frac{w}{2\pi} \int_{-\infty}^{+\infty} \frac{\epsilon_0 k^2 S_e \hat{\phi}^a \hat{\phi}^{a*} dk}{4 \sinh^2(kd) [1 + S_e^2 \coth^2(kd)]} \quad (25)$$

For the excitation represented by Eq. 6, this expression becomes

$$\langle f_z \rangle_t = \frac{w\epsilon_0}{2\pi} |\hat{V}_0|^2 \int_{-\infty}^{+\infty} \frac{k^2 S_e \sin^2 \left[\frac{\ell}{2} (k - \beta) \right] dk}{(k - \beta)^2 \sinh^2(kd) [1 + S_e^2 \coth^2(kd)]} \quad (26)$$

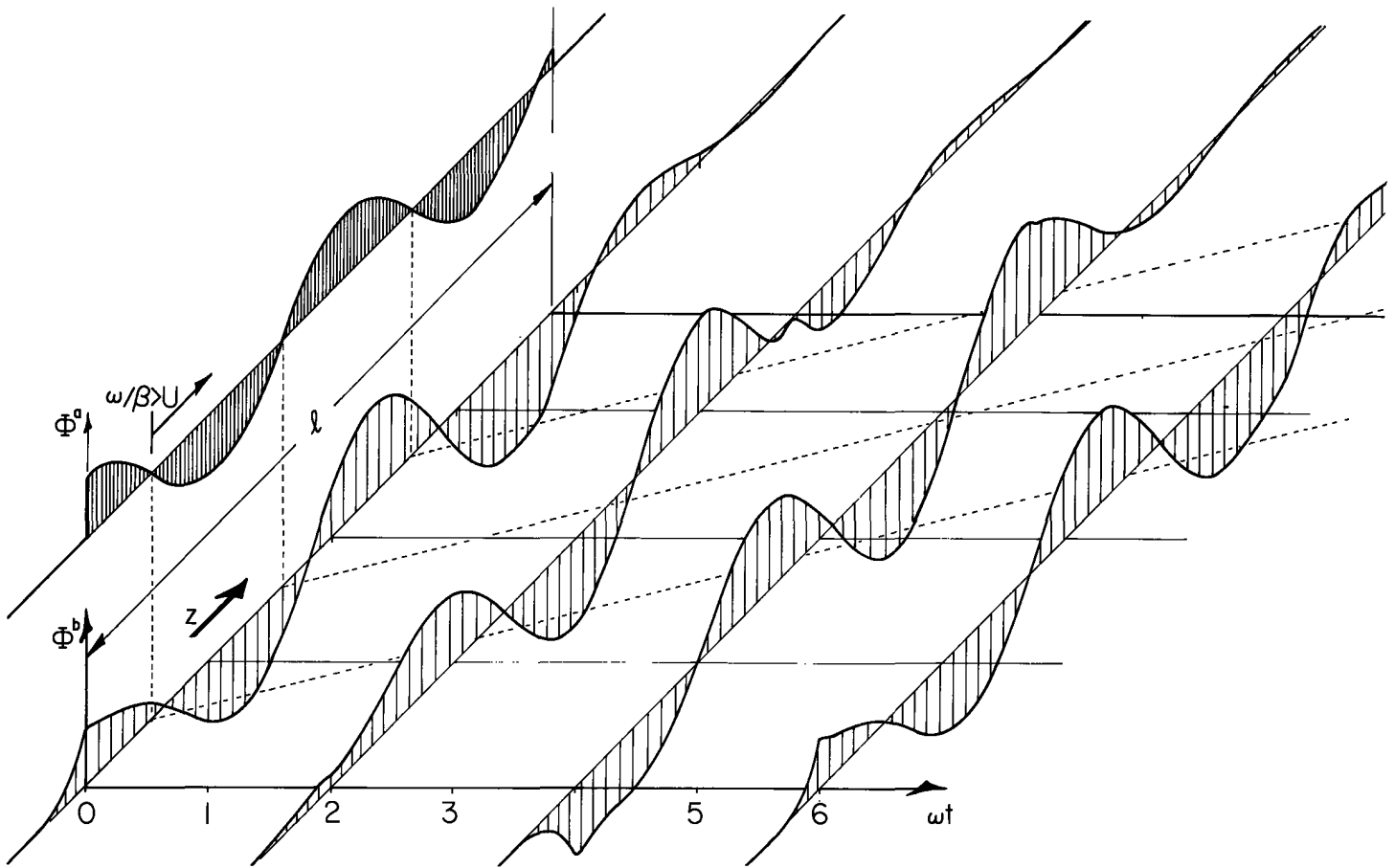


Fig. 5.17.8. Sheet potential Φ^b given by Eqs. 20-23 as a function of z and the normalized time ωt . The excitation potential Φ^a is also shown when $t = 0$. It takes the form of a traveling wave confined to the structure length ℓ with phases following the broken lines in the $z-\omega t$ plane. Note that, in the region under the excitation electrodes, the sheet potential, Φ^b , tends to a spatially periodic response. At any given location z , the fields are temporally periodic with the frequency ω . For the case shown, $\underline{\omega} = 0.5$, $\underline{U} = 0.5$ and $\underline{\beta} = 0.3$ so that $\underline{\omega}/\underline{\beta} = (\omega/\beta)/U > 1$, and the stator-wave phase velocity exceeds the sheet velocity.

Because the integrand of Eq. 26 is positive definite, and has a denominator that increases exponentially for large kd , numerical integration is straightforward. Typical results are illustrated by Fig. 5.17.9. For motor operation, the peak force per unit area and general frequency dependence is diminished by the end effects.

The integration over the Fourier components used to compute the total force in this section is one of two alternative approaches that can be used. In the second approach, the fields (expressed as functions of z) can be used to represent the stress, and this integrated on z to find the total force. The most convenient control volume is one that encloses the sheet, but extends across the air gap so that it has surfaces contiguous with the (a) and (d) surfaces of Fig. 5.17.3. Because the electric shear stress on the (a) and (d) surfaces is confined to the region between $z = 0$ and $z = \ell$ on the (a) surface, the integration reduces to one over that interval only. Care must be taken to include the singularities in E_z that appear at end points of the interval.

Fig. 5.17.9

Normalized force per unit length, Eq. 26, as a function of normalized frequency showing "end effect." The number of poles, $p \equiv (\underline{\beta}/\pi)(l/d)$ (the number of half-wavelengths), is the parameter and \underline{U} and $\underline{\beta}$ are 0.5 and 0.3 respectively. Note that the phase velocity of the drive exceeds that of the material velocity for $\underline{\omega} > \underline{\beta} = 0.3$.

